Open Research Online

The Open University's repository of research publications
and other research outputs

Application of Proton Transfer Reaction Mass Spectrometry to Analytical Science

Thesis

oro.open.ac.uk

Application of Proton Transfer Reaction Mass Spectrometry

to Analytical Science

Sylvia C Miller MSc BSc PGCE

A thesis submitted to The Open University

in the subject of Analytical Sciences

for the degree of Doctor of Philosophy

2014

"Nothing tends so much to the advancement of

knowledge as the application of a new instrument. "

Sir Humphrey Davy

The Open University

Date of Submission: 2 September 2013

Date of Award: 7 July 2014

ProQuest Number: 13835810

A Research Machine

My first introduction to the proton transfer reaction mass spectrometer manufactured by Kore Technology Ltd. was at the premises of Smiths Industries in Watford. This was the instrument which the Molecular Physics group at the University of Birmingham was to have on permanent loan. From the description of Smith's attempts to use it, it occurred to me that it was going to take at least six months to get this working satisfactorily. In the event, it took about a year from delivery to get accurate and useful data.

Had the instrument been fully working, I would not have learned nearly so much about its intricacies and it would have seemed much more of a 'black box'. However, the process of discovering the instrument's features, as well as being able to see its separate functional units, gave a much better feel for how it works: I compare this with the Ionicon Analytik GmbH PTR-Quad-MS in our laboratory which is contained in a washing-machine-sized metal housing from which no conceptual model can be assembled and expertise in its use was already available.

I found the PTR-TOF-MS by turns frustrating, challenging and, occasionally, a joy to work with; for example, my delight on seeing, for the very first time, the pattern presented by the isotopes of chlorine in trichlorobenzene. And then the surprise in seeing an unexpected spectrum from a dichlorobenzene sample only to realise that I had used a deuterated version of the chemical instead of the usual non-deuterated version. Both of these examples are illustrated below.
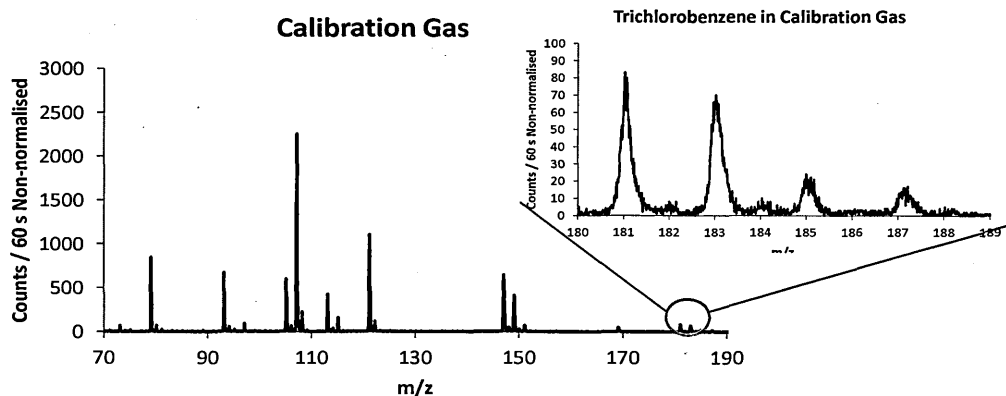
Delight: The spectrum of trichlorobenzene extracted from a calibration gas spectrum at E/N = 140 Td, TCB is present at 100 ppbV ±10%. (parts per billion by volume)
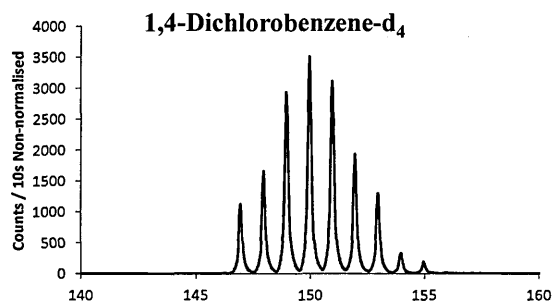
Deuterated   Non-deuterated
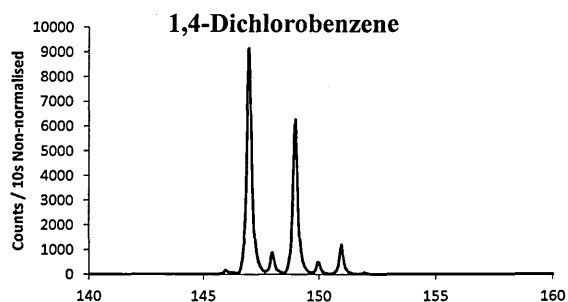
Surprise: Seeing the spectrum on the left instead of the expected outline on the right. The mass spec. never lies!!

Acknowledgments

Thank you to:

This work is dedicated to my mother, who introduced me to

scientific ideas and encouraged me on my scientific journey.

So sad that she is not here now to see the fruits of her efforts.

Abstract

This work concerns a proton transfer reaction time-of-flight mass spectrometer, PTR-TOF-MS, a bespoke model manufactured by Kore Technology Ltd. for Smiths Detection. This instrument achieves 'soft' ionization of volatile organic compounds (VOCs) by proton transfer from protonated water vapour in a reaction chamber at 1 mbar (= 100 Pa). The resulting ions are separated by mass in a field-free time-of-flight tube prior to detection by a multi-channel plate. The instrument was modified to facilitate direct determination of the electric field in the reaction chamber.

Sensitivity measurements determined a value of 4-6 counts per second per parts per billion by volume (ncps ppbv^{-1}) normalised to 10^6 H_3O^+. The calibration gas mixture used in this investigation consisted of 14 compounds, (alkylbenzenes and chlorobenzenes) spanning an m/z range of 78 to 180. Each of these was separately investigated over E/N = 90 to 245 Td to establish fragmentation behaviour and possible interfering contributions. For example, several of the alkylbenzenes fragmented to product ions occurring at m/z 79, the same value as that of protonated benzene. Most of this occurred at the higher E/N values with ethylbenzene a notable exception. The isobaric compounds ethyl benzene and the xylenes exhibit very different fragmentation patterns so enabling differentiation of these two compounds. However, it is not possible to distinguish the individual xylene isomers using this method.

Benchmarking was continued using the hexenol compounds cis-3-, cis-2-, trans-3- and trans-2-hexen-1-ols. This work demonstrated that the same four product ions are seen for all of the hexenol isomers at m/z 39 ($C_3H_3^+$), 41 ($C_3H_5^+$), 55 ($C_4H_7^+$) and 83 ($C_6H_{11}^+$) when reacted with H_3O^+ in a PTR-TOF-MS. A characteristic peak at m/z 99 was seen in trans-2-hexen-1-ol and cis-2-hexen-1-ol at low E/N values (< 140 Td) when the protonated parent ion, m/z 101, is absent. In trans-3-hexen-1-ol and cis-3-hexen-1-ol the MH$^+$ ion at m/z 101 is seen at these lower E/N values but there is no product ion at m/z 99. This suggests a possible method for distinguishing between the 2- and 3-hexenols. It may also be possible to further identify the individual isomers from the differences in the percentage yield of these product ions.

TABLE OF CONTENTS

List of Figures

List of Tables

Acronyms

BR	Branching ratio
BTEX	Benzene, toluene, ethylbenzene and xylenes
CB	Chlorobenzene
CID	Collisional induced dissociation
CIMS	Chemical ionization mass spectrometry
cps	Counts per second
DCB	Dichlorobenzene
DT	Drift tube
DVM	Digital voltmeter
EB	Ethylbenzene
EI	Electron impact
FA-SIFT	Flowing afterglow-SIFT
FA-TMS	Flowing afterglow-tandem mass spectrometry
GC-MS	Gas chromatography mass spectrometry
GD	Glow discharge
HC	Hydrocarbon
HPLC	High-performance liquid chromatography
HV	High voltage
m-	*meta*
mbar	millibar
MCP	Micro-channel plate
MS	Mass spectrometer
ncps	Normalised counts per second
o-	*ortho*
p-	*para*

PA	Proton affinity
Pa	Pascal
PID	Product ion distribution
ppbv	Parts per billion by volume
pptv	Parts per trillion by volume
PTFE	polytetrafluoroethylene
PTR	Proton transfer reaction
SD	Source drift
SIFT	Selected ion flow tube
STP	Standard temperature and pressure
TCB	Trichlorobenzene
TOF	Time of flight
VOC	Volatile organic compound

Chapter 1 Introduction

1.1 Background

Analytical science seeks to investigate the chemical composition and structure of materials in many fields of endeavour. It encompasses the development of new methods and tools, and the analysis and interpretation of data produced. One of the tools with a significant role in this field is the mass spectrometer, an instrument which ionises a substance, generally in gaseous form, and then separates these ions according to their mass-to-charge ratio (m/z). The ions reach a detector and are processed into a spectrum from which identification can be made and structure inferred. There are different techniques for ionising the analyte, e.g. electron impact and chemical ionisation.

The basis of this thesis is the use of a proton transfer reaction - time of flight - mass spectrometer (PTR-TOF-MS), specifically an instrument manufactured by Kore Technology Limited, Ely, UK. PTR-based instruments have been in use since the mid-1990s. There are currently more than 150 operational instruments (Jordan 2009): the majority of these have been manufactured by Ionicon Analytik GmbH, a spin-off company from the Institute of Ion Physics, University of Innsbruck whence the technology originated. Kore instruments are manufactured on a bespoke basis and they are considered to be primarily research tools. Currently, there are approximately 15 Kore PTR-TOF instruments in use. (Kore Technology 2013)

PTR-MS instruments are best used wherever there is a need for the real-time detection and monitoring of trace chemicals in environments (volatile organic compounds or VOCs) where there are many complicating factors, for example, atmospheric pollution or the detection of explosives or drugs. The instrument offers many of the essential characteristics for this type of work: high sensitivity, reduced sample preparation, accuracy and fast response and recovery times.

The research undertaken here aims to exemplify and demonstrate the capabilities of the more unusual Kore time of flight instrument. Consequently, diverse areas have been investigated: food sciences, with a proof-of-principle study of the ageing of pears; environmental studies,

examining the four isomers of hexenol; a detailed investigation into the sensitivity of the instrument which resulted in outcomes with applications in atmospheric chemistry; and a foray into biosciences, looking at quorum-signalling chemicals from bacteria.

1.2   Applications of PTR-TOF-MS Instruments

Prior to the advent of the proton transfer reaction mass spectrometer, the conventional method of identifying VOCs was gas chromatography–mass spectrometry, (GC-MS), or high-performance liquid chromatography (HPLC-MS). The advantages of PTR technology over these and other VOC detection methods are:

- It produces a simpler mass spectrum as a result of the lower energy interactions involved in proton transfer as compared with electron ionisation mass spectrometry.

- Reduced sample preparation is required, unlike GC-MS, so simplifying and speeding up the detection process.

- Limit of detection is in the range of parts per trillion by volume (pptv).

- None of the components of air reacts in the instrument, so air can be used as a carrier gas

PTR-MS instruments have consequently become frequently used by many research groups in such diverse applications as medicine: detecting acetonitrile in smokers' breath (Jordan 1995, Lirk 2003); food: detection of meat spoilage (Mayr 2003, Nhu-Thuc Phan 2012, Heenan 2012); environmental studies: detecting chemicals in typical homes (Jordan 1995), measurement of atmospheric dimethyl sulphide and benzene (Hayward 2002, Inomata 2008, Holzinger 2010), biosciences (Cresp 2011), and security (Mayhew 2010, Agarwal 2011, Whyte 2007). An extended review of additional applications of PTR instruments can be found in Blake *et al.*'s review (2009) and an up-to-date literature review is available in Ellis and Mayhew 2014.

Until recently, all research studies used a quadrupole mass analyser. Lately, PTR instruments with a time of flight analyser (TOF) have been used (Heenan 2012).

1.3   Development of PTR Instruments

Proton transfer reaction is a method of converting an analyte into positively charged ions by the transfer of a proton so that the sample molecules remain intact for subsequent detection. It is derived from 'soft' or chemical ionisation mass spectrometry, (CIMS) introduced by Munson and Field over 40 years ago (Munson 1966) when ion-molecule reaction kinetics were studied by injecting ions into an inert buffer gas that contained a small amount of neutral reactant. This method achieved reactions at thermal or near-thermal collision energies (Fehsenfeld, F. C. *et al.* 1966) but was found to be unsuitable for complex molecular ions: the lack of any ion selection prior to reaction could produce a variety of secondary ions in the discharge source leading to severe complications in the product analysis. This significant problem led to the introduction of the selected ion flow tube (SIFT) technique (Adams and Smith 1976). It was this early work with SIFT that produced most of the kinetic data that guides PTR-MS work today.

In 1993, Lindinger *et al.* (1993) used an ion/molecule-reaction mass spectrometer which exploited CIMS and proved to be the forerunner of today's PTR-MS. The following year they analysed trace organic gases in air (Lagg *et al.* 1994) using a mass-selected H_3O^+ (hydronium) source with a flow drift tube, which combines ion transport by carrier gas (flow tube) and electric field (drift tube). As well as providing a means of ion transport, the electric field also increases the average collision velocity of an ion with the buffer gas thereby reducing the clustering of the hydrated hydronium ions $H_3O^+.(H_2O)_n$, $n = 1,2,3$.

This team in Innsbruck continued to develop the approach to producing protonated species, making two further significant changes (Hansel *et al.* 1995): first, using concepts and methods developed in the 1950's (Little and von Engel 1954), they used a hollow-cathode discharge source that could generate H_3O^+ with high efficiency (> 99.5%) without any need for a mass filter. The second innovation was to replace the flow tube with a relatively short drift tube: instead of using a carrier gas to transport VOCs along the tube, the analyte sample was

directly injected into the drift tube and the unreactive components of the air (N_2, O_2, etc.) served as thermalizing agents.

The PTR-MS has distinct advantages over its predecessor, the SIFT-MS: it is a simpler instrument to operate, there being no necessity to select the reagent ion and its main benefit is its improved detection sensitivity of around two orders of magnitude. SIFT-MS has the advantage of being able to select which ions enter the reaction region, theoretically providing a greater range of possible reagent ions. In practice, however, the reagent ions used tend to be the same as those found in the PTR-MS: NO^+, O_2^+ and H_3O^+. The SIFT's great contribution to the field is its ability to work at thermal energies and so measure absolute rate coefficients. The PTR-MS works at higher energies as result of the electric field in the drift tube but generally there is no need to measure absolute rate coefficients for exothermic H_3O^+ reactions which always occur at the collisional rate, a barrier-less transition. All of the preceding attributes, higher sensitivity, simpler use plus the relatively compact size, have led to a substantial increase in interest in the technique over the past decade (Blake *et al.* 2009).

Most of the work with PTR techniques has used quadrupole spectrometry. These instruments have several disadvantages in comparison with the time of flight detection method as shown in Table 1.1. The PTR ionisation processes require a protonated reagent which reacts

Table 1.1: Comparison of features PTR-Quad-MS and PTR-TOF-MS

	PTR-QUAD-MS	PTR-TOF-MS
Mass resolution ($m/\Delta m$)	≤ 100	At least 1000
Mass range	Rarely exceeds 1000 Da	No theoretical limit
Speed of detection	Slow - Detects limited mass range in one scan	Fast - Detects complete mass range in one spectrum
Sensitivity	pptv	ppbv (Ennis 2005)
m/z detection	Peaks are measured only at integer values	Has a mass precision of ~ 0.1 amu

exothermically with the trace gas of interest. The reaction, however, has a low exothermicity, generally resulting in non-dissociative interactions because there is little excess energy

available to fragment the sample gas. This method generally produces simplified spectra and so enables the analysis of complex gas mixtures, in contrast to electron impact ionisation where higher collision energies produce complicated and often impenetrable results.

A complete description of the PTR-MS development and comparisons with the SIFT-MS and PTR-Quad can be found in Ellis and Mayhew 2014.

The work with this PTR-TOF-MS instrument has mostly used protonated water, H_3O^+ (hydronium) as the reagent, produced by a plasma discharge in a hollow cathode. Sample molecules, M, react with the hydronium in the following way:

$$H_3O^+ + M \rightarrow MH^+ + H_2O$$
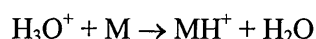
This will only occur if M has a higher proton affinity than that of water (691 kJ mol^{-1}, where 96.5 kJ mol^{-1} = 1 eV)[1]. Generally, most organic compounds have a proton affinity greater than that of water, unlike the main components of air which can therefore be used as the buffer gas for such samples. See §2.1, Table 2.1 for proton affinities for some common chemicals. The positively charged sample molecules can then be analysed, for example, using a quadrupole filter or a time of flight tube.

It is possible to calculate the concentration of molecules in the sample, [M], by measuring the ion counts for $[H_3O^+]$ and $[MH^+]$ and using the following equation:

$$[M] = \frac{1}{kt} \frac{[MH^+]}{[H_3O^+]}$$

where: k = rate coefficient for PTR

t = average time in drift tube (reaction chamber)

This equation holds only if the sample gas concentration is very high compared with the density of H_3O^+. In practice this means that the number of counts of the reagent ions must not change by more than one or two percent on the introduction of the sample i.e. $MH^+ \ll H_3O^+$ (Hayward et al. 2002).

---

[1] http://users.mccammon.ucsd.edu/~blu/Research-Handbook/physical-constant.html Accessed 16/05/2013

A detailed description of the PTR-TOF-MS is given in Chapter 2.

1.4   Areas Investigated

1.1.1   Sensitivity

This was an obvious area of investigation for this relatively unusual instrument. The Molecular Physics department at the University of Birmingham has close links with the team using Ionicon's PTR-MS instruments at the University of Innsbruck (Ionicon Analytik). Hence a comparison of functionality between the instruments used and this Kore Technology manufactured instrument was of interest. The calibration gas used consisted of 14 compounds, (alkylbenzenes and chlorobenzenes) spanning a mass range of 78 to 180.

1.1.2   Benchmarking with Hexenols

The 2010 paper from Demarcke *et al.* examined two of the four hexenol isomers in a PTR-MS quad. This prompted the investigation of all of the four hexenol isomers.

Chapter 2 The Kore Proton Transfer Reaction Time of Flight Mass Spectrometer

"There are too many degrees of freedom for optimisation to proceed simply by working round the whole set of parameters ... A fairly clear mental model of what is happening inside the system is very useful."

From "An update on our thinking regarding the operation of Kore PTR-TOF-MS"

Kore Technology Ltd. January 2006

2.1 Introduction

Proton transfer reaction mass spectrometry was developed to detect very low concentrations of volatile organic compounds (VOCs) in various environments by Lindinger *et al.* in the mid-1990s at the University of Innsbruck. The technique is comprehensively documented in the literature, from the original paper by Hansel *et al.* (1995) to that in the review by Blake *et al.* (2009) and textbook by Ellis and Mayhew (2013). In brief, a proton transfer reaction produces a positively charged ion for subsequent detection in a mass spectrometer, a process which involves exothermic proton transfer between the VOC molecules and H_3O^+ ions, providing that the VOC has a higher proton affinity than that of water. This is a form of chemical ionisation mass spectrometry, (CIMS) introduced by Munson and Field over 40 years ago (Munson 1966). Protonated water, H_3O^+ (hydronium), is produced by a plasma discharge in a hollow cathode. Within the hollow cathode, electron ionisation produces O^+, H^+, H_2^+, OH^+ and H_2O^+. These ions all react with H_2O ultimately producing H_3O^+ (hydronium). There are other methods of producing an ionised reagent, such as a plane electrode dc discharge source (Inomata (2006)) and a radioactive ion source (Hanson *et al.* (2003)).

H_3O^+ ions enter a drift tube reactor where they mix with a constant flow of the sample gas at viscous flow pressures of 1-2 mbar. A very small proportion of the contents of the drift tube is sampled through an orifice (400 μm) at the end of the drift tube. These ions are then steered towards the time of flight tube where they travel in a field-free region, arriving at the detector in a sequence dependent on their mass, the lighter molecules arriving before heavier ones. The resulting spectra for the PTR-TOF show counts per second plotted against *m/z*, where *m* = mass and *z* = charge. The charge always corresponds to *z* = 1 for this ionisation method.

The energy of this reaction is "soft" meaning that fragmentation of the protonated parent ions is minimized. Generally this produces a less complex mass spectrum as compared with that produced by the more standard technique of creating ions through electron impact which substantially fragments the parent molecular species.

The proton affinity (PA) of water is 691 kJ mol^{-1} and transfer of the proton from H_3O^+ occurs only if the analyte has a higher PA than this. Conveniently, many organic species fulfil this criterion whereas the main constituents of air, such as nitrogen, oxygen and carbon dioxide, do not (Table 2.1). Air can therefore act as the buffer gas for the analysis of mixed samples.

Table 2.1: Proton affinities (PAs) of some common chemicals (NIST)

Molecule	PA /kJ mol^{-1}	PA /eV
O_2	421	4.39
N_2	494	5.15
CO_2	541	5.64
Methane	544	5.67
Ethane	596	6.21
Acetylene	641	6.68
H_2O	691	7.20
Benzene	750	7.81
Ethanol	776	8.08
$(H_2O)_2$	808	8.42
Acetone	812	8.46

Compounds with PA < PA of water do not react with H_3O^+ in the PTR-MS

PTR-MS can detect trace gases to parts per trillion by volume (pptv) in seconds. The TOF-MS can achieve a higher mass resolution than the Quad-MS and obtains spectra across the full mass range more quickly. Advantages of the PTR-TOF-MS are primarily its fast response time, high sensitivity and the need for little or no sample preparation.

2.2   Instrument Description

The PTR-TOF-MS is a complex instrument consisting of the following systems:

- Hardware - ion source, PTR chamber, TOF source and flight tube, reflectron, detector

- Electronics – control units for hardware

- Heating elements and controls for the inlet and source areas

- Vacuum systems for the ion source, source drift and PTR chamber (all at around 1 mbar), transfer section (10^{-4} mbar) and TOF tube (10^{-7} mbar), flow rate ~ 100-200 mL/min.

- Software in two parts:

  o GRAMS/AI software that is responsible for data acquisition used for producing the spectra

  o A software interface written by Kore through which experimental details are input: mass range, how spectra will be displayed, filenames, calibration, etc. There are two options for collecting data:

    ⇨ **Single Spectrum**

    Data are collected for a set time and a single spectrum is displayed showing the total counts at each *m/z* value for the requested mass range. An example of this type of collection is shown in Figure 2.5.

    ⇨ **Time series**

    With this method, data are collected, also for a set time but now there is one spectrum for each time interval e.g. for each second. At the end of the collection time a spectrum can be viewed for each time interval as well as a view of the total ion counts' progression over the whole collection period. It is also possible to see a time progression for any of the *m/z* values. An example of this type of collection is shown in Figure 6.15 showing a total ion count for indole for a collection time of 780 s.

The instrument is shown in Figure 2.1 as delivered. It can be divided into four main functional or pressurised sections as shown in the schematic diagram in Figure 2.2.
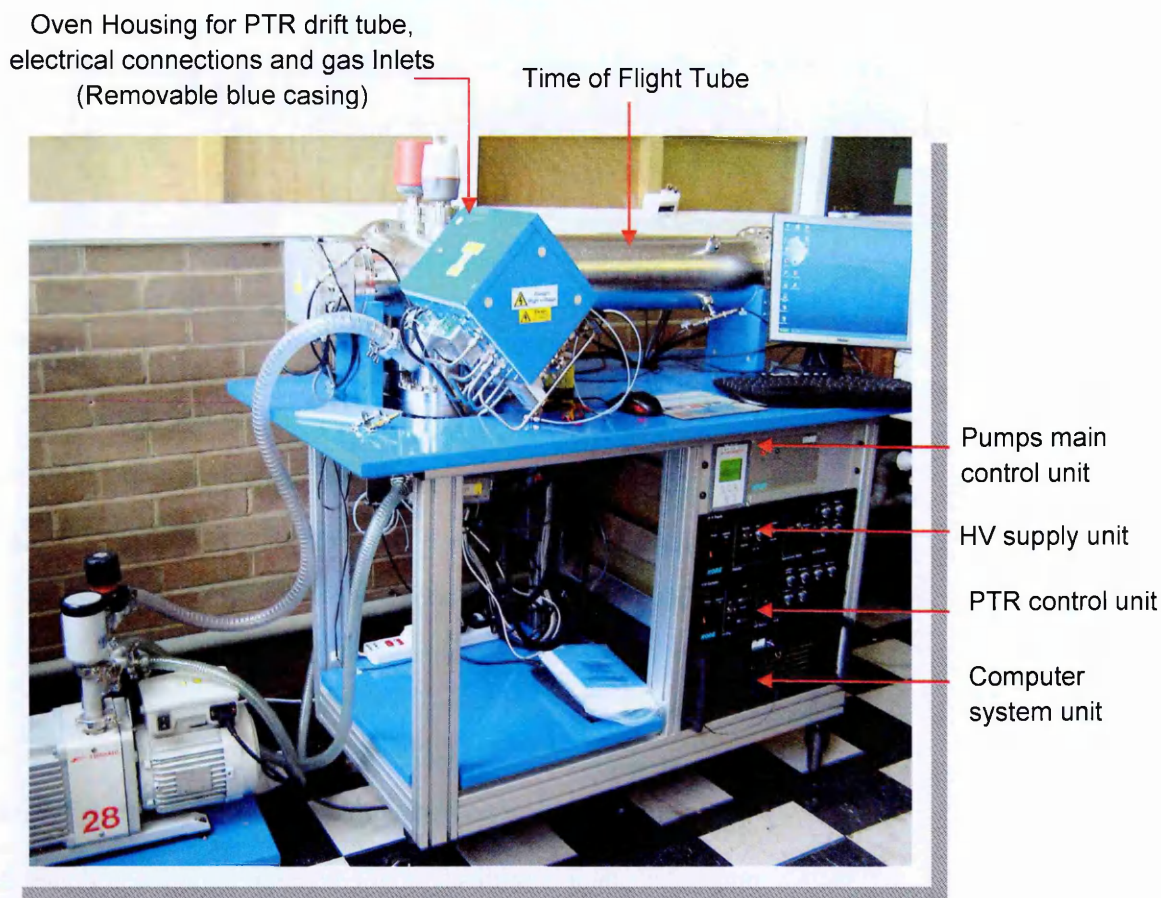
Figure 2.1: PTR-TOF-MS as delivered
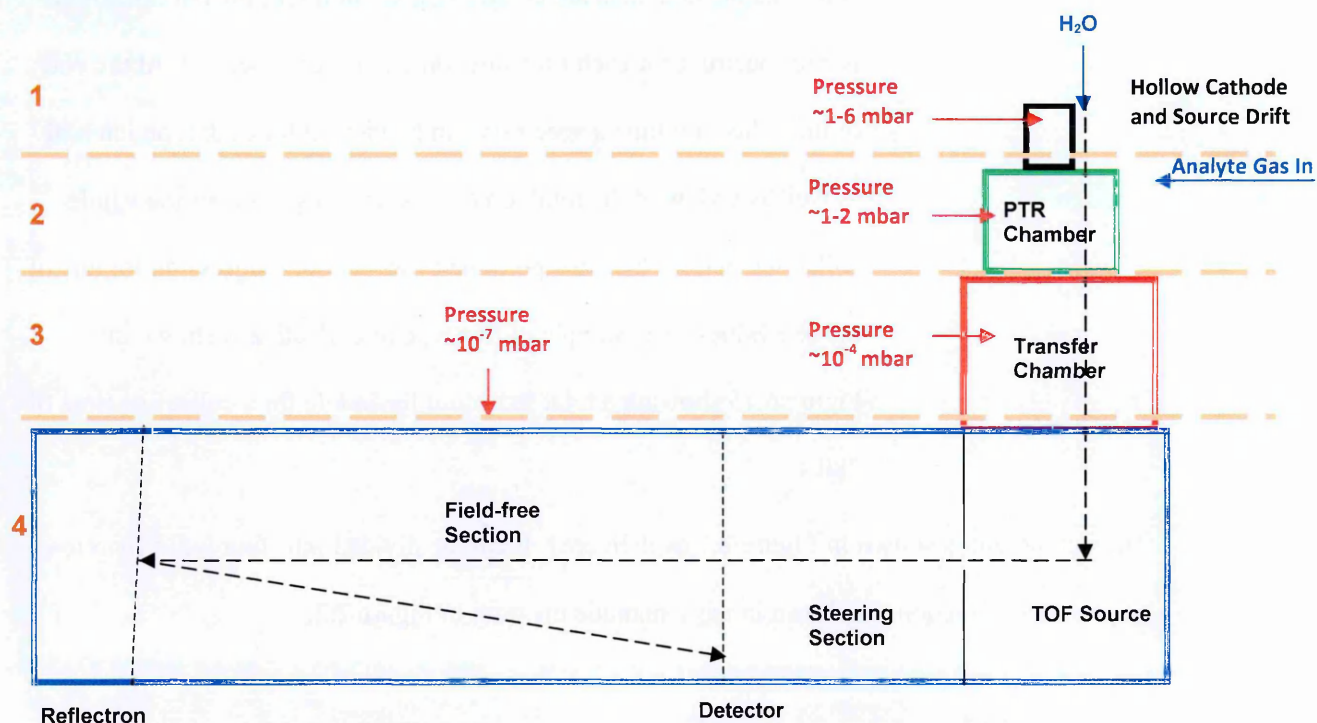
Figure 2.2: PTR-TOF-MS schematic

– – – – – – – Ion flow

Section 1: Hollow cathode and source drift at ~ 1-6 mbar for production of reagent ions H_3O^+.

Section 2: Reaction chamber at ~ 1-2 mbar with viscous flow resulting in many ion/molecule reactions

Section 3: Transfer chamber and optics at ~ 10^{-4} mbar with no ion/ion reactions

Section 4: Time of flight source, steering section and tube with reflection to improve mass resolution at ~ 10^{-7} mbar.

2.2.1 Hollow Cathode and Source Drift

Figure 2.3 shows the hollow cathode (glow discharge GD or plasma discharge, historically) and source drift region (SD). This section produces the primary beam of H_3O^+ ions from the
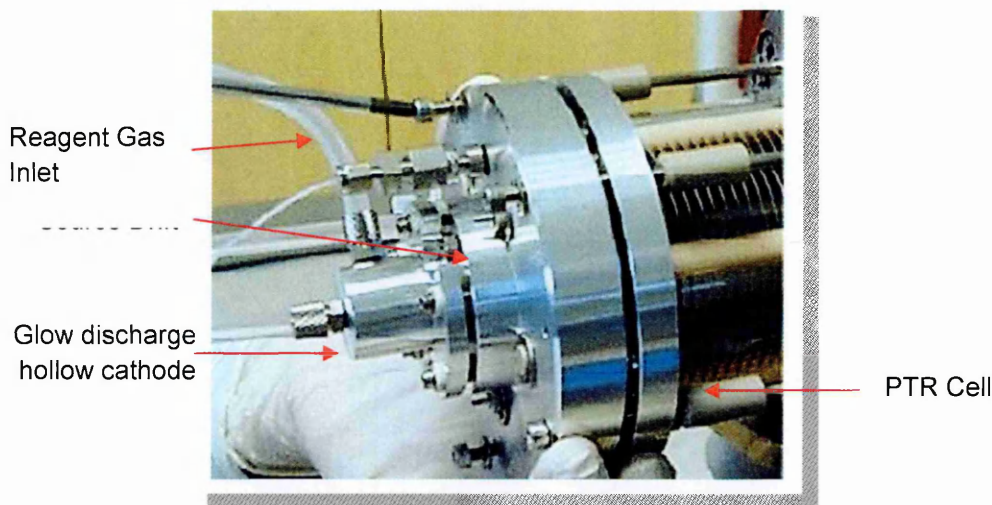
Figure 2.3: PTR assembly
(Courtesy of Kore Technology Ltd. manual z5852M)

water vapour entering the system through the 'Reagent gas' inlet. Inside the glow discharge hollow cathode (aluminium), a plasma forms that typically operates at 1 to 5 mbar and 400-500 V ultimately producing H_3O^+ (hydronium) among other ions. These ions move into a short source drift section and then into the PTR reaction chamber or drift tube (DT).

Ideally, H_3O^+ would be the only ion produced in the hollow cathode region. However, there is some back flow of air from the DT into the hollow cathode, and other species are present, primarily NO^+ and O_2^+, which do not react with H_2O (Blake *et al.* 2009).

2.2.2 PTR Chamber or Drift Tube

The proton transfer reaction cell (PTR or drift tube, DT) is shown schematically in Figure 2.4. The pressure in this section is $\sim$ 1–2 mbar which results in viscous flow conditions so that there are many collisions between the protonated reagent ions and the neutral analyte molecules, M.

There is an electric field, E, along the length of the PTR cell which removes the need for a fast moving carrier gas and therefore powerful pumps, as required for SIFT instrumentation (Blake *et al.* 2009). Changes in E and the pressure (or temperature) determine the collisional

energy conditions and the population of reagent ion clusters. Both of these concepts are described in the following section.
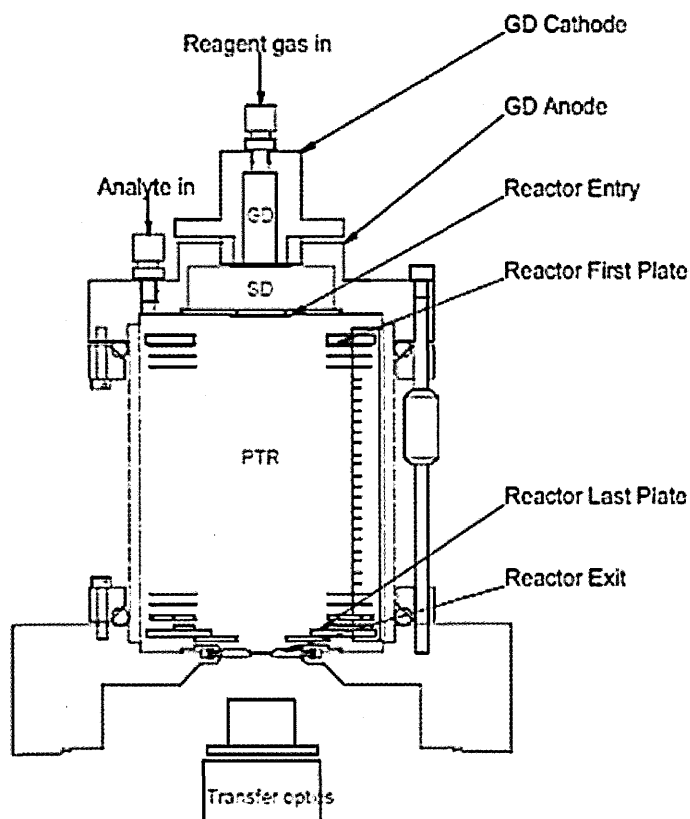
Figure 2.4: Schematic of PTR assembly
GD = Glow discharge or hollow cathode
SD = Source drift region
PTR = Reaction chamber or drift tube (DT)
(Courtesy of Kore Technology Ltd. manual Z-5851-M)

2.2.2.1 Water Clusters and Collisional Energy Conditions

Protonated water clusters, $(H_3O^+).(H_2O)_n$, $n = 0, 1, 2, 3$, can form in the PTR drift tube if the collision energies are sufficiently low. They break up when the clusters have a higher kinetic energy resulting from acceleration in high electric field, E, or a longer mean free path due to a reduced particle density, N, or both. This process is known as collisional induced dissociation (CID). The ratio E/N is used to measure the collisional energy conditions. Figure 2.5a shows spectra taken in laboratory air at two different E/N values, 140 and 200 Td. Figure 2.4b shows the peak at m/z 21, the ^{18}O isotope for H_3O^+ in more detail. The peaks at m/z 19 are not representative of how much H_3O^+ there is in the instrument as this peak has been suppressed (see §2.3.2). Figure 2.5 shows how the

proportions of each of the water clusters, $(H_3O^+).(H_2O)_n$, $n = 0, 1, 2, 3$ is depends on this

E/N which has the SI units V m^2 but is generally given the unit Td, Townsend, where 1 Td

$= 10^{-21}$ V m^2.

Peaks for Water Clusters in Laboratory Air for E/N = 140 and 200 Td

Peaks for m/z 19 and 21 in Laboratory Air for E/N = 140 and 200 Td
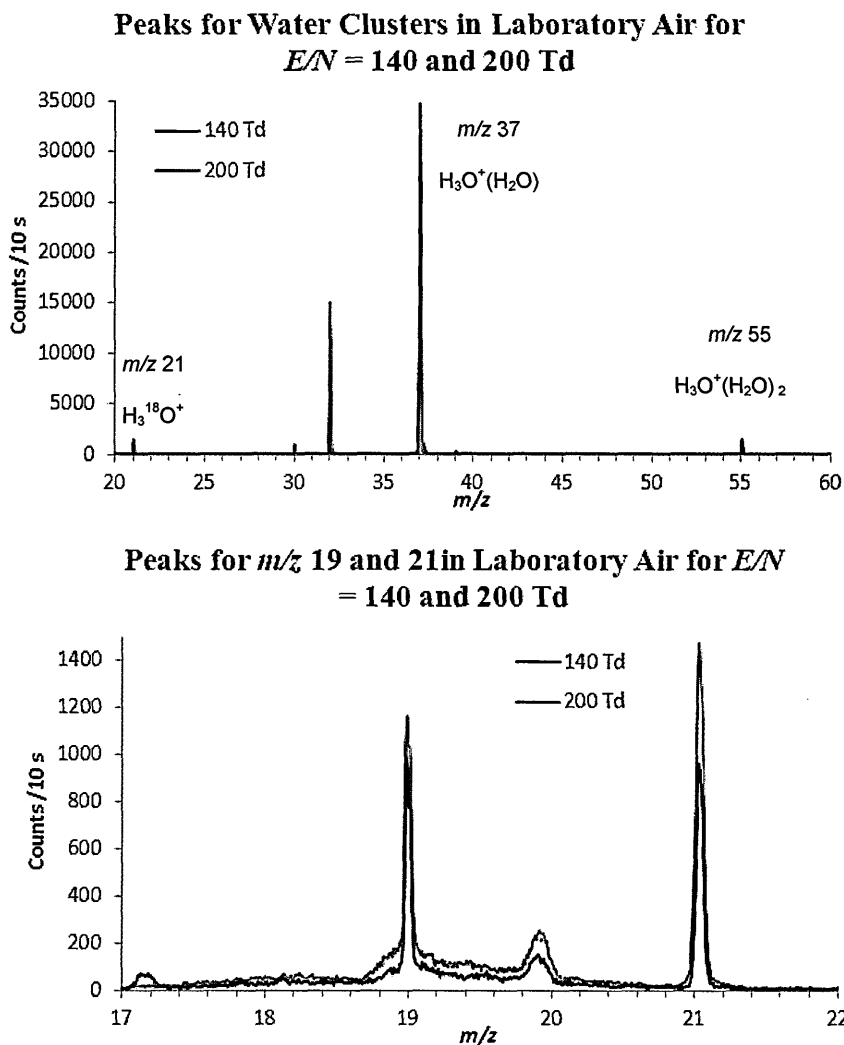
Figure 2.5: Protonated water clusters in the PTR-TOF-MS
a) shows variation in H_3O^+ (m/z 19), $H_3O^+.(H_2O)$ (m/z 37),
$H_3O^+.(H_2O)_2$ (m/z 55) at E/N=140 and 200 Td where E = electric field and N = gas
number density which is temperature and pressure dependent.
b) shows enlarged peaks at m/z 21, protonated ^{18}O isotope of H_3O^+. The peaks at m/z
19 are not representative of how much H_3O^+ there is in the instrument as this peak has
been suppressed.

In the PTR-TOF-MS there is only ~ 30% H_3O^+, m/z 19, at lower E/N values (< 110 Td), the

most abundant ions being $(H_3O^+).(H_2O)$, m/z 37. There is a small but significant amount of

Water Clusters in Laboratory Air PTR-TOF-MS
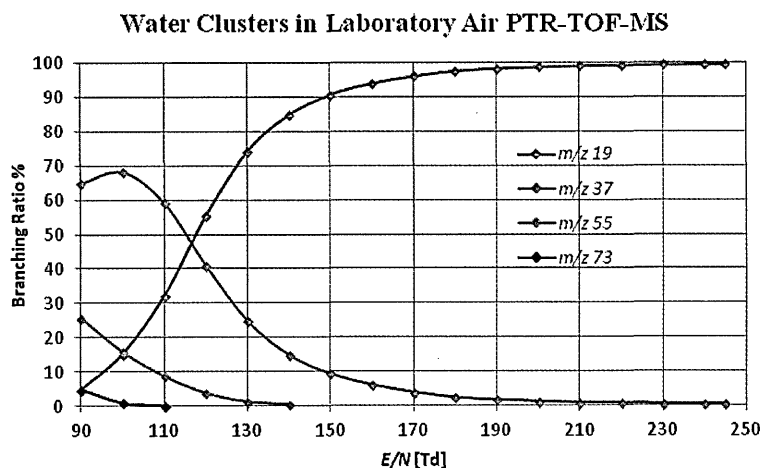
Figure 2.6: Branching ratios for protonated water clusters in the PTR-TOF-MS showing variation in H_3O^+ (m/z 19), $H_3O^+.(H_2O)$ (m/z 37), $H_3O^+.(H_2O)_2$ (m/z 55) and $H_3O^+.(H_2O)_3$ (m/z 73) with changing E/N where E = electric field and N = gas number density which is temperature and pressure dependent.

$(H_3O^+).(H_2O)_2$, m/z 55, and < 5% of $(H_3O^+).(H_2O)_3$, m/z 73, both of which fragment quite

quickly with increasing collisional energy, contributing to the m/z 37 peak. As E/N

increases, m/z 37 reduces and m/z 19 increases.

In general, the analyte, M, reacts with H_3O^+ as follows:

$$H_3O^+ + M \rightarrow MH^+ + H_2O \qquad\qquad [E1]$$

Hence to ensure good sensitivity, it is recommended that optimal operating conditions exist

when the m/z 37 to m/z 19 ratio is 10% to 15% As can be seen in Figure 2.6 this condition

occurs in the PTR-TOF-MS at $E/N \approx$ 145 Td. Figure 2.7 shows the same water-

cluster/energy dependence in the PTR-MS Quad instrument. The graphs show that the drift

tube of this instrument has a much drier environment than that of the Kore instrument, with

its optimal conditions occurring at $E/N \sim$ 115 Td, a much lower amount of m/z 55 and no

m/z 73 at all.
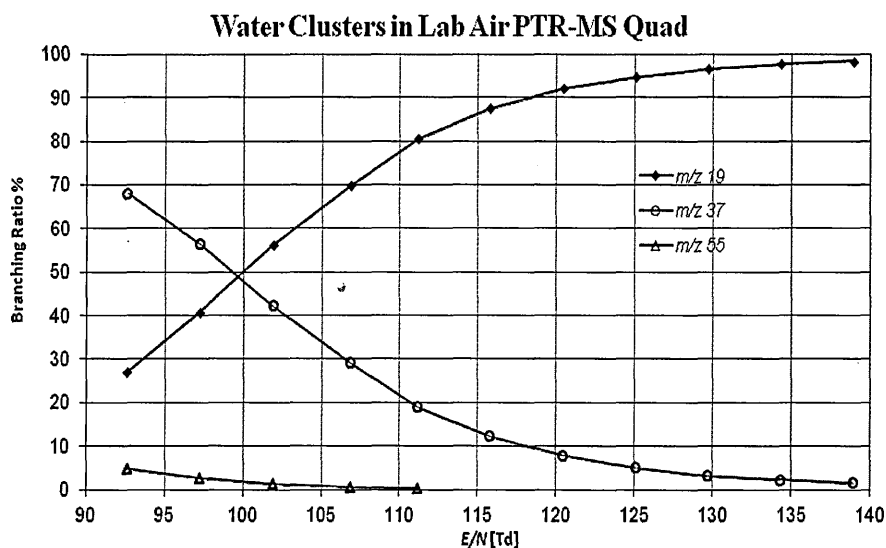
Figure 2.7: Protonated water and protonated water clusters in the PTR-QUAD-MS showing variation in H_3O^+ (m/z 19), $H_3O^+.(H_2O)$ (m/z 37), and $H_3O^+.(H_2O)_2$ (m/z 55) with changing E/N.
(Courtesy of P. Brown, Dept. Mol. Physics, Birmingham University)

The analyte may also react with any water clusters in a ligand-switching reaction shown in equation E2:

$$H_3O^+. H_2O + M \rightarrow H_3O^+.M + H_2O \qquad\qquad [E2]$$
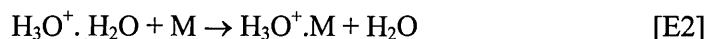
This channel is available when M has a proton affinity $>$ PA (H_2O) and $<$ PA ($H_2O)_2$ and a dipole moment. There are also compounds with proton affinities greater than that of $(H_2O)_2$, (PA = 808 kJ mol^{-1}), which react with both H_3O^+ and $(H_3O^+).(H_2O)$ (de Gouw et al. 2004, Blake et al. 2004) in which case the presence of m/z 37 is not so critical and lower energy conditions can be utilised, e.g. for acetone (PA = 812 kJ mol^{-1}) (Table 2.1). The reaction E1 can proceed as either dissociative or non-dissociative proton transfer. Reactions of the latter type are found to exist when the Gibbs free energy is less than -20.26 kJ/mol to -41.49 kJ/mol (Bouchoux et al. 1996, Bohme et al 1980, House 2008).

There are other conflicting conditions that must also be considered, viz. the amount of O_2^+ and the impact of E/N on the fragmentation of the analyte ions and the reaction time. A higher E/N, i.e. higher collisional energy, not only breaks up protonated water clusters but may also lead to fragmentation of the protonated parent molecules. To limit analyte fragmentation, the PTR-TOF-MS is generally operated at E/N = 140-145 Td. It is also advisable to maintain the ratio of O_2^+ to m/z 19 to $<$ 2% to minimise electron transfer

reactions with the analyte by ensuring a sufficiently high pressure in the glow discharge region. Exceeding these conditions, a higher E/N and more O_2^+, would result in a more complicated mass spectrum.

2.2.2.2 Determining the Electric Field

The magnitude of the electric field, E, is:

$$E = \frac{V}{L}$$

Where V = operating voltage across the drift tube and L = length of the tube.

Figure 2.8 shows the positions of the three electrodes in the PTR drift tube: at the entrance to the drift tube (reactor entry), on plate 26 and at the drift tube exit (reactor exit). The
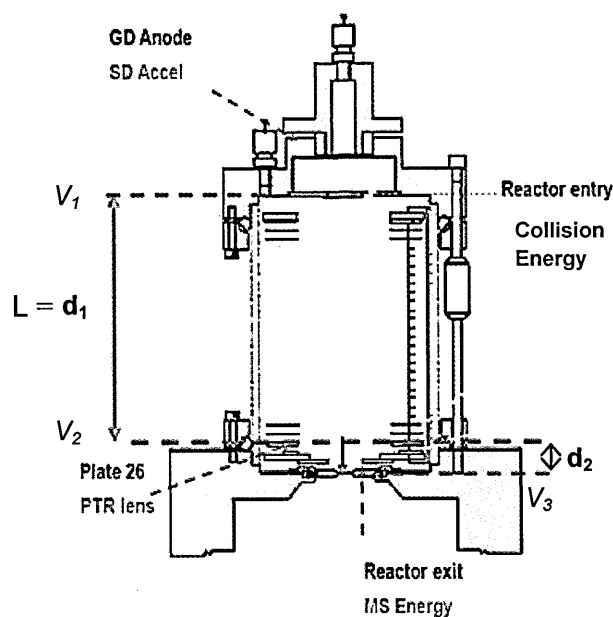
Figure 2.8: Schematic diagram of electrodes in the PTR Drift Tube. (Courtesy of Kore Technology Ltd.)

original reason for having the intermediate electrode at plate 26 was to enable a higher E/N value in this last section of the DT which would break up protonated water clusters. However, this could also lead to the fragmentation of the protonated parent ions. Consequently, it was decided to set these three voltages so that the plate 26 voltage effectively becomes "invisible" to the ions in the DT, i.e. the electric field is constant throughout its length:

$$E = \frac{(V_2 - V_1)}{d_1} = \frac{(V_3 - V_2)}{d_2} = \frac{(V_3 - V_1)}{(d_1 + d_2)} \qquad \text{[E3]}$$

The key voltage that ensures that there is a constant E throughout the drift tube is:

$$V_2 = \frac{d_1 V_3 + d_2 V_1}{(d_1 + d_2)} \qquad \text{[E4]}$$

Where: V_1 = Reactor entry voltage

   V_2 = Plate 26 voltage

   V_3 = Reactor exit voltage

   d_1 = Distance from reactor entry to plate 26 (9.1 cm)

   d_2 = Distance from reactor exit to plate 26 (1.1 cm)

A spread-sheet calculates the voltages to be applied to ensure that V_2 has a value such that the electric field is constant and also calculates a specific E/N value.

Determining Gas Number Density, N

The gas number density, N, is dependent on the temperature and pressure in the drift tube in accordance with:

$$N = \frac{N_A \times T_0 \times P_2}{V_0 \times T_1 \times P_0} \qquad \text{[E5]}$$

Where: N_A = Avogadro's number, (6.022×10^{23} mol^{-1})

   P_2 = Pressure in DT as measured by the pressure meter (millibar, mbar)

   T_1 = DT operating temperature (K)

   T_0 = Standard temperature, 273.15 K

   V_0 = Standard molar volume, 22414 cm^3 mol^{-1} of an ideal gas at STP

   P_0 = Standard atmospheric pressure, 1013.25 mbar

The drift tube is heated by a single heater in the oven casing and the heat is distributed by a fan. A thermocouple on the drift tube itself measures and controls the temperature.

The pressure is measured by a CTR Leybold capacitance manometer gauge, replacing the less accurate Pirani APGX Edwards gauge. There is generally a temperature differential between the DT and the gauge, the DT being at an elevated temperature and the gauge at room temperature (Figure 2.9). The DT maintains a constant pressure as a result of pumping and the introduction of air via the analyte inlet line.

$$P_1 = n_1 k T_1$$

$$P_2 = n_2 k T_2$$
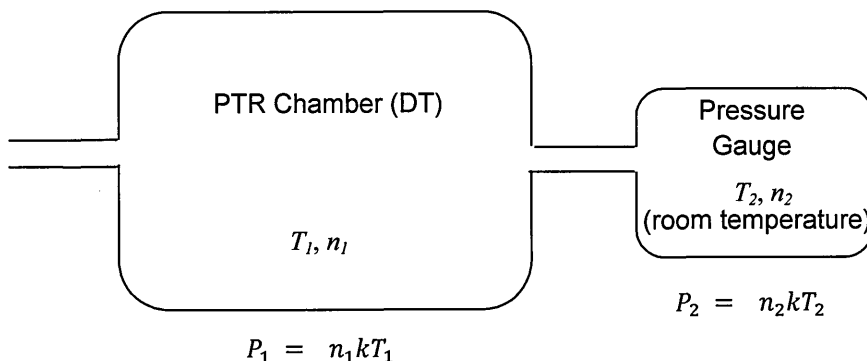
Figure 2.9: Schematic of drift tube and pressure gauge
T = temp. [K]; n = molecule density (no. of molecules m^{-3}); P = pressure [mbar]; k = Boltzmann's constant

In general, the temperature, T_1, used in [E5] is the temperature in the drift tube. However, the system containing the DT and its pressure gauge can be regarded as being a steady state rather than equilibrium environment. This is because energy is being input to maintain the difference in temperature and, therefore, a different number of molecules in each part of this system. From the kinetic theory of gases, the net flux of molecules per unit area of the orifices connecting two chambers is zero (Gombosi, T.E 1994):

$$\frac{1}{4} n_1 \bar{c}_1 - \frac{1}{4} n_2 \bar{c}_2 = 0 \qquad [E6]$$

Where $\bar{c}$ (mean speed) $\propto \sqrt{T}$, T = temperature

$$\therefore n_1 = n_2 \frac{\sqrt{T_2}}{\sqrt{T_1}}$$

$$n_2 = \frac{P_2}{k T_2}$$

$$\therefore n_1 = \frac{P_2}{k} \frac{1}{\sqrt{T_1 T_2}} \qquad [E7]$$

where:

Drift tube variables:

n_1 = number of molecules (m^{-3})

T_1 = temperature (K)

P_1 = pressure (mbar)

Gauge variables:

n_2 = number of molecules (m^{-3})

T_2 = temperature (K)

P_2 = pressure (mbar)

Calculating E/N

The calculation of E/N is now straightforward. Table 2.2 shows a comparison of values for

E/N using $T = \sqrt{T_1 T_2}$ and only the DT temperature, T_1, for the same pressure and voltage

settings. The difference in E/N is ~ 6% with E/N being over-estimated when only the DT

temperature is used in the calculation.

It should be noted that when these temperatures are equal, $T_1 = T_2 = T$, $\sqrt{T_1 T_2} = $ T.

Table 2.2: Comparison of E/N values using T = $\sqrt{T_1 T_2}$ and T = T_1;
DT pressure = 1 mbar, DT temperature (T_1) = 333 K
and room temperature (T_2) = 297 K.

E/N Td	
$T = \sqrt{T_1 T_2}$	$T = T_1$
90	96
95	101
100	106
105	111
110	116
115	122
120	127
125	133
130	138
135	143
140	148
145	153
150	159
155	164
160	170

E/N Collisional Energy Equivalence in eV and Effective Ion Temperature K

The expression for the total kinetic energy of an ion in a drift tube in the laboratory frame

was developed by Wannier (1951) and McFarland (1973) and can be written as:

$$KE_{ion} = \frac{1}{2}mv^2 + \frac{1}{2}Mv^2 + \frac{3}{2}k_bT \qquad \text{[E8]}$$

$$\downarrow \qquad\qquad \downarrow \qquad\qquad \downarrow$$

| Drift energy | Random field energy | Thermal energy |

(Revercomb 1975)

where

m = mass of the ion (kg); M = mass of the buffer gas (kg)

v = drift velocity of the ion (m s^{-1}) T = drift tube temperature (K)

k_b = Boltzmann's constant = $1.3806488 \times 10^{-23}$ m^2 kg s^{-2} K^{-1}

Typically, the thermal energy in PTR-MS instruments is small compared to the total kinetic

energy of the ion, ~ 0.25 eV (Cappellin 2010). However, in terms of energy available for a

reaction, the centre-of-mass kinetic energy must be used which is shown in equation [E9]

(McFarland 1973).

$$KE_{cm} = \frac{3}{2}k_bT + \left(\frac{m_N}{m_N + m_n}\right)\left(KE_{ion} - \frac{3}{2}k_bT\right) \qquad \text{[E9]}$$

where m_N = mass of the neutral molecule.

From this the effective temperature for ion collisions can be determined:

$$T_{eff} = T + \left(\frac{v^2}{3k_b}\right)\left[\frac{m_N(m+M)}{m+m_N}\right] \qquad \text{[E10]}$$

This T_{eff} should be used for calculating reaction rate coefficients. Although rate coefficients

have not been used in this thesis, the above has been included for completeness. However,

collisional energies must be taken into consideration in the fragmentation studies in later

chapters and values for these are provided in Table 2.3.

Table 2.3: Energy [eV)] and effective temperature [T_{eff}] for E/N [Td]

E/N /Td	Energy /eV	T_{eff} /K
90	0.110	854
100	0.136	1054
110	0.165	1275
120	0.196	1518
130	0.230	1781
140	0.267	2066
150	0.307	2372
160	0.349	2699
170	0.394	3046
180	0.441	3415
190	0.492	3805
200	0.545	4216
210	0.601	4649
220	0.659	5102
230	0.721	5576
240	0.785	6072
250	0.852	6588

2.2.3 Transfer Chamber and TOF Source

The analyte ions and fragments leave the DT through a 400 μm diameter aperture and enter the transfer optics chamber (Figures 2.10 and 2.11). The diameter of the drift tube is 7.2 cm. Assuming that the whole of the DT is filled with ions, then only 0.06% of the ions move into the transfer optics chamber. The ion swarm is possibly more centrally concentrated so it may be that not such a large fraction is lost at this stage. The transfer chamber is pumped by a 255 L/s turbo pump which produces a pressure of $\sim 10^{-4}$ mbar representing a reduction of four orders of magnitude compared with the reaction chamber and hence a change from viscous to molecular flow for the ions.

The transfer section holds an extraction electrode and two lensing regions, and determines how much of the ion swarm coming from the reaction chamber is transferred to the TOF-MS.

There are two extreme conditions for this, providing either maximum sensitivity or maximum mass resolution. These conditions are described below.

The ion beam leaving the reaction chamber is attracted into the transfer section by the setting of the control called $T_{extract}$ (Transfer extract) and is focussed by the control called T_{lens}
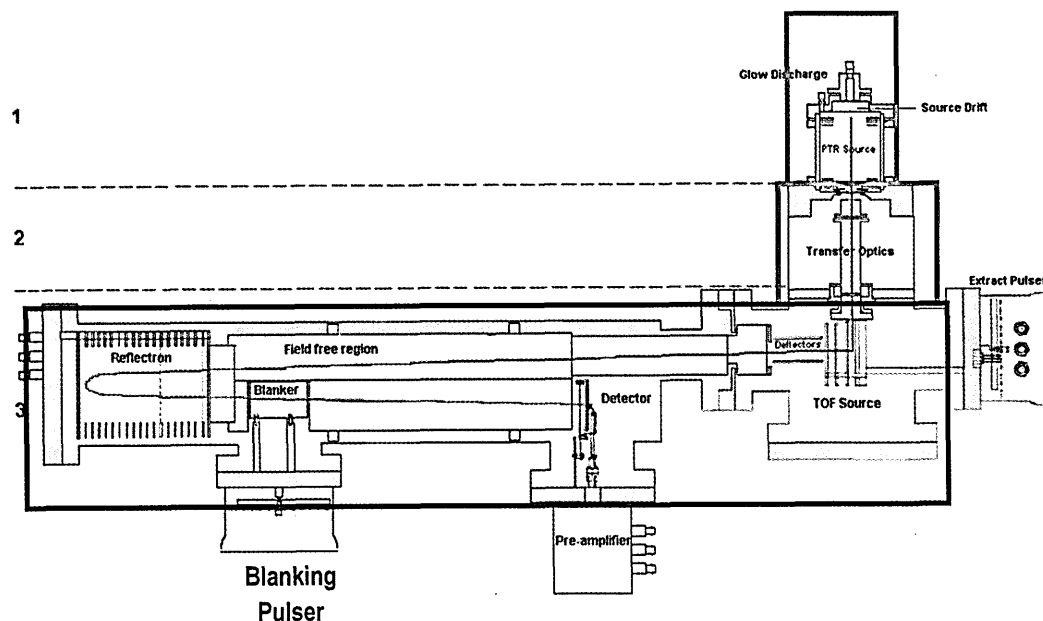
Figure 2.10: PTR-TOF-MS showing the transfer optics and TOF Source regions (Adapted from Kore Technology Ltd. Manual Z-5851-M)
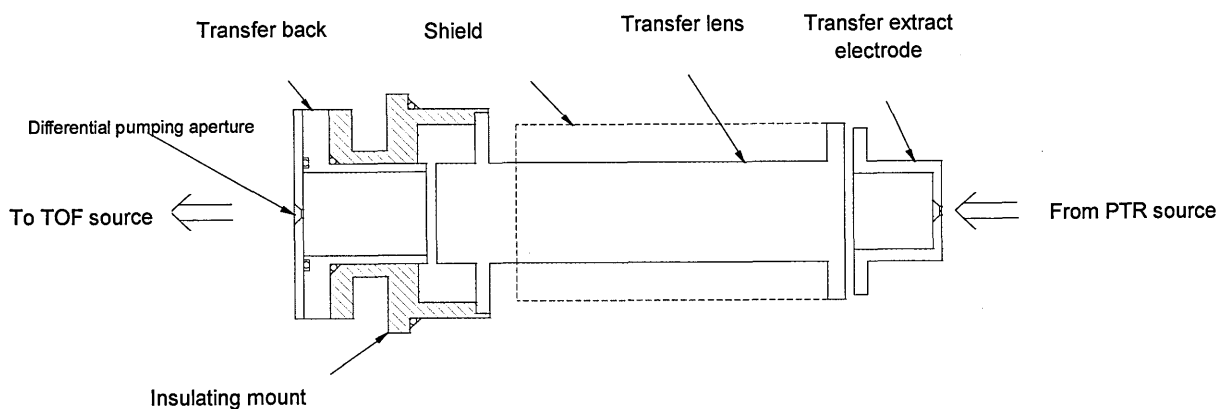
Figure 2.11: Transfer optics chamber (Courtesy of Kore Technology Ltd.. Manual Z-5851-M)

(Transfer lens). The ions then move into the TOF source, where they travel orthogonally to the direction of the detector and are extracted at regular intervals by the TOF source extractor plate: they emerge at a slight angle to the horizontal and are accelerated to the full TOF-MS potential of ~ 2 kV.

In the source the ion beam moves between two charged plates which produce a potential gradient (Figure 2.12). This results in ions at different locations having different energies as
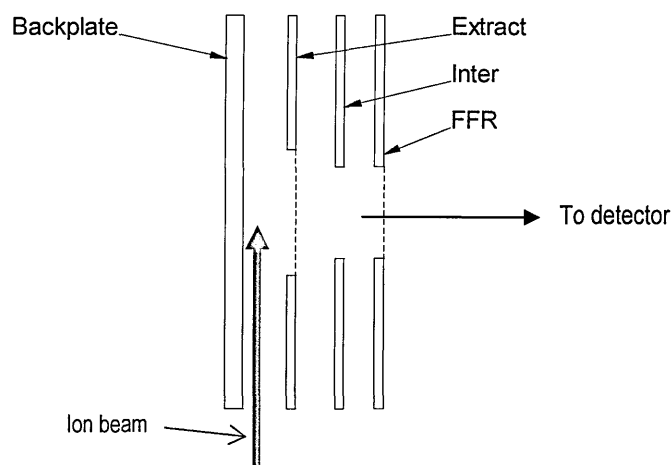
Figure 2.12: TOF source
Extract = Pulsed extraction plate, dashed line = grid
Inter = Intermediate electrode
FFR = Final acceleration electrode
Adapted from Kore Technology manual Z-5851-M

they move into the TOF tube and produces a spread of energies within each *m/z* value, leading to a broadening in the mass peak. The amount of broadening depends on the width of the beam: the narrower the beam, the smaller this is but fewer ions are collected and the sensitivity is reduced.

Alternatively, the beam can be unfocussed to increase the number of ions collected and so increase sensitivity. It is, of course, feasible to create a compromise situation for sensitivity and mass resolution.

2.2.4 Flight Tube and Reflectron

Finally the pulsed ions enter the field-free region of the TOF-MS at a pressure of ~ 10^{-7} mbar, pumped with a 70 L/s turbo pump, where they separate according to their masses They are

focused and reflected in an ion mirror (reflectron) as they move to the detector, a dual micro-channel plate (MCP) type electron multiplier, where their times of arrival are recorded.

The reflectron was developed by Mamyrin (1973) and focuses ions of differing kinetic energy. As the pulse of ions travel down the field free time of flight tube, it spreads into groups of ions with the same mass with an energy spread within each group. This is because the acceleration given to each ion depends on its position at the time of experiencing the impulse into the time of flight tube. So, as each mass group arrives at the reflectron, the more energetic ions travel further into it, so taking a slightly longer path to the detector. The less energetic ions of the same mass travel a shorter distance into the reflectron, taking a shorter path overall to the detector (Figure 2.13).
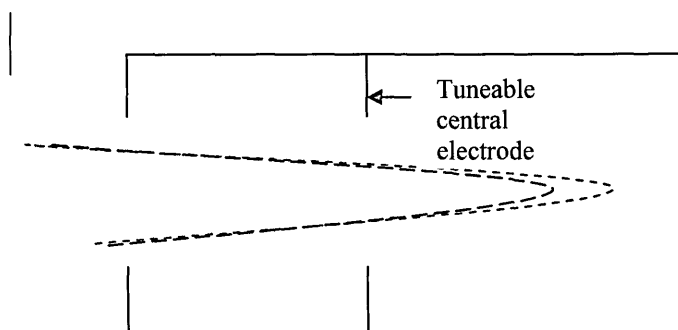
Figure 2.13: Reflectron schematic
Showing the different paths taken by ions of same mass with differing energies through the reflectron (Fast = red; Slow = black)

A clear exposition of the workings of the reflectron is given at Jordan TOF Products (Jordan TOF[2]). The more energetic ions are the most difficult to control and, when included in the measurements, tend to result in a lower resolution with more spreading of the peak. The central electrode of the reflectron can be adjusted so that the most energetic ions hit the back of the reflectron and are lost to the signal, so the reflectron then operates as a low-pass energy filter, resulting in an improvement in resolution.

The time of arrival at the detector of a protonated molecule of mass m is proportional to $\sqrt{m}$

$$E = \frac{1}{2}mv^2$$
[E9]

---

[2] Jordan TOF http://www.rmjordan.com/Resources/Tutorial.pdf (Accessed 12/03/2013)

since every ion is given the same amount of energy, E:

where m = mass and v = velocity

If the length of the field free tube = l and the time to traverse this = t, equation [E9] becomes:

$$E = \frac{1}{2}mv^2 = \frac{m}{2}\frac{l^2}{t^2} \qquad \text{[E10]}$$

Hence: $\qquad t = \frac{lm^{1/2}}{(2E)^{1/2}}$

$$t = Cm^{1/2} \quad \text{where} \quad C = \frac{l}{(2E)^{1/2}} \qquad \text{[E11]}$$

Software then converts the times of arrival at the detector into masses to produce a spectrum of number of counts against m/z.

2.2.5 Operating Conditions

Table 2.4 shows the temperatures, ion counts and ratios for normal operating conditions used in the studies presented in this thesis. Pressures are shown when the PTR-TOF is in use (under load) and when running but inactive (no load).

Table 2.4: Normal operating conditions: temperatures, pressures, voltages, ion counts and ratios.

Parameter	Under Load	No Load
PTR Temperature	333 K	333 K
PTR Pressure	≈ 1.00 mbar	≈ 0.04 mbar
GD Pressure	≈ 1.30 mbar	≈ 0.03 mbar
AIMX pressure (TOF tube)	7.0×10^{-7} mbar	$\approx 6 \times 10^{-9}$ mbar
WRG pressure (Transfer section)	7.0×10^{-5} mbar	$\approx 2.3 \times 10^{-6}$ mbar
Flow rate into PTR	100ml min^{-1}	-
E/N	≈ 144 Td	-
V_{CE}	354 V	-
V_{PTR}	48.9 V	-
V_{MS}	9.7 V	-
Total ion counts at 60°C	$\approx 20,000$ s^{-1}	-
m/z 21 counts at 60°C	$\approx 450 - 560$ s^{-1}	-
Ratio m/z 37: m/z 19	< 5%	-
Ratio m/z 32:(m/z 19+ m/z 37)	< 4%	-

2.3   Optimisation of the Instrument

2.3.1   Modifications

The instrument required several modifications before being fit for purpose.

2.3.1.1   Measuring and Monitoring *E/N*

To determine the electric field, *E*, in the drift tube, it is necessary to measure the voltages at three points in the tube: at the entrance, at Plate 26, part way down the tube and at the exit (see §2.2.2.2 for further details). However, none of the three voltages could be measured on the delivered instrument until a digital voltmeter (DVM) and control unit were added (Figure 2.14).

Pressure gauge

Pressure gauge controller

DVM for electrodes in drift tube

Drift tube electrode switching unit
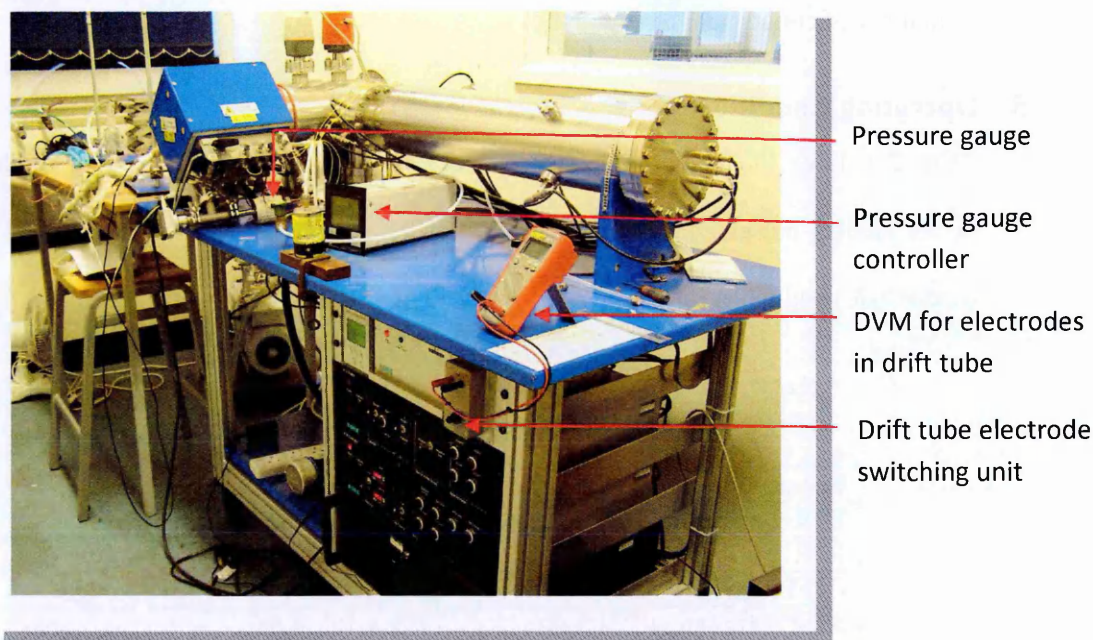
Figure 2.14: Modifications to the PTR-TOF-MS Kore instrument.

In order to calculate and monitor *E/N*, it is necessary to know the pressure and temperature in the drift tube. A reliable thermocouple already existed but a more accurate pressure gauge was added. The method for calculating *E/N* is given in §2.2.2.2. To alter *E/N*, the pressure in the drift tube is held constant, thus keeping *N*, the gas number density constant, and the voltages across the drift tube are varied.

2.3.1.2 Isolating the Water Container

The original isolating tap for the water chamber had been removed by Smiths. Reinstating this enabled venting only of this container, and not the whole instrument, when more water is required (Figure 2.15).
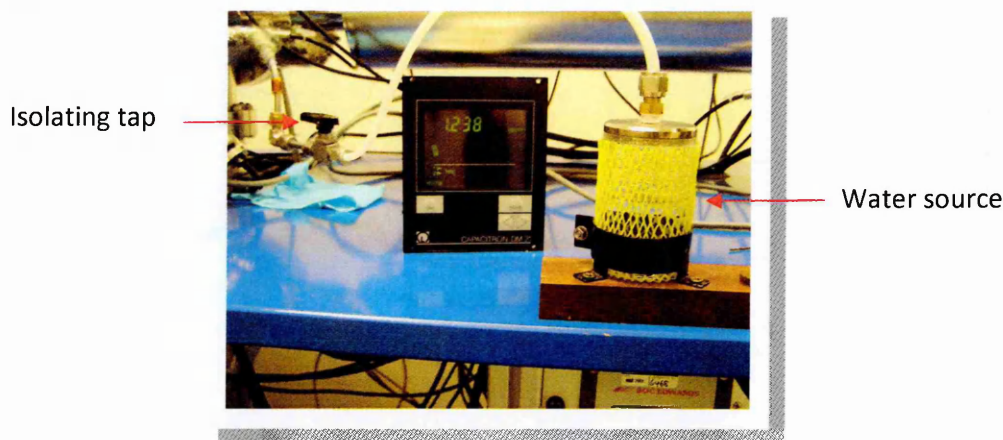
Figure 2.15: Isolating tap for water chamber

2.3.2 Eliminating Reagent Ions at the Detector

After ions have been reflected by the reflectron, there is a component referred to as a blanking pulser (see Figure 2.10) which is designed to prevent H_3O^+ ions (*m/z* 19) reaching and damaging the detector. The blanking pulser consists of two plates, one permanently connected at the field free region potential and the other pulsed such that all ions passing through the plates when the pulse occurs are diverted away from the path of the detector. The time at which this pulse occurs is controlled by a delay potentiometer.

The graph in Figure 2.16 shows the average counts for a collection time of 10 s for *m/z* 19 and *m/z* 21 as the delay setting is varied as measured on the potentiometer (range 1–10). This clearly shows how ions at *m/z* 19 are prevented from reaching the detector as the delay potentiometer moves from 6.0 to 6.4 and that the optimal setting for these ions, i.e. the minimum level detected, is when the delay setting is ~ 6.1 to 6.2. As the delay setting is increased, ions at *m/z* 21 are diverted from the detector, with a minimum number reaching the detector when the blanking pulser is set at a delay of 6.4 to 6.6.

Counts vs Delay Settings
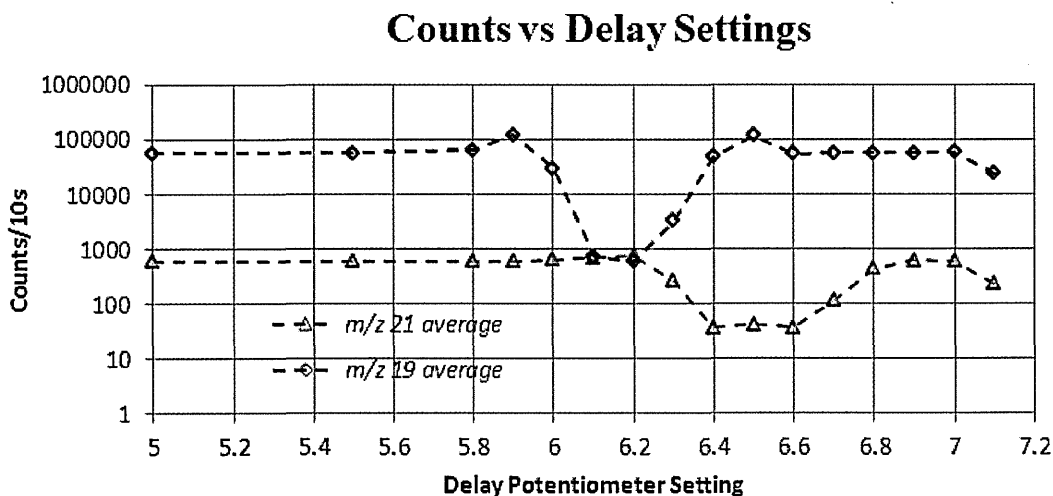
Figure 2.16: H_3O^+ (*m/z* 19) and isotope $H_3^{18}O^+$ (*m/z* 21) signal change on varying the blanking pulser delay potentiometer setting. The points show an average of two sets of data.

The *m/z* 19 results show some unexpected data at delay settings 5.9 and 6.5: the number of counts increase as the delay setting moves from 5.8 to 5.9 and then the number of counts reduce as the delay setting moves from 6.5 to 6.6. When displayed on a linear scale (Figure 2.17), the change in counts seen at these delay settings is ~ 100% and the reason for this is shown in the spectra in Figures 2.18a), b), c) and d): at a delay setting where there is no blanking for *m/z* 19, the detector becomes saturated due to dead-time issues and the peak has the shape shown in Figure 2.17a) at potentiometer delay setting = 5.8, and in Figure 2.17d), potentiometer delay setting 6.6. These spectra show the typical saturated shape of a double peak with many ions missing from the signal. As the delay setting is changed and blanking becomes effective, more of the *m/z* 19 ions can initially be detected, so increasing the number of detected counts. The peak shape assumes its more regular shape (Figure 2.17b) for potentiometer delay setting 5.9 and Figure 2.17c) for potentiometer delay setting 6.5.

These changes for m/z 19 at the cusps of the blanking effects are interesting but unimportant

as the instrument is only operated in the range 6.1 to 6.2, the actual signal being calculated

from the ^{18}O isotope at m/z 21
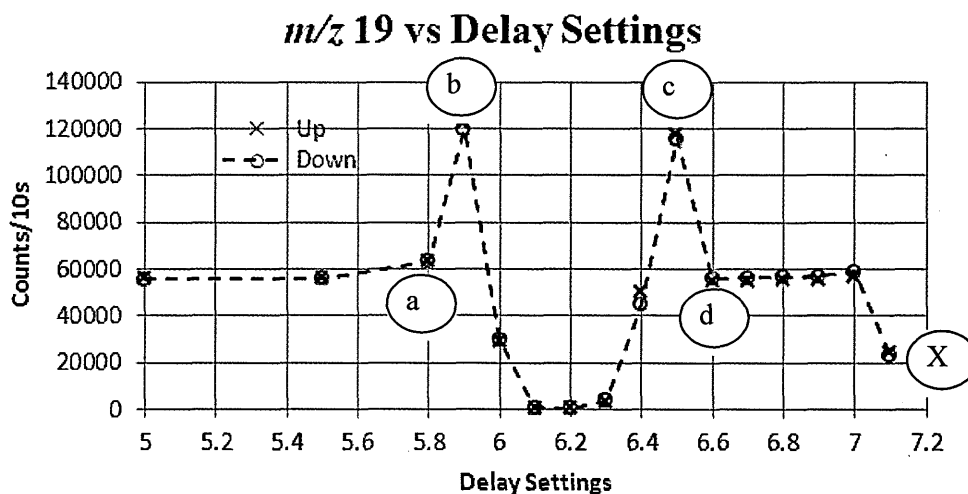
Figure 2.17: m/z 19 signal as the potentiometer called delay varies.
Points a) to d) refer to the spectra in Figure 2.18 below.
Increased (up) and decreased (down) measurements are shown.
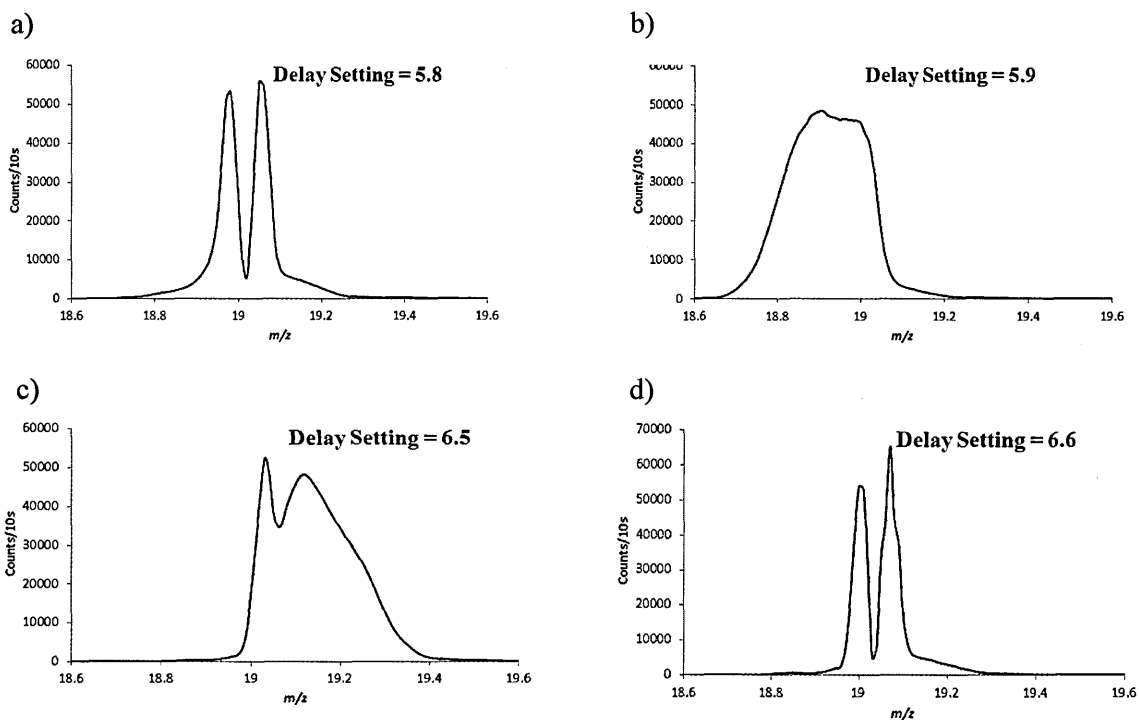
Figure 2.18: m/z 19 peaks at the delay settings 5.8 (a), 5.9 (b), 6.5 (c) and 6.6 (d)
as shown in Figure 2.17.

However, as Figure 2.19 shows, there is a similar, but smaller, increase for m/z 21 between

m/z 21 vs Delay Settings
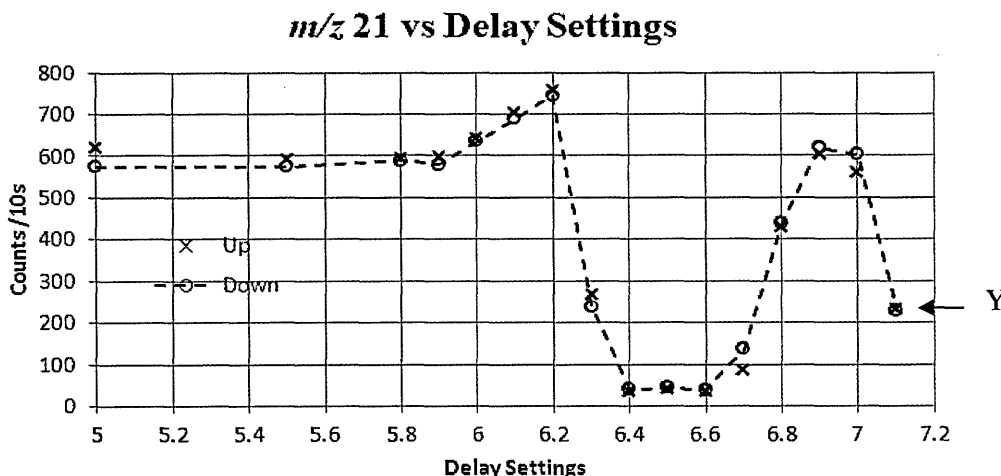
Figure 2.19: m/z 21 signal vs delay setting
Shows an increase in signal from delay setting 5.9 to 6.2.
Results for increased (up) and decreased (down) delays

delay settings 5.9, counts = 589, to 6.2, counts = 751. The graph shows a linear increase in these counts, both when measurements were taken as the delay setting was increased (up) and then decreased (down). This increase cannot be accounted for in the same way as for m/z 19 above, as at no time is the signal at the detector saturated for m/z 21 ions.

Also, since the counts vary according to Poisson statistics, the variation at delay 5.9 for counts 581 (down measurements) is expected to be $\sqrt{581} = \pm 24.1$. The actual variation seen is $\sim$ 54 (635-581 Table 2.5). Consequently, the differences observed here are considered to be real as they fall outside of these statistical fluctuations and, taken over the delay range of 5.9 to 6.2, amounts to a $\sim$ 27% difference.

Table 2.5: m/z 21 counts for potentiometer delay settings 5.9 to 6.2

Delay	Counts up N_{up}	$\sqrt{N_{up}}$	Counts down N_{down}	$\sqrt{N_{down}}$
5.9	597	24.4	581	24.1
6.0	642	25.3	635	25.2
6.1	704	26.5	691	26.3
6.2	756	27.5	746	27.3

This implies that for a delay setting of 6.2, which is optimal for removing H_3O^+ ions from the detector, the corresponding isotope count at m/z 21 would appear to be approximately 27%

higher than that found for a delay setting of ≤ 5.9. It would therefore appear that, as the blanking effect moves the m/z 19 ions away from the detector, the initial effect is to increase the number of m/z 21 ions reaching the detector. This same effect of optimising the m/z 21 signal can be achieved by using the X deflector steering plates which also deflect the ion beam towards the detector. A query to Kore Technology regarding this issue resulted in the advice always to optimise m/z 21 with the X deflectors whenever the delay setting is changed. Points X and Y in Figures 2.17 and 2.19 respectively represent an anomaly in the workings of the PTR-TOF. They have not been further investigated.

Oxygen

A short test using oxygen as the primary ion (O_2^+) showed that blocking of the m/z 32 signal occurs at a delay setting of ~ 6.9 and that the m/z 34 signal was also depleted.

2.4   Experimental Methods

2.4.1   Preventing Dilution of VOCs from Biological Sources

The headspace above a biological sample can sometimes be required not to become diluted by a carrier gas. A method of overcoming this dilution problem is to have a small expandable
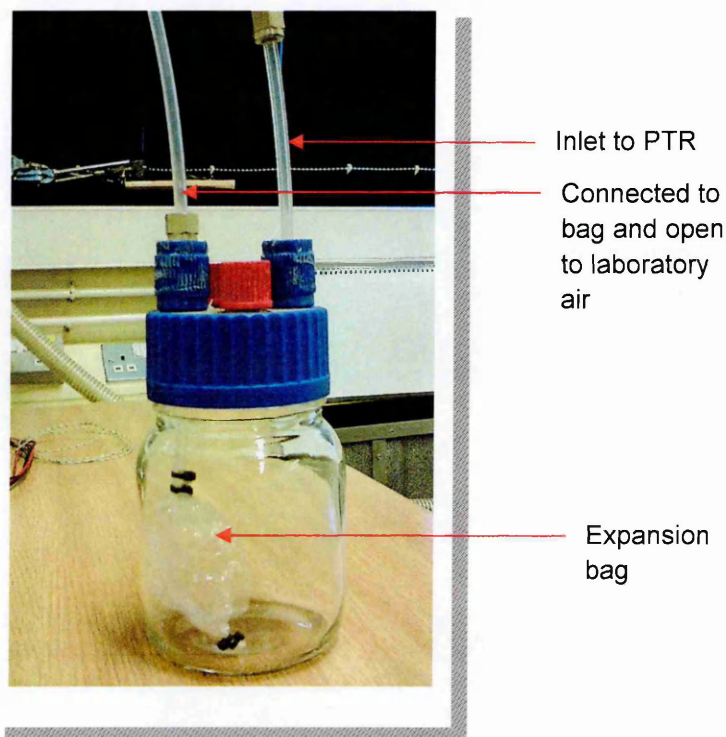
Figure 2.20: Equipment with an expansion Nalophan® bag to prevent sample VOC dilution

'bag' within the sample container which is open to the laboratory air such that it can expand and replace the volume left by the evacuated headspace gases (Figure 2.20). The apparatus here consists of a 500 mL Schott glass bottle with a four-way polytetrafluoroethylene (PTFE [Teflon]) bottle cap and flexible PTFE tubes and fittings. Two of the cap openings (in red) are permanently closed. Inside the bottle is a small Nalophan® bag made from poly-(ethylene terephthalate) film and closed with cable ties, connected to laboratory air through a PTFE tube. The other tube is connected to the PTR. Nalophan® was selected as it is frequently used in SIFT and GC-MS VOC detection, albeit for sample storage rather than for the purpose described here (Turner 2013, Beghi and Guillot 2008). This apparatus was trialled during proof of concept work involving the ageing of pears.

2.4.2   Heated Inlet Line

Some molecules and ions take a long time to reach a constant flow through the instrument and are referred to as being 'sticky'. Such conditions were encountered in the calibration gas (Chapter 3) and in the proof of concept works: detecting indole and when examining the ageing of pears. One way of overcoming this problem is to heat the inlet line into the PTR-MS by wrapping heating tape around the inlet line. Examples are shown in Figures 2.21 and 2.22
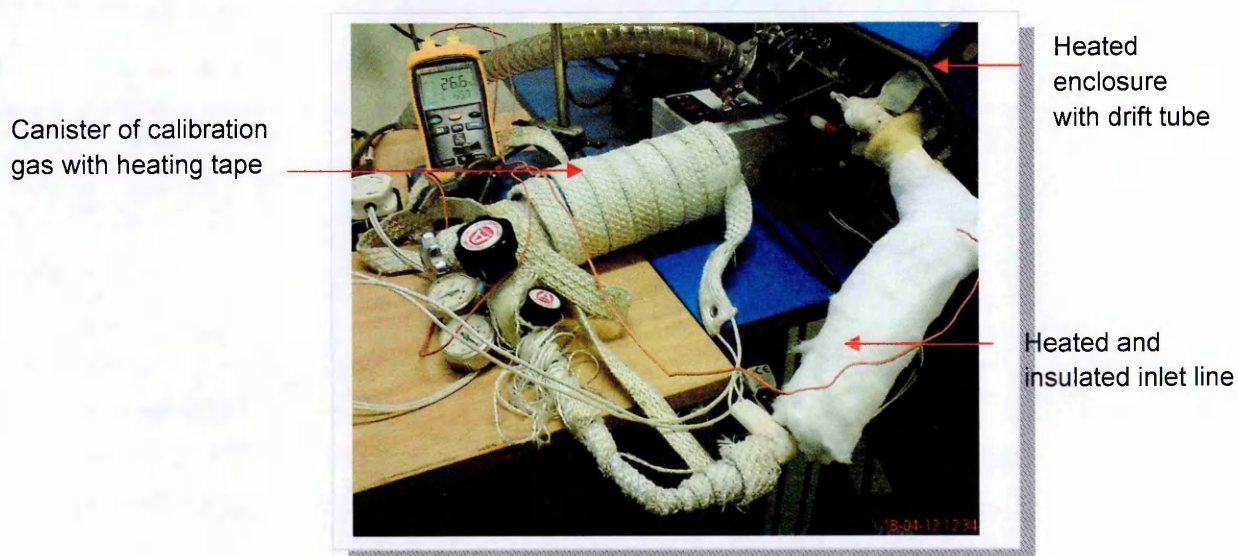
Figure 2.21: Calibration gas canister with heating tapes
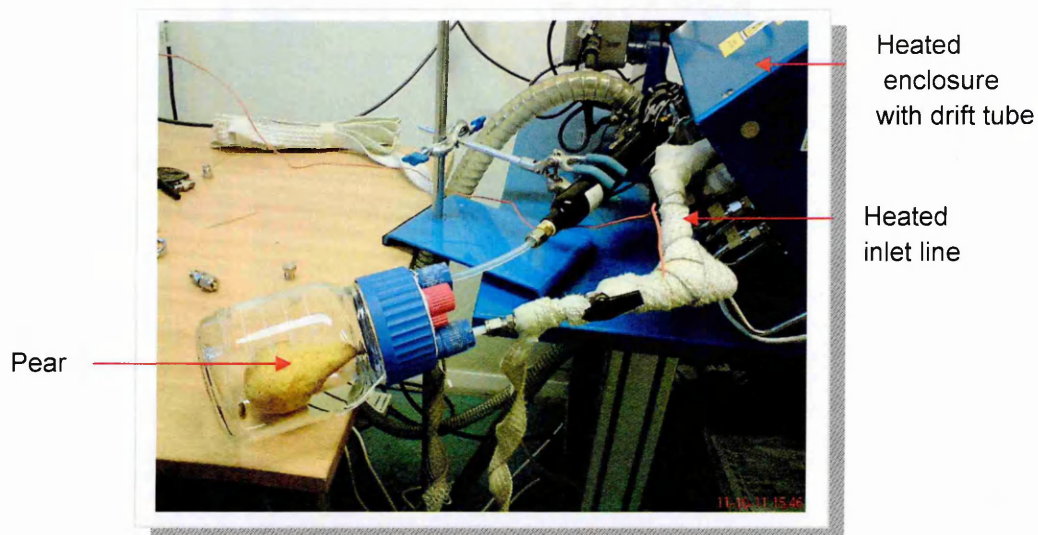
Figure 2.22: Experimental setup with heated inlet line

2.4.3 Methods of Introducing Samples into the PTR-MS

Different apparatus was used depending on the type of sample being investigated e.g. solid indole, liquid hexenols, pears or a bacterial medium. The container for pears is shown in Figure 2.22, a motorised syringe used for the hexenols is shown in Figure 2.23 and the
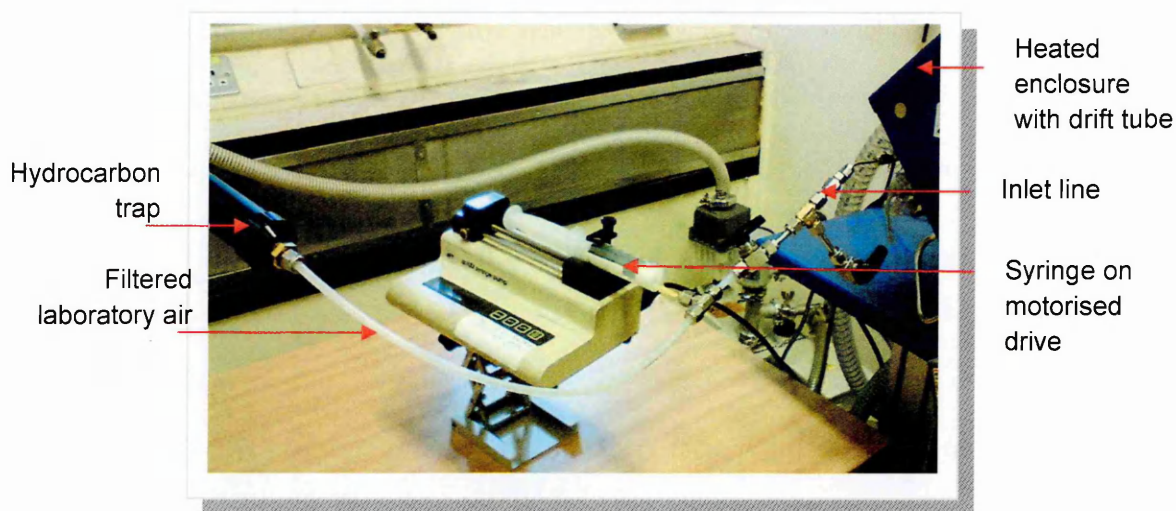
Figure 2.23: Experimental setup with motorized syringe

container used for indole and the alkyl and chloro- benzenes is shown in Figure 2.24.
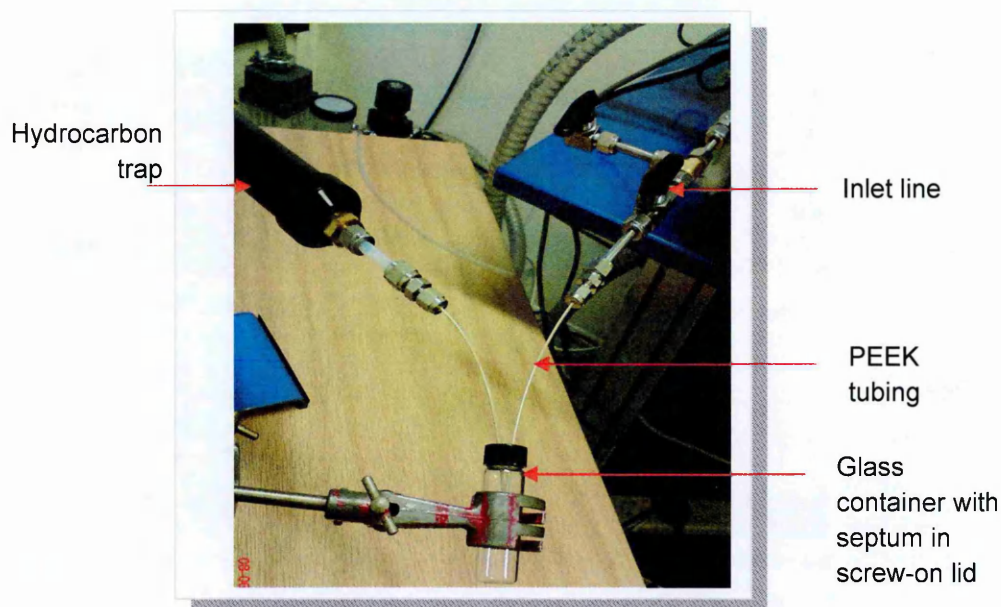
Figure 2.24: Experimental setup with glass container and PEEK tubing syringe

2.5 Data Considerations

2.5.1 Ion Detection, Counting and Errors

The device for detecting ions used in this Kore instrument is a dual micro-channel plate (MCP) type electron multiplying detector (Burle Long-Life™ channel plate). It is also worth noting that secondary electron emission at each dynode is a statistical process, and, at the level of individual ions, the output current from the detector for each incoming ion event follows a Poisson distribution. Hence errors in the number of counts, N, at any m/z is $\pm \sqrt{N}$.

2.5.2 Calculating Counts for Water Clusters $H_3O^+.(H_2O)_n$, $n = 0, 1$

The reagent ions used throughout the investigations presented in this thesis was H_3O^+ and it is important to know its intensity (counts per second). However, this spectral peak is always saturated, or hardly present at all if the delay setting has been used (§2.5.5). It is therefore necessary to calculate the intensity from the $H_3^{18}O^+$ isotope peak at m/z 21, (abundance of the ^{18}O isotope is 0.205(14) %) (NIST) :

$$[H_3O^+] = [H_3^{18}O^+] \times 487$$

Similarly for the first water dimer at m/z 37, $H_3O^+.(H_2O)$ for low E/N values it is necessary to use the ^{18}O isotope at m/z 39:

$$[37] = \frac{[39] \times 487}{2}$$

where:

The division by 2 is a consequence of there being two oxygen atoms in this cluster.

[37] = Number of counts at m/z 37

[39] = Number of counts at m/z 39

2.5.3 Fragments at m/z 39

Product ion fragments frequently occur at m/z 39 e.g. Chapter 3. This is the same peak at which the ^{18}O isotope (abundance 0.205%) of the first water dimer, $H_3O^+.(H_2O)$ (m/z 37), appears. The method used to estimate these counts is to calculate the ^{18}O isotope counts expected from m/z 37 and subtract this from the actual counts at m/z 39:

$$[Counts]_{prod} = [Counts]_{39} - \frac{[Counts]_{37} * 2}{487}$$

m/z 39 product ion counts	m/z 39 total counts	m/z 39 ^{18}O isotope counts

Dead-time issues prevent the detector from registering all of the ions at this m/z. Consequently, this method is only reliable for E/N values > 140 Td as the m/z 37 signal is saturated at values lower than this.

2.5.4 Normalising Ion Counts

Different investigations often require different ways of handling data. For example, calculation of branching ratios uses values for one m/z as a percentage of the total counts for of all the m/z values being considered. In this case, the raw counts can be used. If, however, a comparison of raw counts is required, then these counts must be normalised generally to 10^6 counts at m/z 19 as the analyte signal is dependent on this signal:

$$[M_N^+] = \frac{[M^+] \times 10^6}{[H_3O^+]}$$

where:

$$[M_N^+] = \text{Number of normalised counts for an } m/z$$
$$[M^+] = \text{Number of un-normalised counts for the } m/z$$
$$[H_3O^+] = \text{Number of counts at } m/z \text{ 19}$$

The denominator can change, depending on the proton affinity of the compound – if the PA is close to that of the first water dimer, $(H_2O)_2$, PA = 808 kJ mol^{-1}, then the sum of the counts at m/z 19 and m/z 37 is used.

2.5.5 Reproducibility of Data

A convenient method of checking for the reproducibility of data is to take measurements as E/N is increased and then decreased. These two sets of readings are referred as 'up' and 'down' in the text. It was not always possible or necessary to take reading in this way e.g. for pears, readings were taken for one E/N value only. Where possible, three readings at each E/N value were taken as a means of eliminating possible rogue values. An average of these readings was used.

2.6 Summary

This chapter provides a description of the hardware, some operating characteristics and enhancements to the Kore PTR-TOF-MS instrument. There were several faults to correct before being able to use it, not least of which was the ability to detect voltages in the reaction chamber in order to calculate the energy conditions therein. This having been done, the following chapters describe the areas of investigation undertaken to prove that satisfactory results could be achieved when compared with other such instruments.

Chapter 3 – Characterising the PTR-TOF-MS

3.1 Background

As mentioned in Chapter 1, there are only a small number of Kore PTR-TOF-MS instruments in use and there are no detailed accounts for the determination of such instruments' sensitivity - the total number of a protonated parent ions and fragments resulting from ion-molecule and collision-induced dissociation (CID) reactions per integration time per parts per billion by volume (ppbv), normalised to 10^6 reagent ions. In view of this, a detailed study of the sensitivity of this PTR-TOF-MS was made using a standard calibration gas (Restek, Scott/Air Liquide TO-14A Aromatics Mix) chosen for its wide range of VOCs and molecular weights. The constituents of this calibration gas are detailed in

Table 3.1: Details of the gas used to calibrate the sensitivity of the Kore PTR-TOF-MS.

Compound	Molecular Formula	Protonated[a] Mass [amu]	Proton Affinity (PA) kJ mol^{-1}	ppbV[b]
Benzene	C_6H_6	79.05	750.4[d]	110
Toluene	C_7H_8	93.07	784.0[d]	110
Styrene	C_8H_8	105.07	839.5[c]	96
m-Xylene (1,3-Dimethylbenzene)	C_8H_{10}	107.09	812.1[c]	110
o-Xylene (1,2-Dimethylbenzene)	C_8H_{10}	107.09	796.00[c]	110
p-Xylene (1,4-Dimethylbenzene)	C_8H_{10}	107.09	794.40[d]	110
Ethylbenzene	C_8H_{10}	107.09	788.00[c]	110
Chlorobenzene	C_6H_5Cl	113.02	753.1[c]	110
1,2,4-Trimethylbenzene	C_9H_{12}	121.10	826.36[f]	100
1,3,5-Trimethylbenzene	C_9H_{12}	121.10	836.2[c]	100
1,2-Dichlorobenzene	$C_6H_4Cl_2$	146.98	711.3[d]	99
1,3-Dichlorobenzene	$C_6H_4Cl_2$	146.98	730.96[e]	99
1,4-Dichlorobenzene	$C_6H_4Cl_2$	146.98	701.67[e]	100
1,2,4-Trichlorobenzene	$C_6H_3Cl_3$	180.94	NA	100

[a]For the atomic masses the major isotopes of carbon and chlorine were used, i.e. ^{12}C and ^{35}Cl (actual to 2 decimal places 34.97).
[b]ppbV supplied by manufacturers accurate to ±10%
Sources for PA:
[c] = http:// http://webbook.nist.gov/chemistry/pa-ser.html (Accessed 03/05/2012);
[d] = Hunter and Lias (1998);[e] = Borisov and Garrett (1998);
[f] = Stone, Li and Turner (1986)

Table 3.1.

It is normally assumed that proton transfer reactions are non-dissociative with fewer species being produced than those for electron impact spectrometry. However, other investigations (e.g. Sulzer, 2012; Demarcke, 2009; Shen, 2012) and this present one show that this is not always the case: higher energy conditions in the reaction chamber can result in ions undergoing not just dissociation as a result of

excess energy after protonation, but also collision-induced dissociation. These mechanisms impact on a

sensitivity investigation such as this, where a wide range of energy conditions are to be used: it is

therefore essential to know how the individual species behave over the energy range in order to be able

correctly to assign mass peaks to their correct VOC.

An example of fragmentation as a function of E/N is shown in Figure 3.1 which shows the % branching

ratios (often referred to as product ion distribution PID) of species from protonated ethylbenzene. A

significant product ion occurs at m/z 79 which, in a mixture of VOCs, could be taken to be protonated

benzene, (also m/z 79) for E/N values as low as 120 Td. This would result in an overestimation of the

Ethylbenzene (Protonated Ion m/z 107)
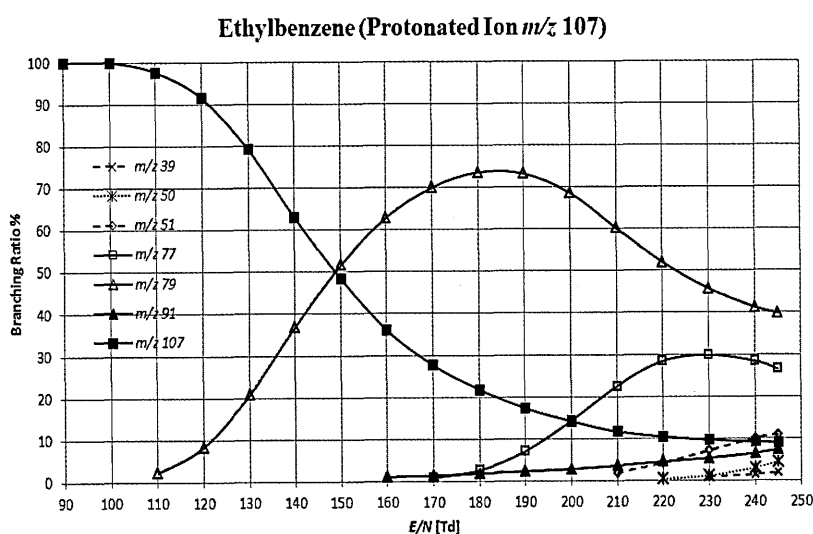
Figure 3.1: Fragmentation behaviour with changes in E/N of ethylbenzene:
the largest fragment is m/z 79 starting to appear at E/N = 110 Td.
'm/z' is unitless with m = molecular or atomic mass and z = number of
charges carried by the ion. For the PTR-MS, z =1.

benzene concentration in a complex chemical environment such as the atmosphere where other VOCs

also fragment to an ion with m/z 79. Consequently, to ensure an accurate signal for each of the

calibration gas compounds, the fragmentation and product ion distribution of the 14 compounds were

investigated as a function of E/N before studying this calibration gas.

These compounds separate into two groups: aromatic hydrocarbons (alkylbenzenes) Figure 3.2 and

chlorobenzenes Figure 3.3.

Benzene C_6H_6
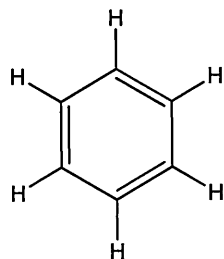
Styrene
$C_6H_5CH_2CH$
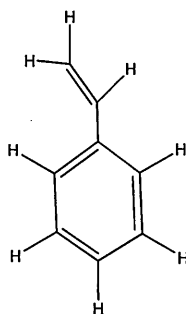
Ethylbenzene
$C_6H_5CH_3CH_2$
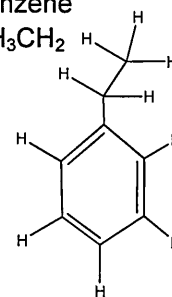
Toluene
Methylbenzene
$C_6H_5CH_3$
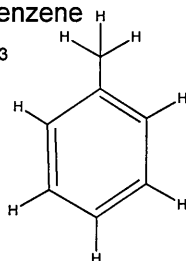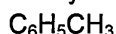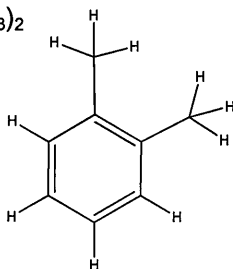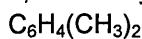
o-Xylene
1,2-Dimethylbenzene
$C_6H_4(CH_3)_2$

m-Xylene
1,3-Dimethylbenzene
$C_6H_4(CH_3)_2$
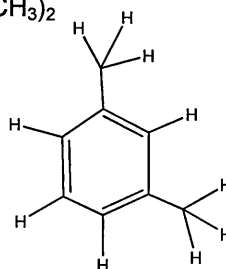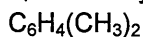
p-Xylene
1,4-Dimethylbenzene
$C_6H_4(CH_3)_2$
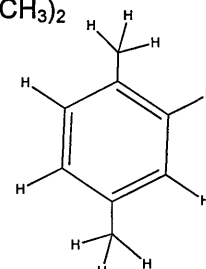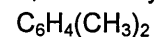
1,2,4-Trimethylbenzene
$C_6H_3(CH_3)_3$
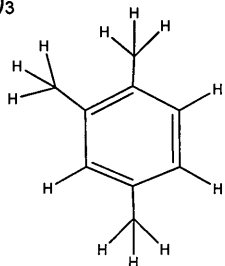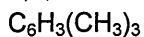
1,3,5-Trimethylbenzene
Mesitylene
$C_6H_3(CH_3)_3$
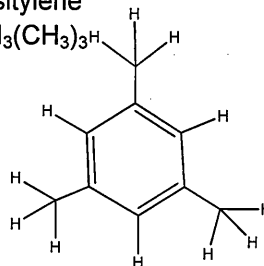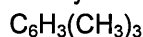
Figure 3.2: Molecular structures for the alkylbenzenes:
benzene, toluene, styrene, ethylbenzene, xylenes and trimethylbenzenes

All of the alkylbenzene components of this calibration gas are found in the atmosphere of industrial

environments (Table 3.2). These are the so-called BTEX chemicals (benzene, toluene, ethylbenzene,

trimethylbenzenes and xylenes) which are mainly attributable to traffic and the burning of fossil fuels

(Buczynska 2009, Lin 2011, EUGRIS): 1,3,5-trimethylbenzene has been shown to be the most active

Table 3.2: Compounds and *fragments identified by PTR-MS in ambient air (Blake 2009 adapted from de Gouw and Warneke 2007)

m/z	Compound
28	HCN
31	HCHO
33	Methanol
42	Acetonitrile
45	Acetaldehyde
47	Formic acid
54	Acrylonitrile
57	Butenes, methyl *tert*-butyl ether, butanol
59	Acetone
61	Acetic acid
63	Dimethylsulfide
69	Isoprene, furan
71	Methyl vinyl ketone, methacrolein
73	Methyl ethyl ketone
75	Hydroxy acetone
77	Peroxy acetyl nitrate (PAN)*
79	Benzene
81	Monoterpenes, hexenal
83	Hexenol, hexanal*, hexenylacetate methylfuran, isoprene hydroxyl carbonyls
85	Ethyl vinyl ketone
87	2-methyl-3-buten-2-ol c_5 carbonyls, methacrylic acid
91	peroxypropionyl nitrate (PPN)
93	Toluene
95	2-vinylfuran phenol
99*	Hexanal
101	Isoprene hydroperoxides
103	peroxymethacrylic nitric anhydride (MPAN)
105	Styrene, peroxyisobutyric nitric anhydride (PiBN)
107	C_8 aromatics
115	Heptanal*
121	C_9 aromatics
129	Octanal naphthalene
135	C_{10} aromatics
137	Monoterpenes
139	Nopinone
143	Nonanal
149	C_{11} aromatics methylchavicol
151	Pinonaldehyde
163	C_{12} aromatics

pollutant in the production of ozone in the atmosphere (Derwent 2000). Benzene, toluene, styrene and

xylene are used in the manufacturing of new materials and consequently are also commonly found in indoor environments (Lee 2005).

The following chlorobenzene compounds were investigated here:

- Chlorobenzene, C_6H_5Cl, (Figure 3.3a,) has one hydrogen atom replaced in benzene by a chlorine atom and has a molecular weight (m.w.) of 112.01 amu, with a protonated m.w. of 113.02 amu

- Dichlorobenzene, $C_6H_4Cl_2$, (Figure 3.3b), has two chlorine atoms which replace two of the hydrogen atoms on the benzene ring. There are three isomers, o-, m-, and p-dichlorobenzene, each denoting a different arrangement of the Cl atoms: 'o' denotes Cl atoms in positions 1 and 2; 'm' denotes Cl atoms in position 1 and 3 (Fig 3.3bi) and 'p' denotes Cl atoms in positions 1 and 4 (Fig 3.3bii).

- Trichlorobenzene, $C_6H_3Cl_3$, (Figure 3.3c), has three chlorine atoms which replace three of the hydrogen atoms on the carbon ring in benzene. The one used here is 1,2,4-trichlorobenzene.
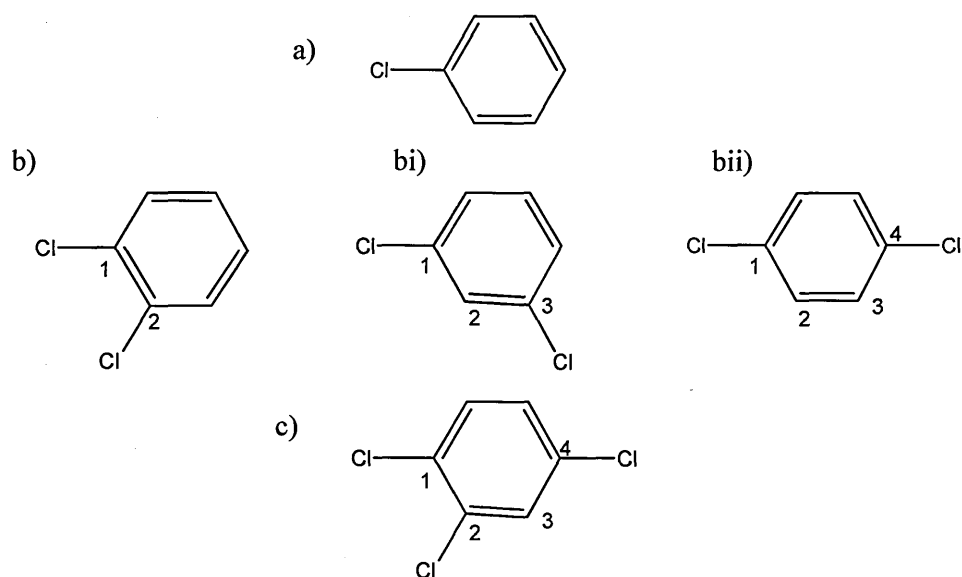
Figure 3.3: Molecular structures for the chlorinated compounds:
a) chlorobenzene,
b) 1,2-dichlorobenzene (o-DCB); bi) 1,3-dichlorobenzene (m-DCB); bii) 1,4-dichlorobenzene (p-DCB);
c) 1,2,4-trichlorobenzene

All sources of chlorobenzenes in the environment are man-made, being used, for example, as pesticide carriers, in air fresheners, and in the synthesis of other organic chemicals (Malcolm 2004). It follows, therefore, that investigation of these individual compounds is likely to be of interest to the environmental science community.

This work extends the comprehensive measurements of VOCs in the atmosphere taken by de Gouw and Warneke, 2007, where a quadrupole PTR-MS was used.

3.2 Experimental Procedures

The experimental work for the sensitivity measurements is divided into two sections: study of the individual chemicals comprising the calibration and then an investigation of the calibration gas itself. Initially, the individual chemicals were studied for the reasons mentioned above, i.e. to determine each one's fragmentation behaviour and product ion distribution over a wide E/N range so that a more accurate measure could be made when the mixture of VOCs was subsequently examined in the calibration gas.

All the chemicals for this investigation were purchased from Sigma Aldrich with purities shown in Table 3.3.

Two filters were attached to the inlet tube through which buffer air was drawn from the laboratory: a hydrocarbon (HC) filter (Supelpure HC, Supelco, Bellefonte, PA.) to reduce environmental influences and a

Table 3.3: Purities for compounds in calibration gas

Compound	Purity
Benzene	$> 99.9\%$
Toluene	$\geq 99.5\%$
Styrene	$\geq 99\%$
m-Xylene (1,3-Dimethylbenzene)	99+%
o-Xylene (1,2-Dimethylbenzene)	97%
p-Xylene (1,4-Dimethylbenzene)	99+%
Ethylbenzene	$\geq 99.5\%$
Chlorobenzene	99.8%
1,2,4-Trimethylbenzene	98.7%
1,3,5-Trimethylbenzene	99.3%
1,2-Dichlorobenzene	99.9%
1,3-Dichlorobenzene	99.4%
1,4-Dichlorobenzene	$\geq 99\%$
1,2,4-Trichlorobenzene	$\geq 99\%$

moisture filter (Big Moisture Trap, Supelco) to reduce moisture from the incoming airflow. The range of voltages that can be applied to the drift tube (DT) enables an E/N range of 90 Td to 250 Td (Table 3.4). E/N was altered by varying the potentials at the entry to the drift tube (Collision Energy) and on the intermediate terminal (PTR Lens).

Conditions in the DT were pressure = 0.81 mbar and temperature = 333 K.

Table 3.4: Drift tube voltages for E/N range used for
individual compound investigation

E/N /Td	Drift Tube Voltage /V
90	180
100	200
110	218
120	237
130	256
140	275
150	294
160	313
170	332
180	351
190	370
200	388
210	408
220	427
230	445
240	464
245	474
250	483

3.2.1 Individual Compounds

Two spectra were acquired for E/N = 90 Td to 240 Td in steps of 10 Td. A final reading was taken at 245 Td because the 250 Td reading was not always reliable: the hollow cathode worked only intermittently.

E/N was increased (up) and then decreased (down), to ensure reproducibility. The same method for introducing the sample into the PTR-TOF-MS was used for each liquid phase compound. Only one, 1,4-dichlorobenzene, was a solid. The vapour pressures of these volatile aromatic compounds are very high and the major issue was to ensure that the reagent ion signal was not significantly reduced by the introduction of the sample which led to the signal being monitored before taking measurements. To achieve this, for the liquid compounds a 1 mL syringe was used to transfer one drop of liquid into a small glass vessel which was then filled with cotton wool to help reduce the flow of analyte into the instrument.

§3.3 describes the alkylbenzenes and §3.4 the chlorobenzenes. The following data are presented for each compound:

- A mass spectrum comparing two E/N values, 140 Td and 245 Td showing non-normalised counts. Mass spectra are taken from one series of data, generally as E/N was increased.

- % Branching ratios (BR %)

  This describes compound fragmentation as E/N is varied: the signals for the protonated parent ion and each product ion are shown as percentages of the sum of all products. Product ions with low percentages are expanded in a second BR. The branching ratios are an average of data taken as E/N was increased and then decreased.

3.2.2 Calibration Gas

The E/N range was 100 Td to 240 Td using steps of 20 Td. The calibration gas container was heated to 60°C, DT temperature was 60°C and the inlet line was heated to 70°C. The gas was studied using two different techniques:

- Varying E/N with the drift tube pressure held constant at 0.8 mbar.

  Three sets of data were taken, i) an 'up' run (E/N = 100 Td to 240 Td); ii) a 'down' run (E/N = 240 Td to 100 Td); iii) a second 'up' run. The first two sets were taken consecutively; the third set was started 4020 s after the 'down' run. Although the system had been allowed to equilibriate before starting to take measurements, the first two sets of data showed particularly low signals for trichlorobenzene at m/z 181, a seemingly very 'sticky' molecule which took a long time to detect in the instrument. Both of these sets of readings were subsequently discarded.

- Varying the pressure at constant E/N = 140 Td.

  Two sets of data were taken, the first varying the drift tube pressure from 0.8 mbar to 1.32 mbar, and the second reducing the drift tube pressure back to 0.8 mbar to ensure reproducibility of the data. E/N was held at 140 Td for both of these sets of measurements.

3.3   Alkylbenzenes

Results for the alkylbenzene compounds are given in §3.3.1 and a discussion of the data can be

found in §3.3.2.

3.3.1   Results

Spectra and branching ratios are show for fragments and protonated parent ions for each compound.

3.3.1.1   Benzene C₆H₆

Benzene was investigated over the *E/N* range 90 Td to 248 Td and mass spectra at two of

these values, 140 Td and 245 Td, are shown in Figure 3.4. The protonated parent peak at
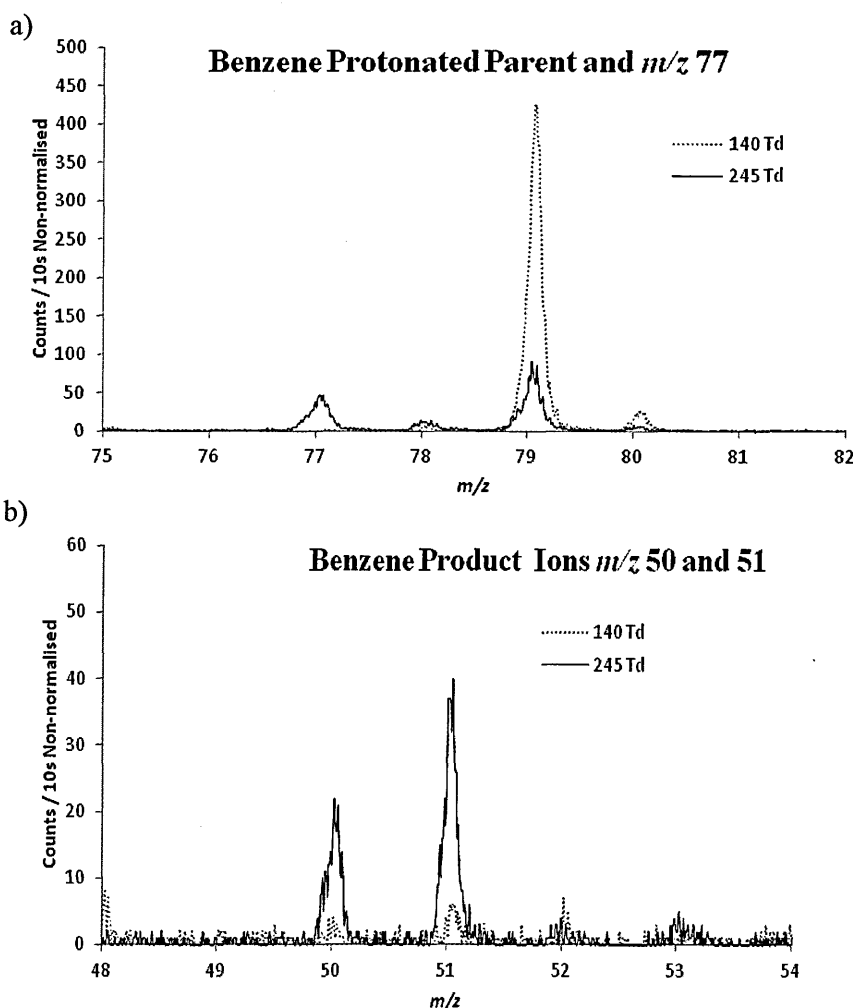
Figure 3.4: Mass spectra for benzene at E/N = 140 Td and 245 Td
a) peaks for protonated benzene at m/z 79 and b) fragments at m/z
50 and 51.

m/z 79 is the major signal at both of these energies. The product ion distribution or

branching ratios describe the fragmentation of benzene over the full E/N range (Figure 3.5).

This shows that the protonated benzene ion $C_6H_7^+$, m/z 79, starts to fragment at $E/N > 180$

Td, losing H_2 to form the fragment at m/z 77, $C_6H_4^+$. As the energy increases, fragmentation

continues with m/z 79 decreasing and m/z 77 increasing. At ~ 200 Td, product ions at m/z

39, 50 and 51 appear, $C_3H_3^+$, $C_4H_2^+$ and $C_4H_3^+$ respectively.

a)
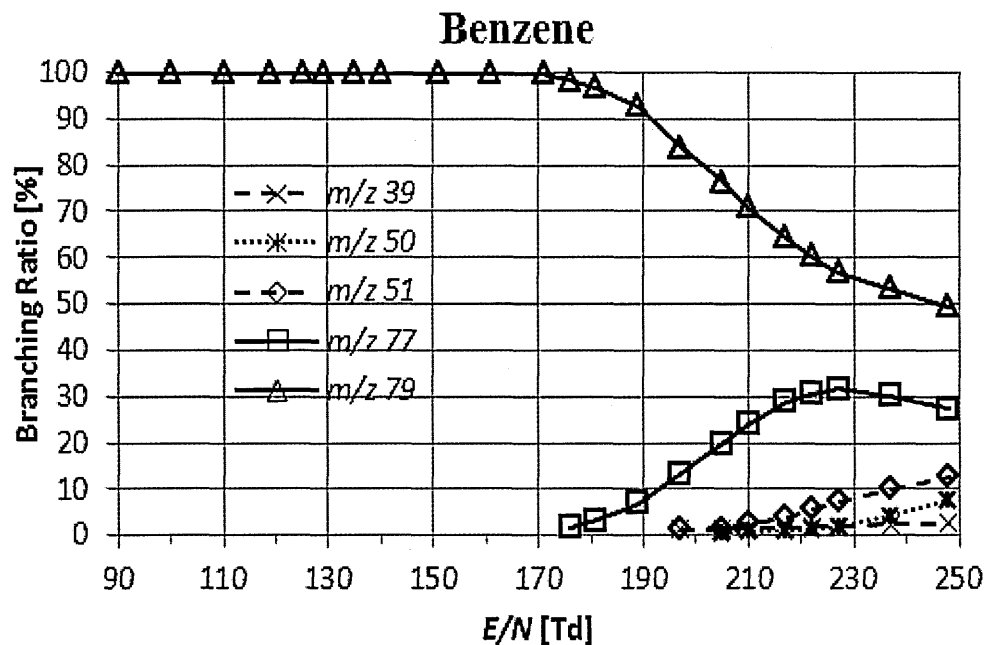
b)
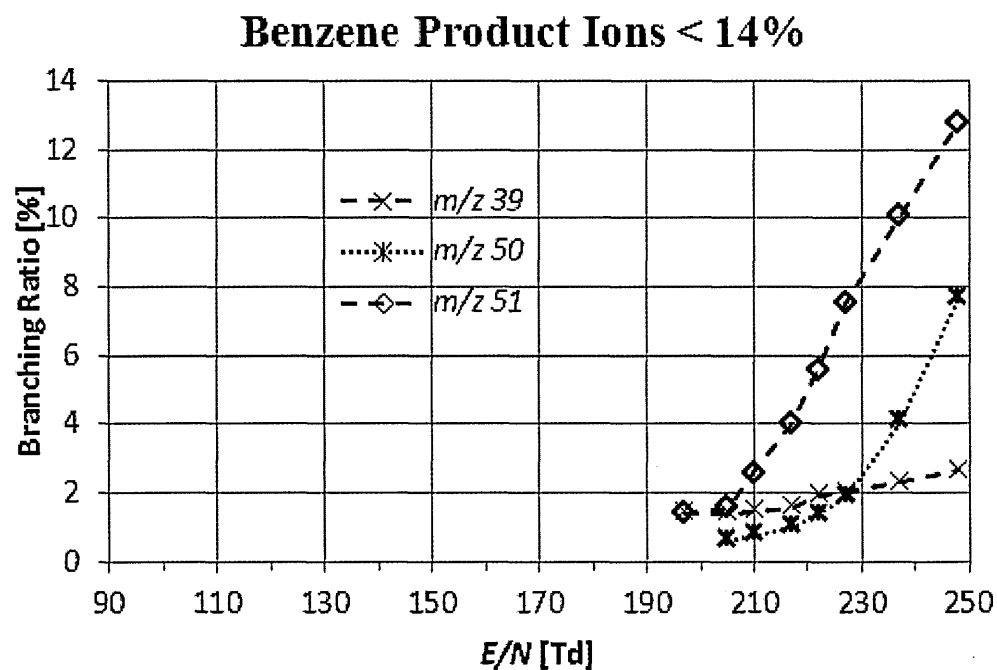
Figure 3.5: Branching ratios for benzene
b) shows minor products in greater detail

3.3.1.2   Toluene C₆H₅CH₃

A comparison of mass spectra for toluene at E/N = 140 Td and E/N = 250 Td are shown in
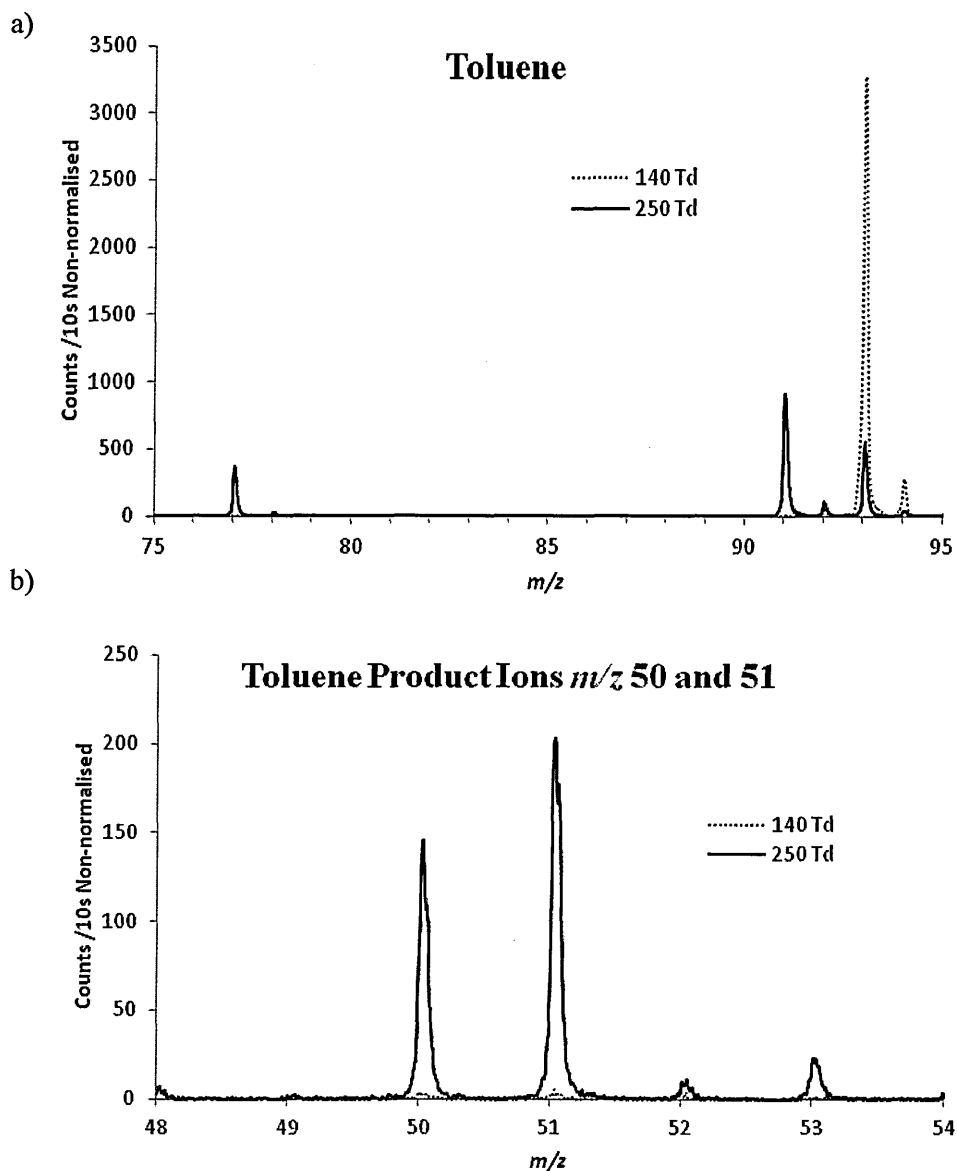
Figure 3.6: Mass spectra for toluene at E/N = 140 Td and 250 Td
a) shows peaks for protonated toluene at m/z 91 and a fragment at
m/z 77. b) shows fragments at m/z 50 and 51.

Figure 3.6. At E/N = 250 Td the protonated toluene signal at m/z 93 (C₆H₅CH₃H⁺) is less

than that of the product ion at m/z 91. It can also be seen that, even at high E/N, there is no

product ion at m/z 79, although a signal at m/z 77 is observed. The fragmentation behaviour

of toluene is shown in the branching ratio diagrams (Figure 3.7) as E/N is varied from 90 Td

to 250 Td. Toluene starts to fragment at E/N = 150 Td, losing H₂ to form the product ion at

m/z 91, C₇H₇⁺. This is a commonly found fragment ion called the tropylium cation. (See

a)

b)
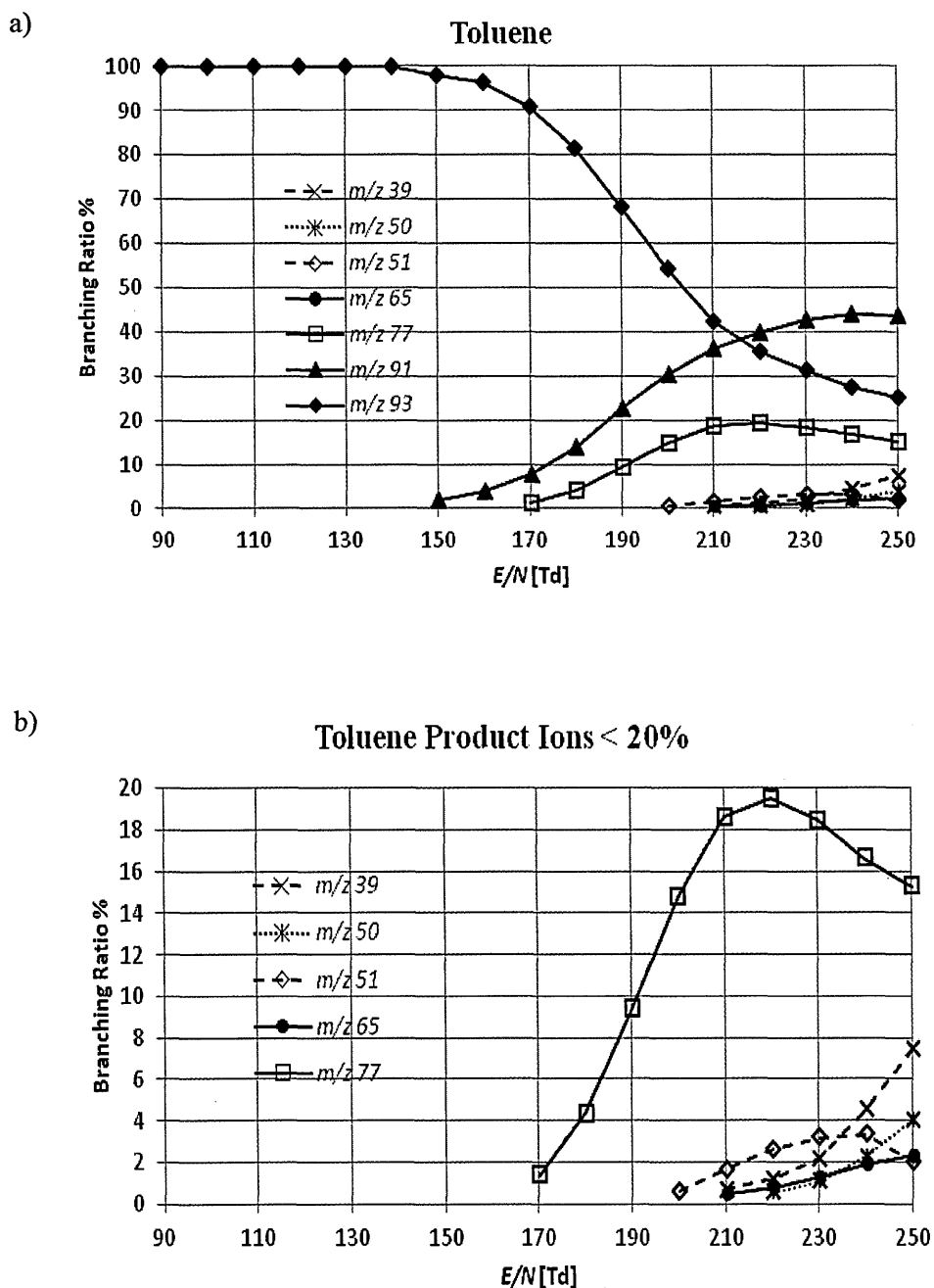
Figure 3.7: Branching ratios for toluene
b) shows minor products in greater detail

§3.3.2 for further information.) At $E/N \approx 170$ Td, m/z 77 appears, $C_6H_5^+$, with m/z 51

$(C_4H_3^+)$ following at 200 Td. Product ions at m/z 39, $(C_3H_3^+)$, m/z 50 and m/z 65 occur as

E/N increases > 210 Td.

3.3.1.3   Styrene C₆H₅CH₂CH

A comparison of mass spectra for styrene at $E/N = 140$ Td and $E/N = 250$ Td are shown in

Figure 3.8. Unlike toluene, styrene fragments to a product ion at m/z 79, as well as an ion at

m/z 77. The presence of m/z 79 in this spectrum is important when considering the calibration

gas and sensitivity calculations, as an adjustment for these counts must be made in order to

obtain an accurate value for the benzene content of the gas.

a)

b)
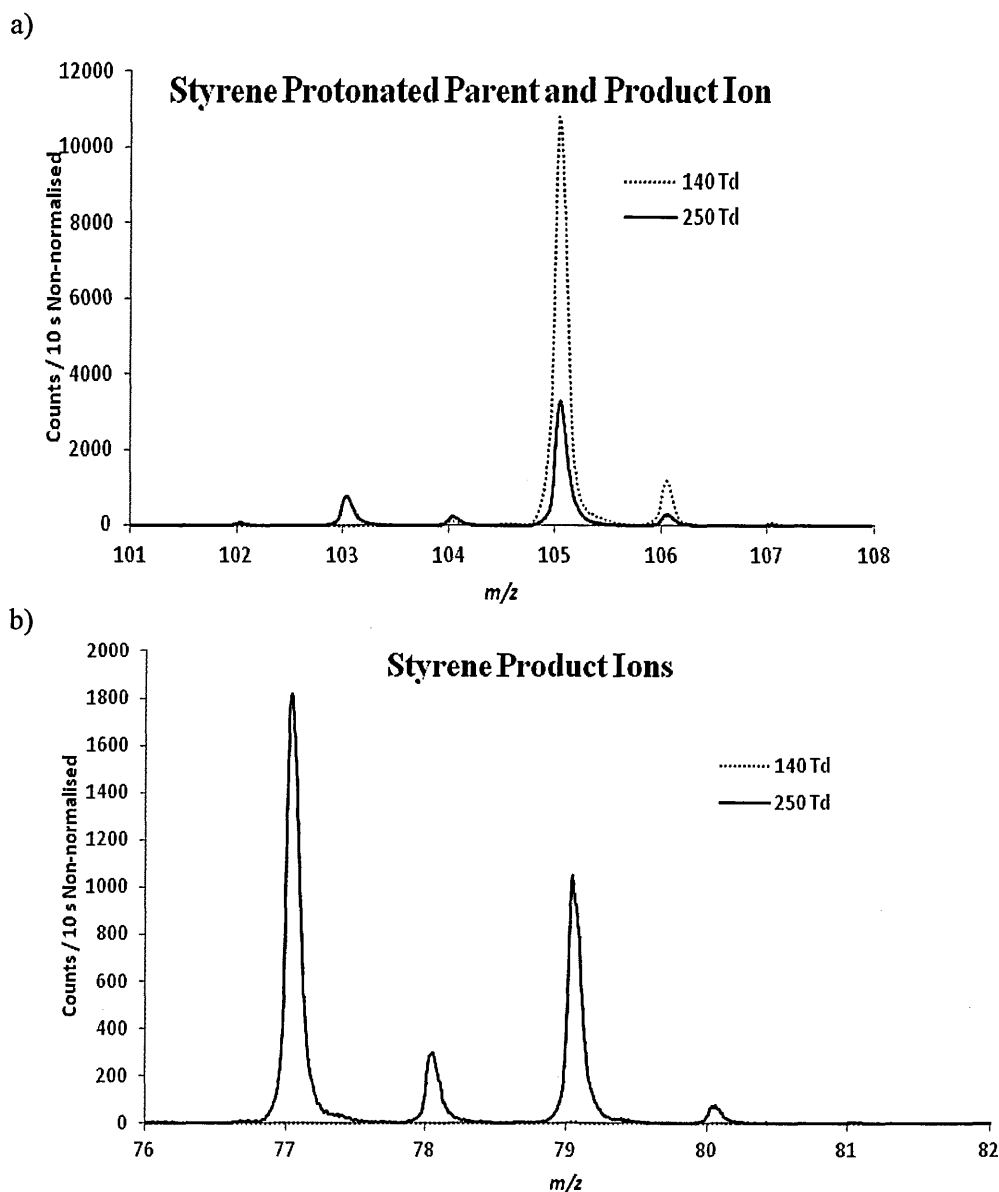
Figure 3.8: Mass spectra for styrene at $E/N = 140$ Td and 250 Td
a) shows peaks for protonated styrene at m/z 105 and a fragment at
m/z 103. b) shows fragments at m/z 77 and 79.

The fragmentation behaviour of styrene is shown in the branching ratio diagrams (Figure 3.9) as E/N is varied from 90 Td to 250 Td. Styrene starts to fragment at $E/N = 170$ Td, where the product ions at m/z 77, 79 and 103 appear. Product ions at m/z 51, $C_4H_3^+$ and m/z 50, $C_4H_2^+$, appear at $E/N > 220$ Td.

a)

b)
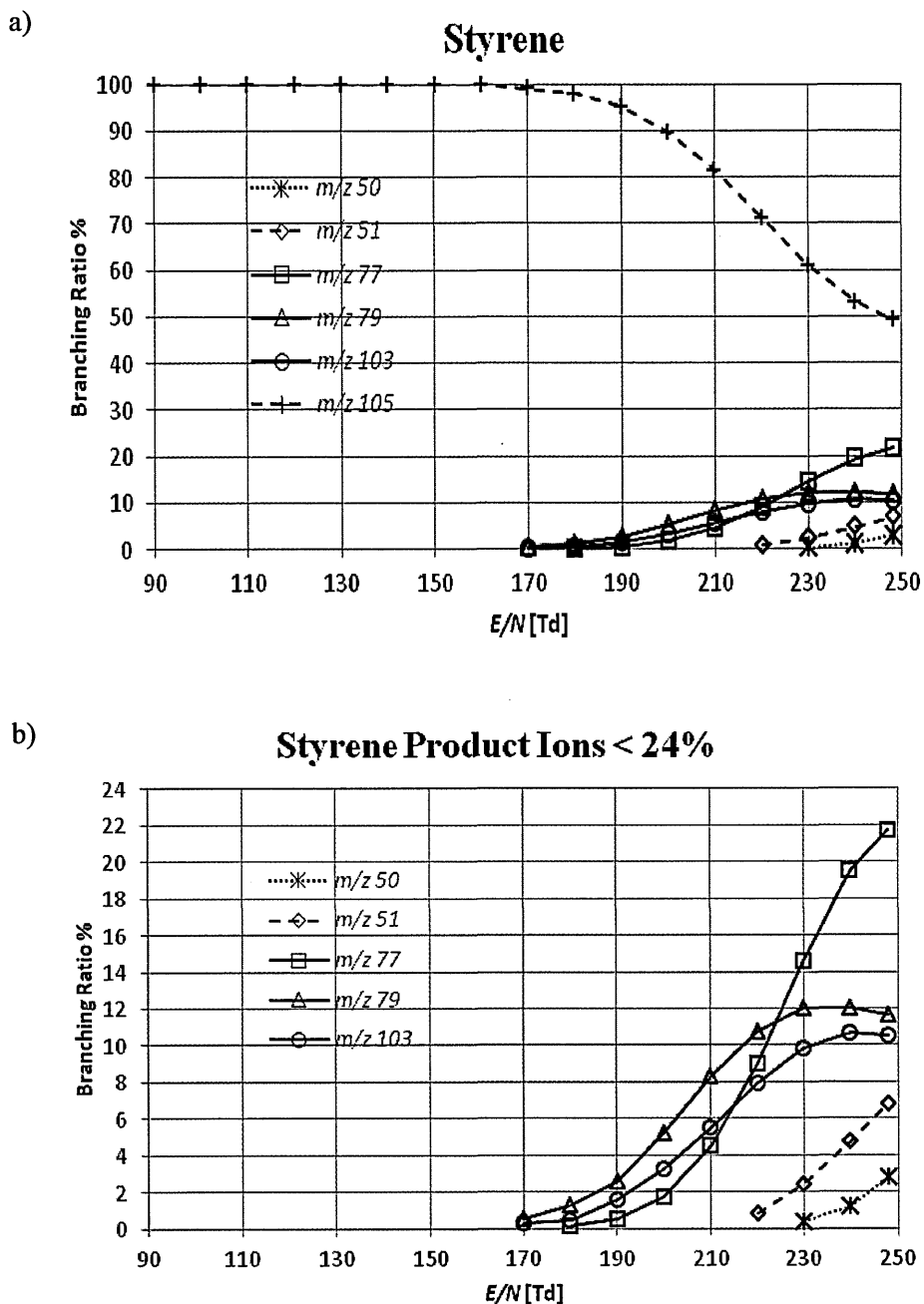
Figure 3.9: Branching ratios for styrene
b) shows minor products in greater detail

3.3.1.5   Xylenes $C_6H_4(CH_3)$

Figure 3.12a) and b) show the mass spectra at $E/N = 140$ Td and 245 Td for p-xylene, taken

to exemplify all three xylenes. (The molecular structures of the xylenes can be found in

Figure 3.2.)

a)

b)
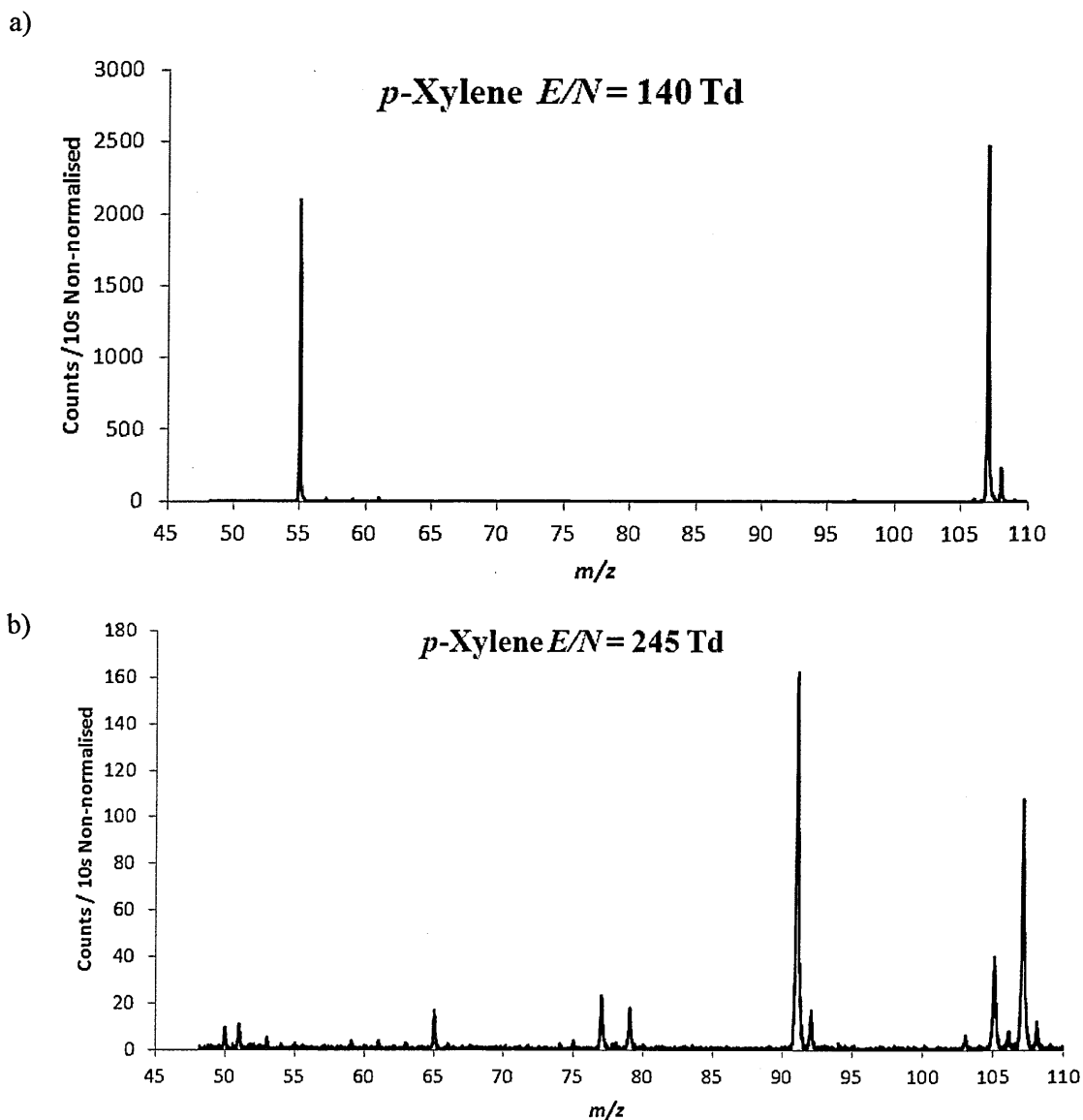
Figure 3.12: Mass spectra for protonated p-xylene
a) shows peaks at $E/N = 140$ Td and b) at 245 Td

The branching ratio graph, Figure 3.12a) shows that p-xylene starts to fragment at $E/N = 140$

Td, where m/z 105, $C_8H_9^+$ appears. However, this small amount of m/z 105 cannot be seen in

the mass spectrum for $E/N = 140$ Td. Although the xylenes are isobaric with ethylbenzene,

their fragmentation patterns are very different, with the xylenes showing few product ions

until E/N = 160 – 180 Td. A comparison of these compounds is developed in §3.3.2.1. At

$E/N \approx$ 160 Td, the product ion m/z 91, $C_7H_7^+$ appears: this is the major fragment for all the

xylenes for E/N values greater than 225 Td.

a)

b)
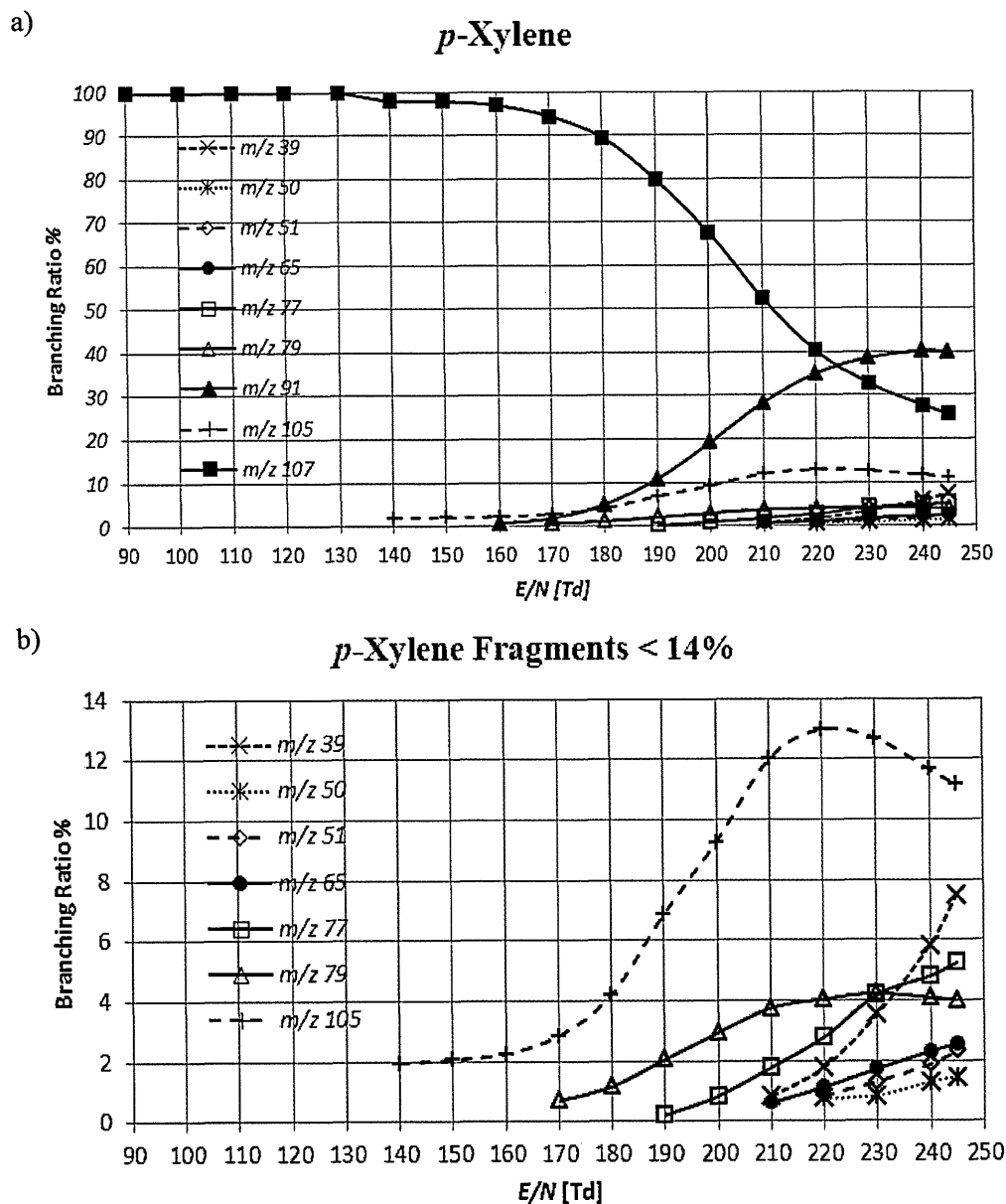
Figure 3.13: Branching ratios for p-xylene
b) shows minor products in greater detail

Branching ratios for *m*- and *o*-xylenes are shown in Figure 3.14 and 3.15. The branching ratios for all three isomers are so similar that it is not possible to differentiate between them using this method.

a)

m-Xylene

b)

m-Xylene Fragments < 14%
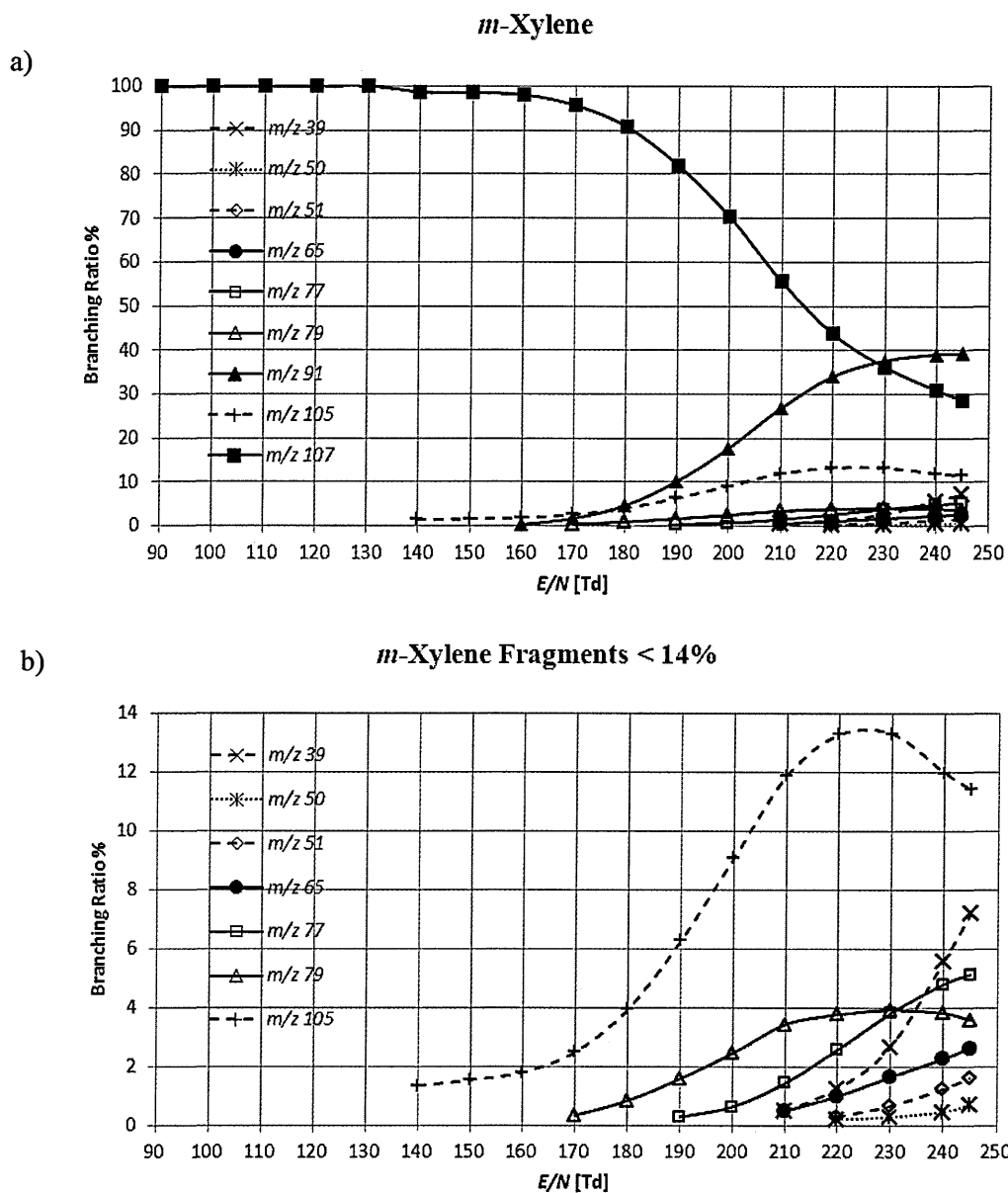
Figure 3.14: Branching ratios for *m*-xylene
b) shows minor products in greater detail

a)

o-Xylene

b)

o-Xylene Fragments < 14%
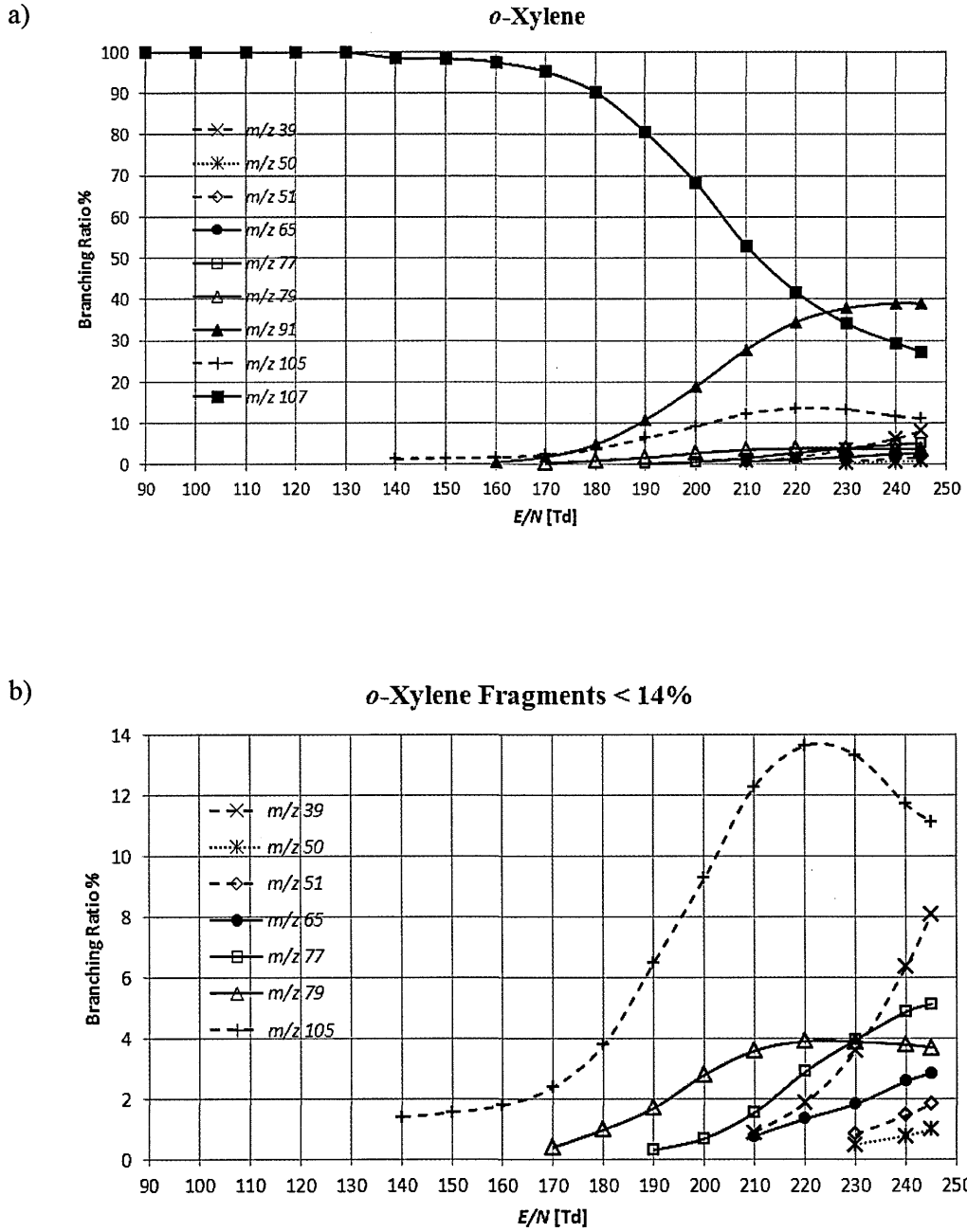
Figure 3.15: Branching ratios for o-xylene
b) shows minor products in greater detail

3.3.1.6 Trimthylbenzenes $C_6H_3(CH_3)_3$

Figure 3.16a) and b) show the mass spectra at E/N = 140 Td and 245 Td for 1,3,5-trimethylbenzene, taken to exemplify both of the trimethylbenzenes studied here. (The molecular structures of the trimethylbenzenes can be found in Figure 3.2) Figures 3.17 and

a)

b)
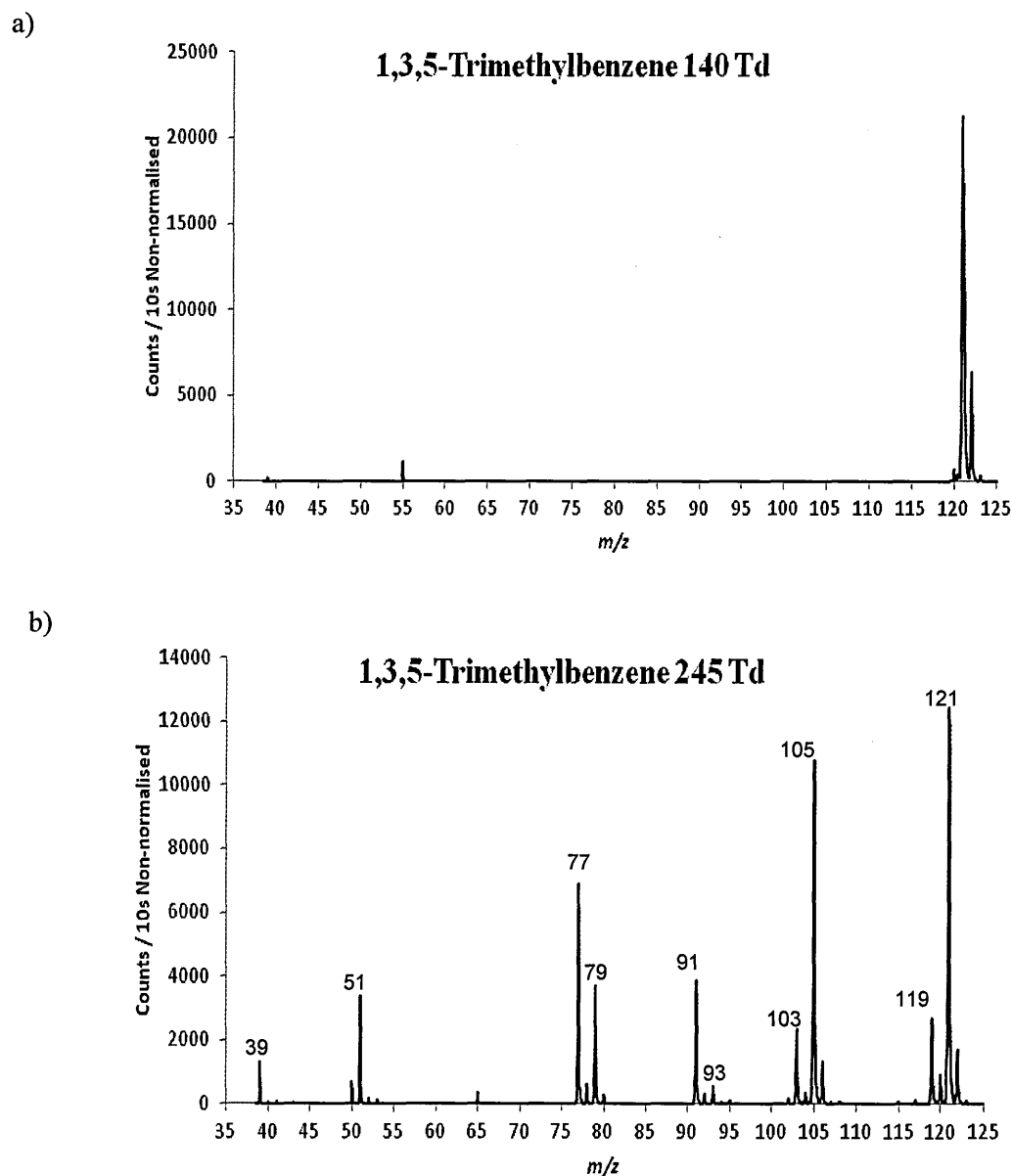
Figure 3.16: Mass spectra for 1,3,5-trimethylbenzene at a) E/N = 140 Td and b) 245 Td

3.18 show the branching ratios for the two trimethylbenzene isomers as E/N is varied from 90 Td to 245 Td. It can be seen that trimethylbenzene starts to fragment at E/N = 160 Td, where m/z 105, $C_6H_7^+$ and m/z 119 (loss of H_2) appear. For 1,3,5-trimethylbenzene, m/z 119

does not appear until E/N = 170 Td. At 190 Td, the fragments m/z 91, $C_7H_7^+$, and m/z 77,

$C_6H_5^+$, occur.

a)

1,2,4-Trimethylbenzene
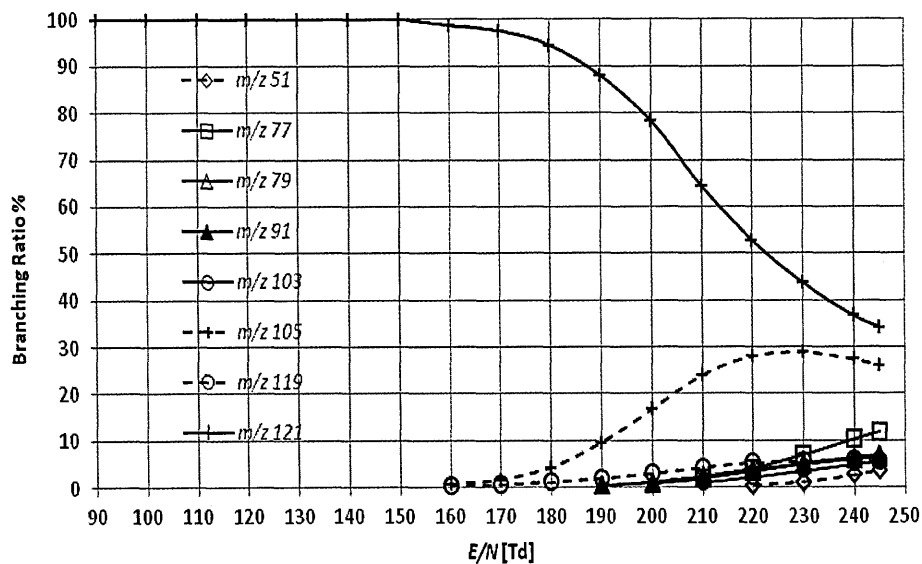
b)

1,2,4-Trimethylbenzene Product Ions < 12%
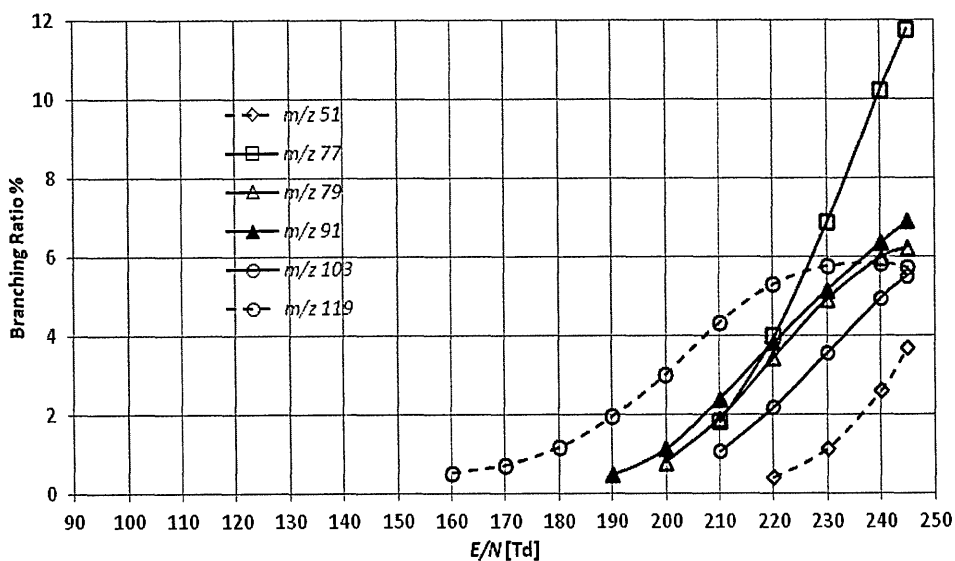
Figure 3.17: Branching ratios for 1,2,4-trimethylbenzene
b) shows minor products in greater detail

a)

1,3,5-Trimethylbenzene

b)

1,3,5-Trimethylbenzene Product Ions < 12%
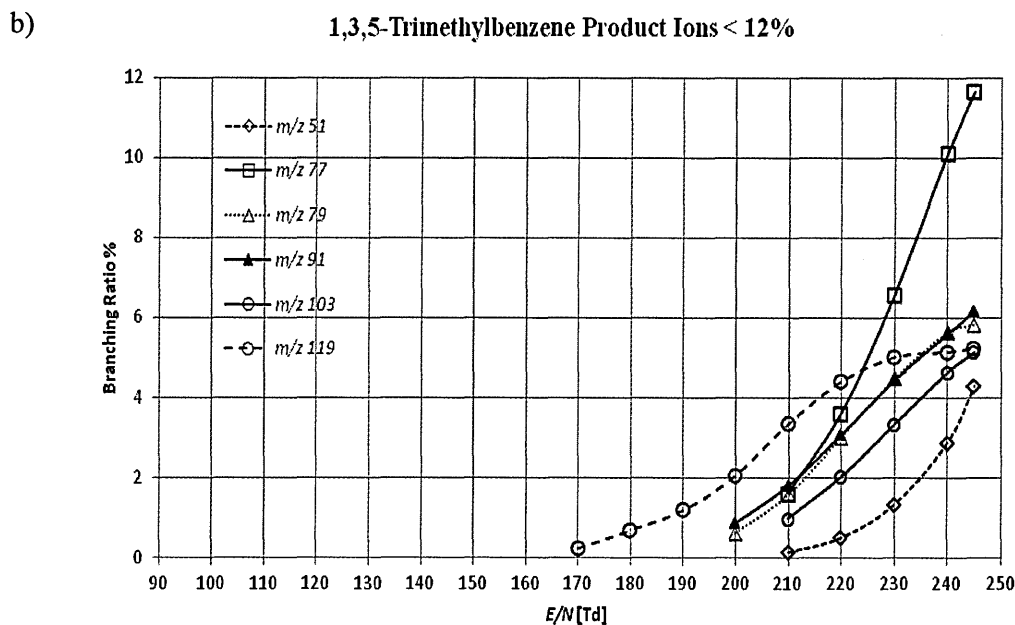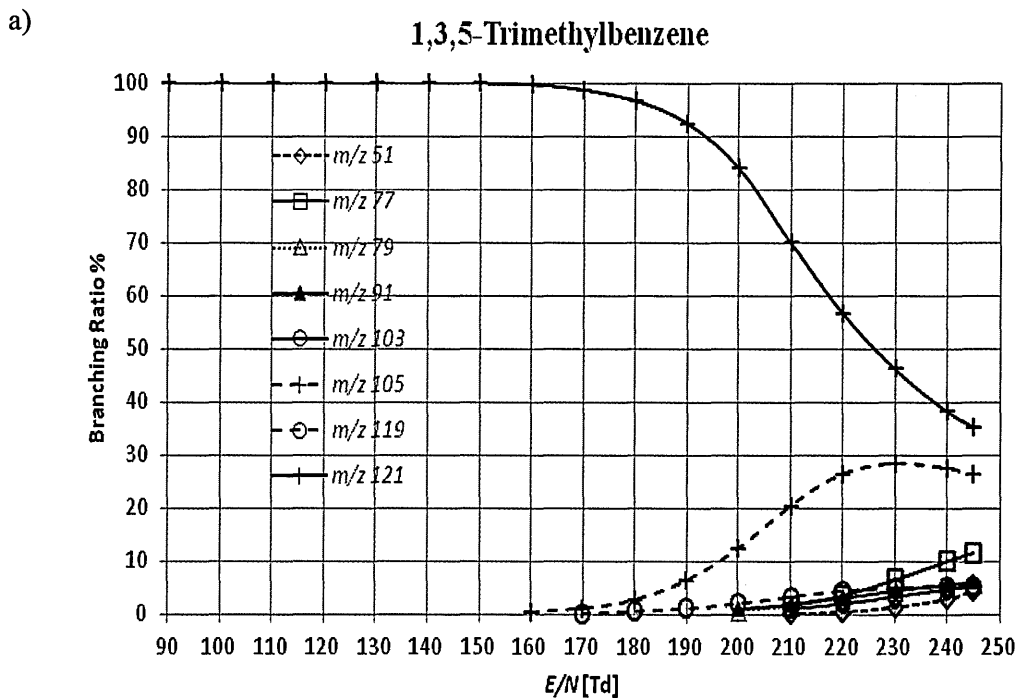
Figure 3.18: Branching ratios for 1,3,5-trimethylbenzene
b) shows minor products in greater detail

3.3.2   Discussion

The branching ratios show that most of these compounds do not fragment significantly until $E/N > 150$ Td, the main exception being ethylbenzene which produces $\sim 10\%$ *m/z* 79 at $E/N = 120$ Td. The *m/z*, proposed formula and percentage of each product ion for each compound are shown in Table 3.5 at 140 Td and at 245 Td, the highest value used here.

These data show that, at sufficiently high energy values, all of the alkylbenzene compounds tested fragment to produce ions at:

- *m/z* 51 and 77;

- *m/z* 79 except toluene;

- *m/z* 39 except styrene and the trimethylbenzenes.

From this it can be seen that benzene appears to be the most stable of these compounds retaining 50% of the parent ion at 245 Td. This is a direct result of the resonance structure of the electrons and bonding in the benzene ring (Cooper 1986). Ethylbenzene is the least stable with only 9% of the parent ion remaining at 245 Td. It is also interesting to note that none of the compounds fragment to a product ion at *m/z* 93 where protonated toluene is found. This may be of interest for environmental science considerations (see §3.3.2.1).

All of the compounds except toluene have a product ion at *m/z* 79, the same *m/z* value as protonated benzene.

Table 3.5: Percentage product ions found at $E/N = 140$ Td and 245 Td.
Shaded cells represent MH^+ values: m/z 79 = benzene, m/z 93 = toluene, m/z 105 = styrene, m/z 107 = ethylbenzene (EthylB) and xylenes, and m/z 121 = trimethylbenzenes (TriMB)

E/N Td / m/z	Formula	Benzene 140	245	Toluene 140	245	Styrene 140	245	EthylB 140	245	o-Xylene 140	245	m-Xylene 140	245	p-Xylene 140	245	1,2,4-TriMB 140	245	1,3,5-TriMB 140	245
39	$C_3H_3^+$	-	3	-	7	-	-	-	2	-	7	-	8	-	8	-	-	-	-
50	$C_4H_2^+$	-	8	-	4	-	3	-	4	-	1	-	1	-	1	-	-	-	-
51	$C_4H_3^+$	-	13	-	2	-	7	-	11	-	2	-	2	-	2	-	6	-	4
65	$C_5H_5^+$	-	-	-	2	-	-	-	-	-	3	-	3	-	3	-	-	-	-
77	$C_6H_5^+$	-	27	-	15	-	22	-	27	-	5	-	5	-	5	-	13	-	12
79	$C_6H_7^+$	100	50	-	-	-	12	37	40	-	4	-	4	-	4	-	6	-	6
91	$C_7H_7^+$			-	44	-	-	-	7	-	39	-	39	-	40	-	7	-	6
93	$C_6H_5CH_3H^+$			100	25														
103	$C_8H_7^+$					-	11	-	-	-	-	-	-	-	-	-	5	-	5
105	$C_8H_9^+$					100	49	-	-	2	11	2	11	2	11	-	25	-	26
107	$C_8H_{11}^+$							63	9	98	29	98	27	98	26				
119	$C_9H_{11}^+$															-	5	-	5
121	$C_6H_3(CH_3)_3H^+$															100	30	100	35

m/z 39, 50, 51, and 77

Product ions at *m/z* 39, 50, 51 and 77 normally appear in the electron impact (EI) spectra of all alkylbenzenes (Budzikiewicz *et al.* 1967). A product ion at *m/z* 51 ($C_4H_3^+$) can be produced by *m/z* 79 as a result of its losing ethylene, C_2H_4; *m/z* 77 can lose C_3H_2 to form the simplest aromatic species, $C_3H_3^+$ (*m/z* 39), the cyclopropenyl ion (Breslow and Groves 1970).

m/z 91 Tropylium ion

The tropylium cation, $C_7H_7^+$, is a well-recognised species in alkylbenzene EI mass spectra: its production from ionised or protonated toluene is one of the most investigated processes in gas-phase ion chemistry (Chiavarino *et al.* 2012, Lifshitz 1994). It is not surprising, therefore, to see this appearing in the PTR spectra for all of the alkylbenzenes here except for benzene (MH^+ *m/z* 79) which has an *m/z* too low to form a product ion at *m/z* 91, and styrene, where *m/z* 91 starts to appear only at the highest *E/N* values and then reaches a maximum of ~ 0.2%. However, *m/z* 91 does not coincide with the MH^+ peaks of any of the calibration gas compounds so is of no further interest except to describe, briefly, how it is formed:

- From toluene $C_6H_5CH_3H^+$ *m/z* 93

   Loss of 2 amu H_2:

$$C_7H_9^+ \longrightarrow C_7H_7^+ + H_2$$
$$\textit{m/z } 93 \qquad\qquad \textit{m/z } 91$$
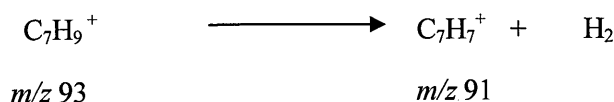
- From ethylbenzene and xylenes $C_8H_{11}^+$ *m/z* 107

   Loss of 16 amu CH_4:

$$C_8H_{11}^+ \longrightarrow C_7H_7^+ + CH_4$$
$$\textit{m/z } 107 \qquad\qquad \textit{m/z } 91$$
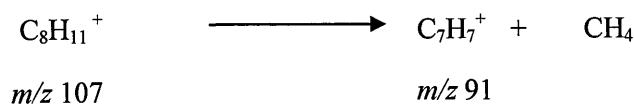
- From trimethylbenzenes $C_9H_{13}^+$ m/z 121

Loss of 30 amu C_2H_6

$$C_9H_{13}^+ \longrightarrow C_9H_7^+ + C_2H_6$$

$$m/z\ 121 \qquad\qquad\qquad m/z\ 91$$
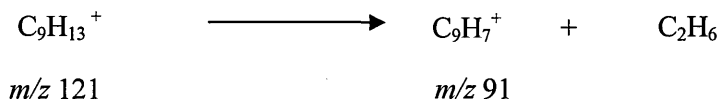
3.3.2.1 Comparison of the Isomeric Compounds Ethylbenzene and Xylenes (C_8H_{10})

The E/N investigation of individual compounds of the calibration gas demonstrates how

fragmentation behaviour over a wide range of E/N values can be used to discriminate

a)

b)
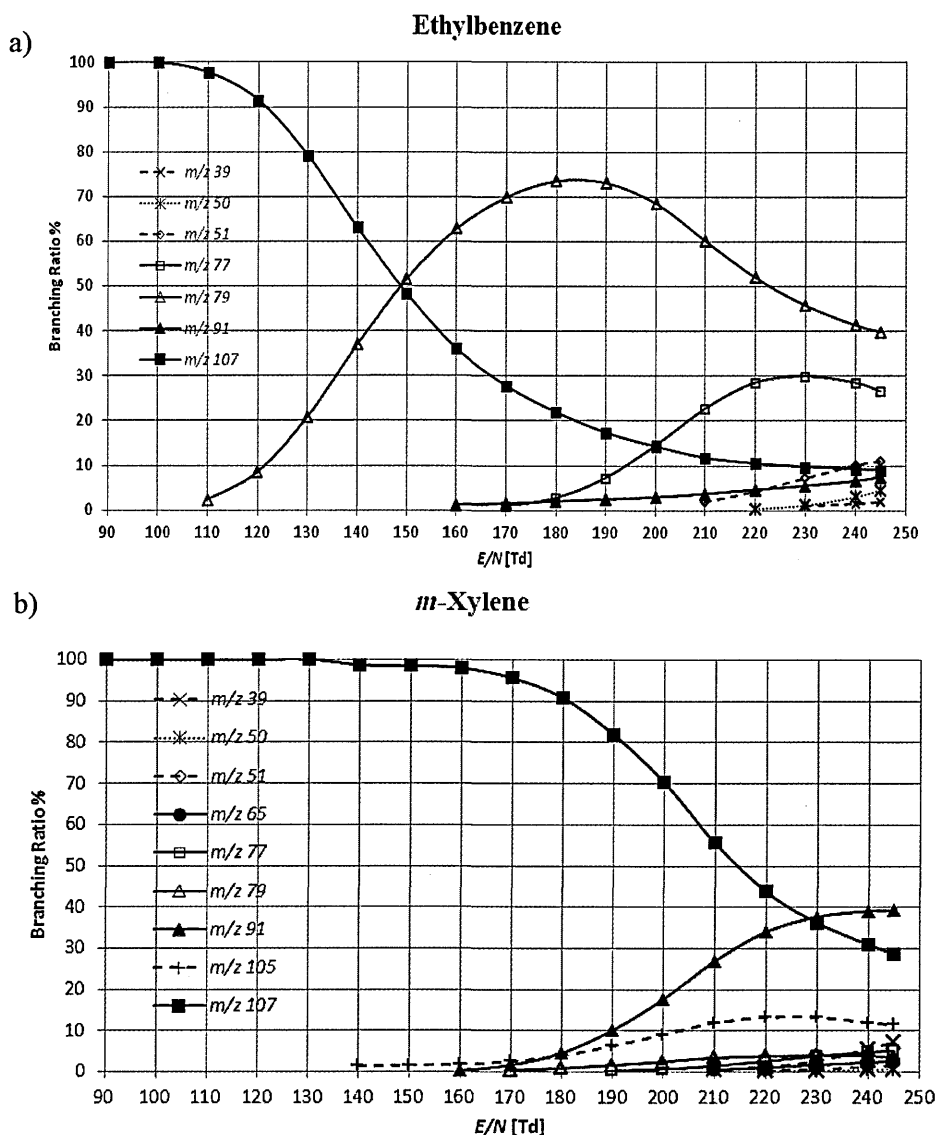
Figure 3.19: Fragmentation behaviour with changes in E/N
a) ethylbenzene: the largest product ion is m/z 79 appearing at $E/N =$ 110 Td; b) m-xylene: the largest product ion is m/z 91, with m/z 105 (styrene) appearing at $E/N =$ 140 Td

between isomeric compounds (Figure 3.19, repeats of Figs 3.11 and 3.14). Even at 'normal'

operating E/N values (*i.e.* 140 Td) there are noticeable differences with ethylbenzene which

is reduced by almost 40% to produce m/z 79. The branching ratio graphs above show that

one of xylene's product ions, m/z 105, appears at E/N = 140 Td. Ethylbenzene does not give

a product ion at m/z 105, so a peak at m/z 105 from a gas mixture with a peak at m/z 107

would indicate the presence of xylene, providing that no styrene was initially present in the

mixture. This could be checked at E/N < 140 Td and if no peak at m/z 105 were present, then

sampling the gas mixture at 140 Td $\geq E/N \leq$ 165 Td might provide data to give an estimate

of the relative quantities of xylene and ethylbenzene. (Note: trimethylbenzene also produces

an ion at m/z 105 at $E/N \geq$ 170 Td.)

As a proof of concept, an analysis using known values from the calibration gas (described in

§3.2.2) is shown below. Consider a sample of gas mixture tested at 120 Td and 140 Td

which produced the data shown in Figure 3.20.

a)

b)
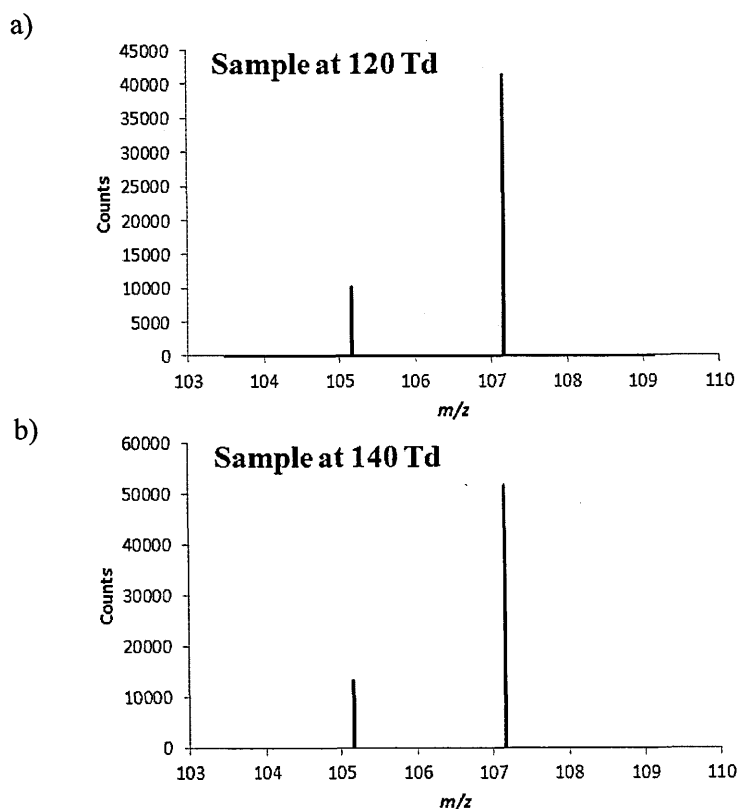
Figure 3.20: Samples of gas mixture at E/N = 120 Td and 140 Td

Branching ratios show that neither styrene (m/z 105) (Figure 3.9) nor xylene (m/z 107)

(Figure 3.13) breaks up at 120 Td, so, at this E/N there is 100% of each species with no contribution being made to styrene from the xylenes. At 140 Td, there is still 100% of styrene but the xylenes have fragmented to yield an average of 2% product ions at m/z 105 (Table 3.6). A difference in normalised counts is therefore expected at m/z 105 at the two

Table 3.6: Percentage of compounds remaining at E/N = 120 Td and 140 Td.

E/N /Td	m/z 105 Styrene	m/z 107 Xylenes	m/z 107 EthylB*
120	100%	100%	92%
140	100%	98%	63%

*Values for ethylbenzene are given for comparison but there is no contribution from this to m/z 105.

E/N values: some of this difference is due to a reduction in counts because of the decrease in reaction time in the drift tube and an increase from the contribution from the xylenes. The overall increase is 1483 non-normalised counts representing the 2% contribution from the xylenes.

The values for this example have been taken from those for the calibration gas where the actual contribution from the xylenes to m/z 105 is 680 non-normalised counts at 140 Td. The calculated (reverse) value results in a total xylene count of 92663, which is 41029 counts more than actually detected at m/z 107.

In an environment with no background peak at m/z 105, the relative amounts of ethylbenzene and xylenes could be found more accurately as it would be possible to work at just one E/N value and so avoid the inherent problems encountered by comparing values at different E/Ns. However, this is generally not the case – styrene is produced by exhaust fumes and so is commonly found in the atmosphere, outdoors in concentrations of 0.06-4.6 ppb and indoors 0.07-11.5 ppb (ToxGuide for Styrene). It is therefore necessary to have a method of identifying the extra counts contributed from xylene and, from the foregoing example, this does not seem to be possible. Further work in this area is not, however, ruled out since at least one author (Karl *et al.* 2001) considers that it would be possible to reconstruct the original concentration providing one distinct ion can be identified.

3.4   Chlorobenzenes and Calibration Gas

Results and discussions are set out in the following sections. Results for the calibration gas itself are included here for completeness and in particular to enable the further discussion of product ions at m/z 95 and m/z 129.

3.4.1   Results

Branching ratios and spectra for fragments and protonated parent ions are given for each compound.

3.4.1.1   Chlorobenzene C_6H_5Cl

Figure 3.21a) shows mass spectra for chlorobenzene and product ions at E/N = 140 Td, 210 Td and 245 Td. The peak at m/z 55 for 140 Td is the water trimer: this ceases to exist at the higher E/N values. Product ions occur at m/z 39, 50, 51, 77 and 95 and the protonated parent, MH^+, at m/z 113. The signal at m/z 39 is not included in the mass spectra as its very large signal at lower E/N values would overwhelm the other peaks shown here.

Figure 3.21b) shows a magnified mass spectrum at 245 Td. This shows more clearly how the

a)

b)
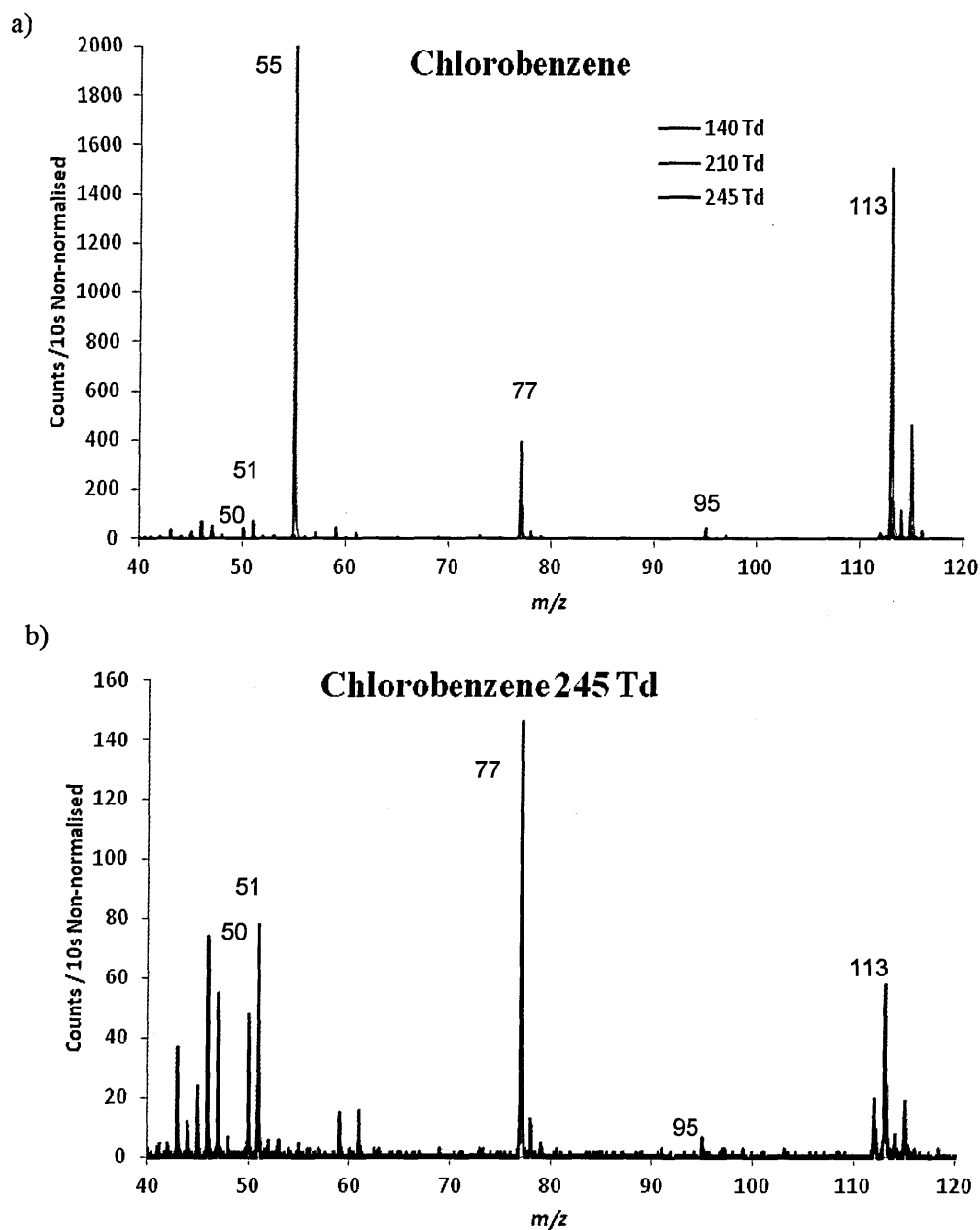
Figure 3.21: Mass spectra for chlorobenzene:
a) E/N =140 Td, 210 Td, 245 Td; b) E/N = 245 Td expanded scale

signal at m/z 77 is greater than that of the protonated parent ion at m/z 113.

Branching ratio curves in Fig 3.22 show the behaviour of the product ions over the whole E/N

range.

a)

b)
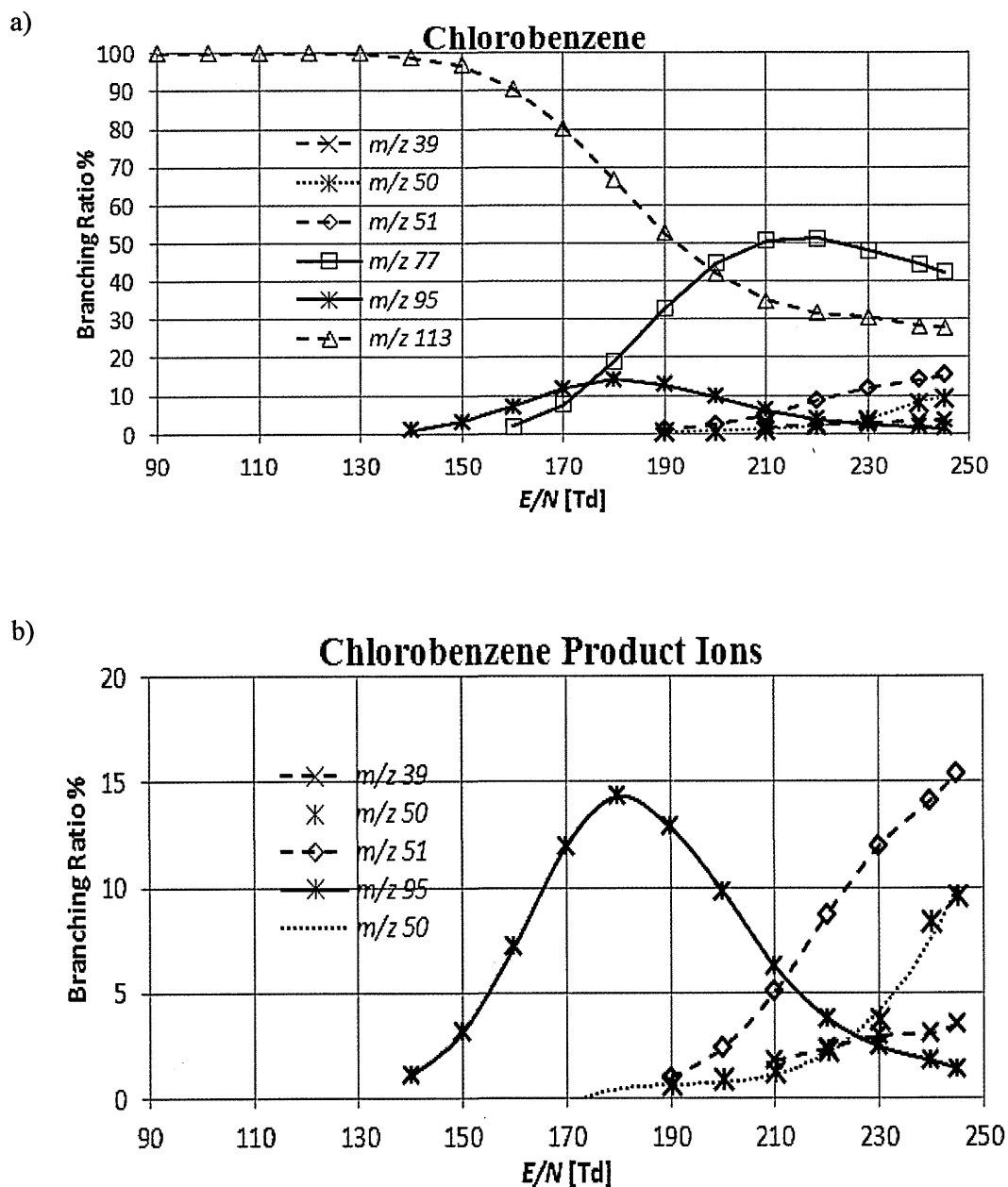
Figure 3.22: Branching ratios for chlorobenzene

None of the fragments at m/z < 113, *viz.* m/z 39, 50 and 51 contain a Cl atom and can, in fact, be compared with the fragments from benzene itself (Table 3.5). This seems to suggest that fragmentation occurs by the loss of the Cl atom. One might expect to see the chlorine atom in a product ion but this has not been found, not even at m/z 49, CH_2Cl^+ (Figure 3.23).

a)

b)
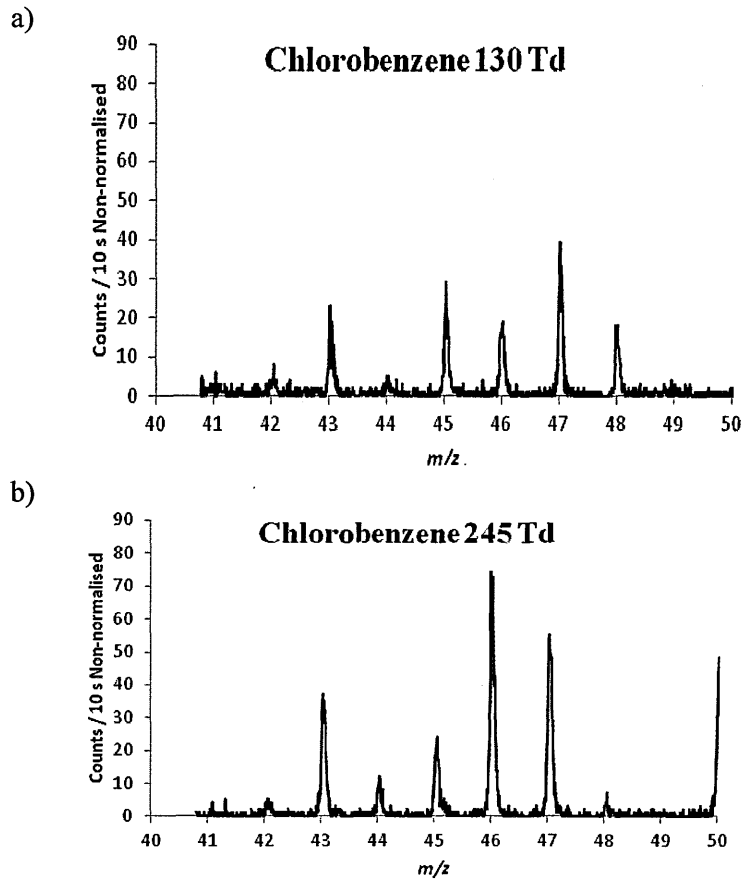
Figure 3.23: Spectra of chlorobenzene at E/N = 130 Td and 245 Td showing no signal at m/z 49.

Peaks for the protonated ion and isotopes of chlorobenzene, C_6H_5Cl, are shown in Figure 3.24: they occur at m/z 113 ($C_6H_5ClH^+$), m/z 114 ($^{13}CC_5H_5ClH^+$), m/z 115 ($C_6H_5{}^{37}ClH^+$), and m/z 116 ($^{13}CC_5H_5{}^{37}ClH^+$). The peaks at m/z 113 and m/z 115 represent the ^{37}Cl bearing ions. The separation of 2 amu arises because the two isotopes of chlorine have atomic masses of 35 amu and 37 amu, The relative abundance of these isotopes is approximately 3:1 (^{35}Cl: ^{37}Cl)
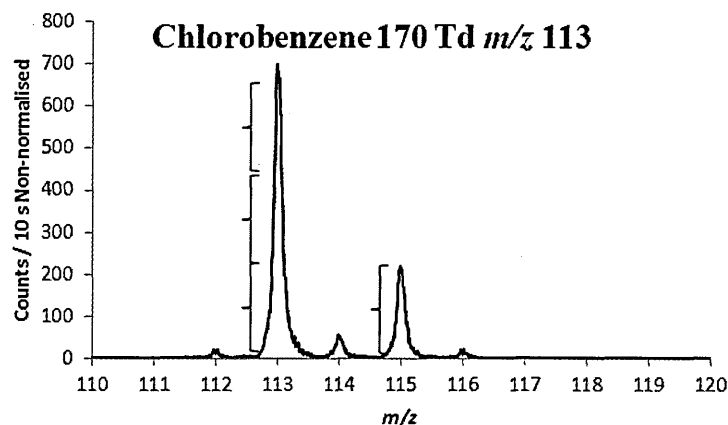
Figure 3.24: Peaks for protonated chlorobenzene.

and these proportions can be seen in the relative heights of the peaks at m/z 113 (~700 counts) and m/z 115 (~210 counts) which gives a proportion of 100:30. The integrated counts under the peak is, in fact, a more appropriate basis for the ratio, giving 13416:4149 = 100:31.

Further discussion of the product ions from chlorobenzene is given in §3.4.2.

3.4.1.2 Dichlorobenzenes C₆H₄Cl₂

Figures 3.25a) and b) show the mass spectra at E/N = 140 Td and 245 Td for m-dichlorobenzene, taken to exemplify the three dichlorobenzenes. (Structures for the isomers can be found in Figure 3.3b, bi and bii.)

a)

b)
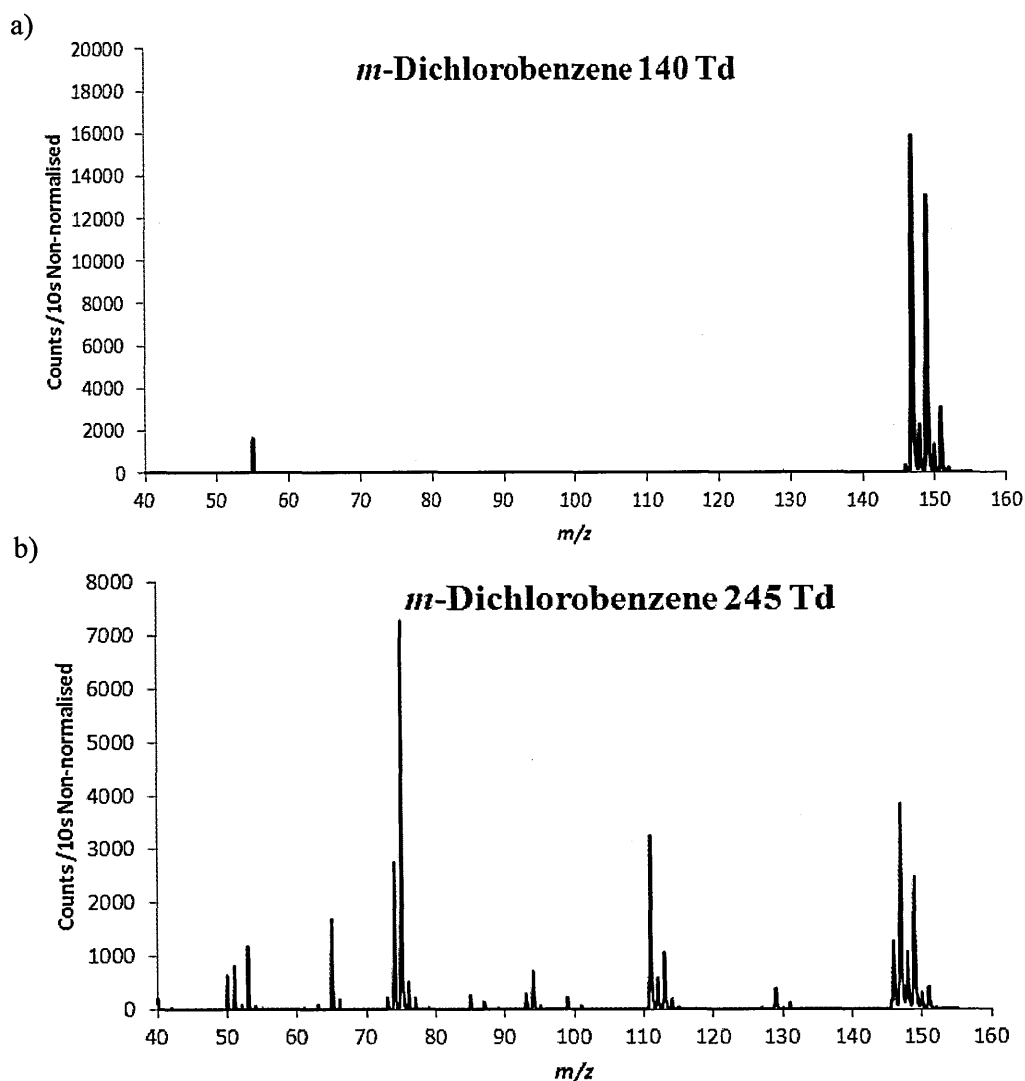
Figure 3.25: Mass spectra for m-dichlorobenzene at a) E/N = 140 Td and b) 245 Td

Figures 3.26, 3.27 and 3.28 show the branching ratios for the three dichlorobenzene isomers as E/N is varied from 90 Td to 245 Td. It can be seen that m/z 111, $C_6H_4Cl^+$ is the first fragment to appear at $E/N = 170$ Td for all three isomers. Peaks at m/z 50, 51, 53 and 99 contribute 2% or less to the branching ratios and, since they have no bearing on the calibration gas constituents, have not been given any further consideration.

a)

b)
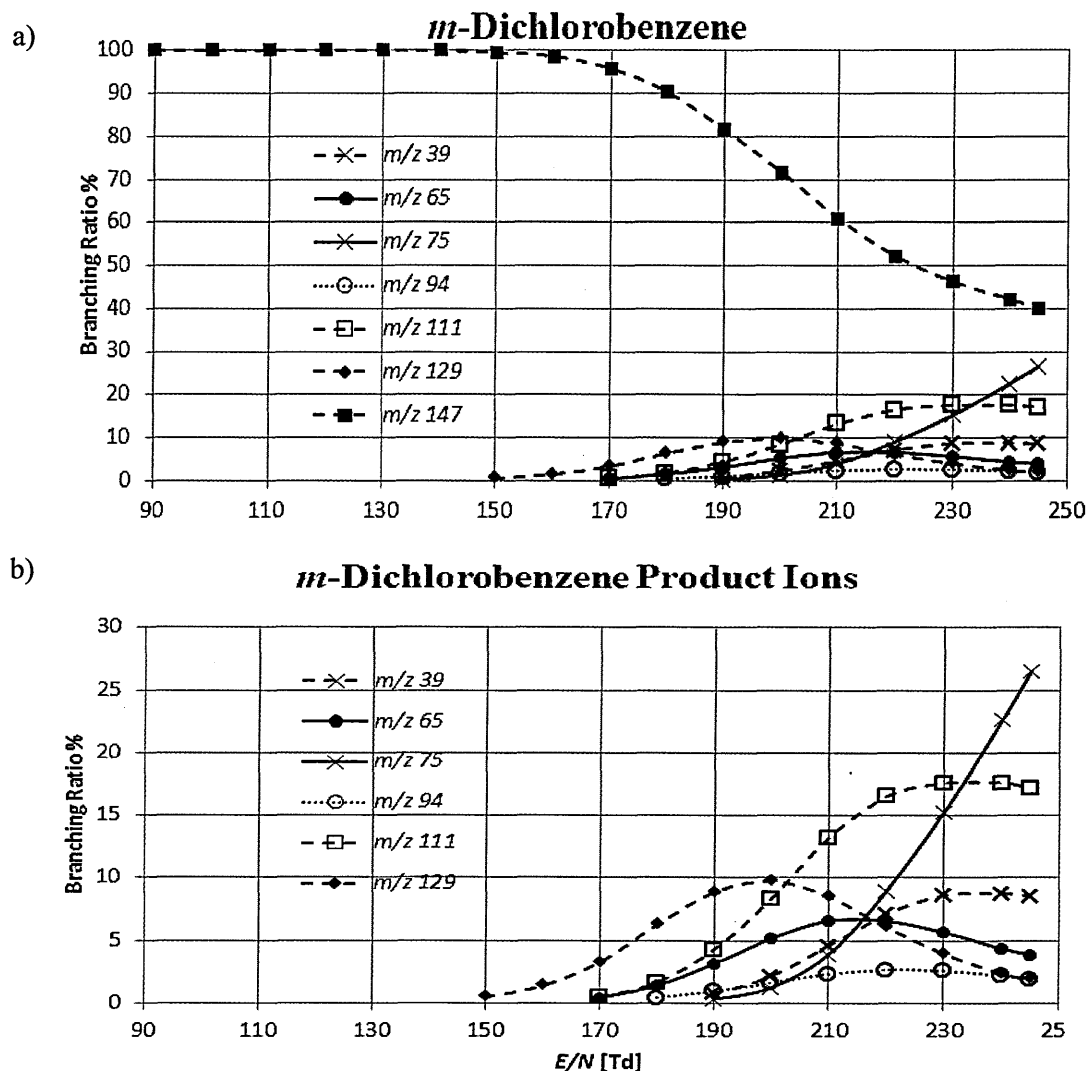
Figure 3.26: Branching ratios for m-dichlorobenzene

a)

o-Dichlorobenzene

Legend:
- – ✕ – m/z 39
- – ● – m/z 65
- – ✕ – m/z 75
- ⋯○⋯ m/z 94
- – ☐ – m/z 111
- – ◆ – m/z 129
- – ■ – m/z 147

X-axis: E/N [Td]
Y-axis: Branching Ratio %

b)

o-Dichlorobenzene Product Ions

Legend:
- – ✕ – m/z 39
- – ● – m/z 65
- – ✕ – m/z 75
- ⋯○⋯ m/z 94
- – ☐ – m/z 111
- – ◆ – m/z 129

X-axis: E/N [Td]
Y-axis: Branching Ratio %
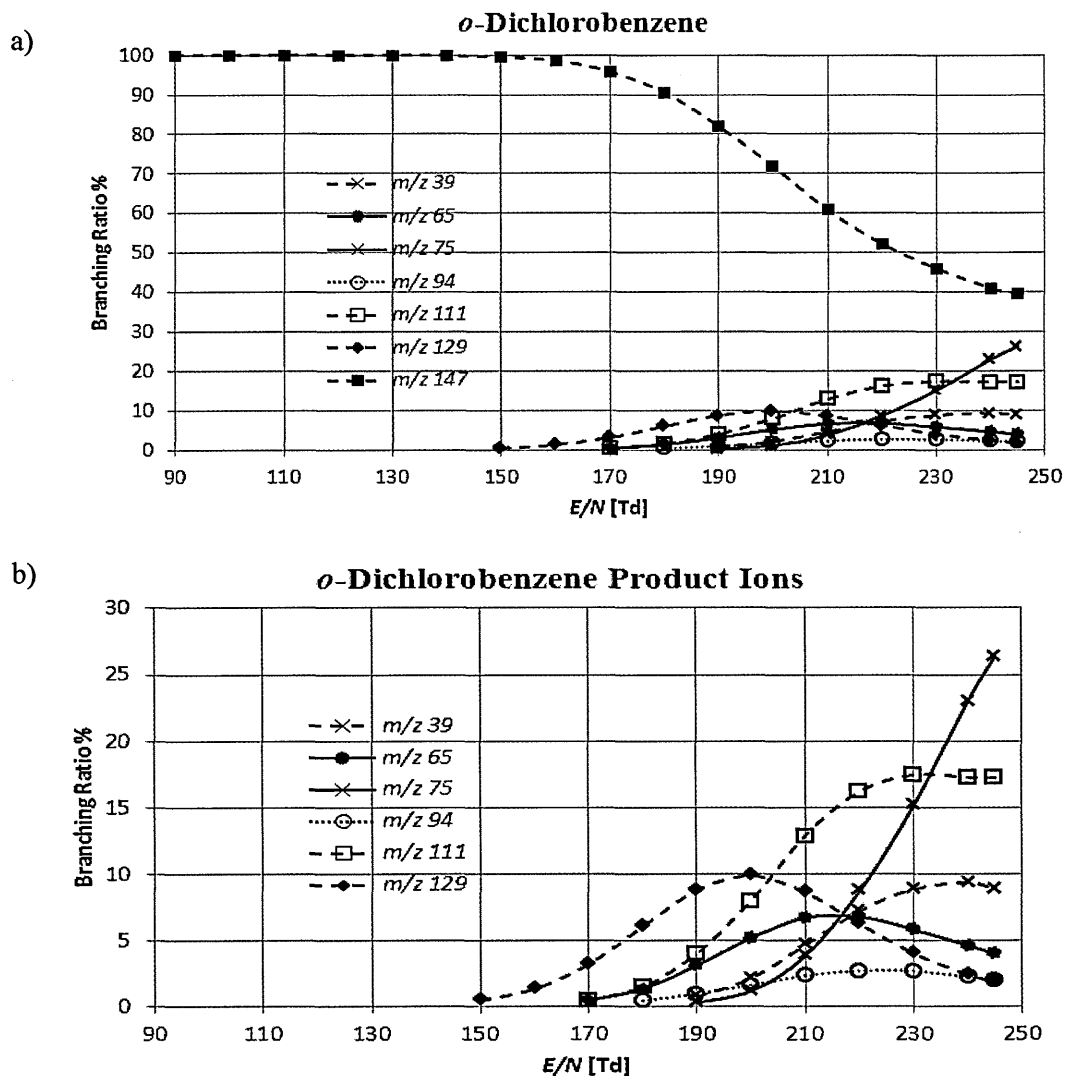
Figure 3.27: Branching ratios for o-dichlorobenzene

a)

p-Dichlorobenzene

b)

p-Dichlorobenzene Product Ions
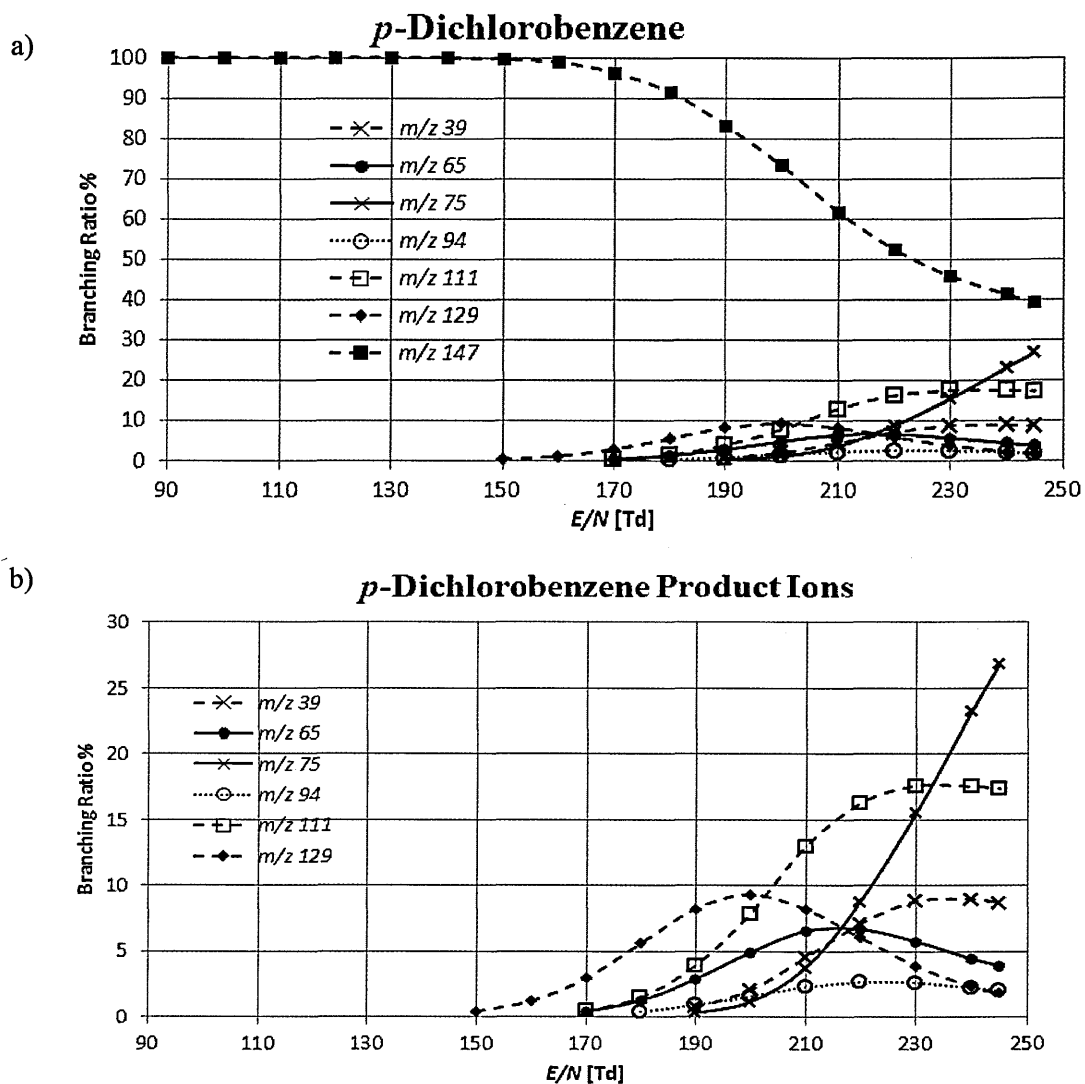
Figure 3.28: Branching ratios for *p*-dichlorobenzene

Protonated *p*-Dichlorobenzene at *m/z* 147 (1,4-C$_6$H$_4$Cl$_2$H$^+$)

Figure 3.29 shows an expanded spectrum for the protonated parent ion in 1,4-C$_6$H$_5$Cl$_2$$^+$, (*p*-dichlorobenzene) with the MH$^+$ peak at *m/z* 147. The series of peaks shows the characteristic

Figure 3.29: Spectrum of protonated parent ion at *m/z* 147 showing isotope peaks in *p*-dichlorobenzene.

pattern of a chlorine compound containing two chlorine atoms: three peaks relating to the chlorine isotopes: MH$^+$, MH$^+$ + 2 and MH$^+$ + 4. These arise because of the three possible combinations of the isotopes occurring on each of the two chlorine atoms where the probability of finding a ^{35}Cl atom is 0.75 and the probability of finding a ^{37}Cl is 0.25 (Table 3.7). The ratio of the three possible combinations is 9 : 6 : 1, very close to the ratio for the peaks seen at MH$^+$, MH$^+$ + 2 and MH$^+$ + 4 in Figure 3.29 above.

Table 3.7: Possible ways of combining isotopes for two Cl atoms

Isotope Combination	Probability 0.75 for ^{35}Cl 0.25 for ^{37}Cl	Ratio	Peak Counts	Peak Counts Ratio
C$_6$H$_4$^{35}Cl^{35}Cl	¾ × ¾ = 9/16	9	233909	8.8
C$_6$H$_4$^{35}Cl^{37}Cl C$_6$H$_4$^{37}Cl^{35}Cl	(¾ × ¼) × 2 = 6/16	6	155032	5.8
C$_6$H$_4$^{37}Cl^{37}Cl	(¼ × ¼) = 1/16	1	26595	1

Further discussion of product ions found in the dichlorobenzenes can be found in §3.4.2.

3.4.1.3   1,2,4-Trichlorobenzene $C_6H_3Cl_3$

Figure 3.30a) and b) show the mass spectra at E/N = 140 Td and 245 Td for 1,2,4-

a)

b)

Figure 3.30: Mass spectra for 1,2,4-trichlorobenzene:
At a) E/N = 140 Td with the peak at m/z 147 enlarged and b) at E/N = 245 Td

trichlorobenzene. (See Figure 3.3 for the molecular structure.)

The spectrum in Figure 3.30a) at E/N = 140 Td shows a peak at m/z 147. This is, in fact, due

to the presence of a dichlorobenzene impurity shown in the enlargement in this figure.

However, the peaks in Figure 3.30b at m/z 146, 148 and 150 at E/N = 245 Td are the result

of MH^+ losing a Cl atom.

Figure 3.31 shows the branching ratios for 1,2,4-trichlorobenzene as E/N is varied from 90

Td to 245 Td. Here it is clearly shown that 1,2,4-trichlorobenzene starts to fragment at 170

Td, losing Cl to produce $C_6H_3Cl_2H^+$ at m/z 146.

a)

b)

Figure 3.31: Branching ratios for 1,2,4-trichlorobenzene

Protonated 1,2,4-Trichlorobenzene at m/z 181 (1,2,4-$C_6H_3Cl_3$)

Figure 3.32 shows a spectrum of the protonated parent peaks for 1,2,4-trichlorobenzene with

the MH^+ peak at m/z 181. These peaks show the characteristic pattern of a compound

containing three chlorine atoms. There are now four peaks relating to the chlorine isotopes:

MH^+ (m/z 181), $MH^+ + 2$ (m/z 183), $MH^+ + 4$ (m/z 185) and $MH^+ + 6$ (m/z 187). These arise

because of the possible combinations of the two isotopes.

The abundance of $^{37}Cl:^{35}Cl$ is 33%, i.e. the number of counts for ^{37}Cl is one third of that of the counts for ^{35}Cl (see Figure 3.24). Consequently the probability of finding a ^{37}Cl is one in four, i.e. 25%. However this probability is not exactly 25%, but is 24.24% (Hitzfield *et al.* 2011). If the ratio were exactly 25%, then the first and second peaks in this spectrum would have identical heights, but this is not the case, as can be seen in Figure 3.28. Ratios for both 25% and 24.24% probabilities are shown in Table 3.8.

Figure 3.32: Spectrum of MH$^+$ at *m/z* 181 in 1,2,4-trichlorobenzene

Further discussion of product ions found in 1,2,4-trichlorobenzene can be found in §3.4.2.1

Table 3.8: Comparison of isotope distributions for three Cl atoms
with 25% and 24.24% probability for ^{37}Cl
Data from the spectrum in Fig 3.27 are closer to the 24.24% values

m/z	Isotope Combination	Probability $^{37}Cl = 0.25$ $^{35}Cl = 0.75$	% Theory	Probability $^{37}Cl = 0.2424$ $^{35}Cl = 0.7576$	% Theory	Peak Counts	% Exper.
181	$C_6H_3{}^{35}Cl^{35}Cl^{35}Cl$	$\frac{3}{4} \times \frac{3}{4} \times \frac{3}{4} = 27/64$	100	$(0.7576)^3 = 0.4348$	100	68934	100
183	$C_6H_3{}^{35}Cl^{37}Cl^{35}Cl$ $C_6H_3{}^{37}Cl^{35}Cl^{35}Cl$ $C_6H_3{}^{35}Cl^{35}Cl^{37}Cl$	$(\frac{3}{4} \times \frac{3}{4} \times \frac{1}{4}) \times 3 = 27/64$	100	$(0.7576 \times 0.7576 \times 0.2424) \times 3 = 0.4174$	96	63104	91.5
185	$C_6H_3{}^{37}Cl^{37}Cl^{35}Cl$ $C_6H_3{}^{37}Cl^{35}Cl^{37}Cl$ $C_6H_3{}^{35}Cl^{37}Cl^{37}Cl$	$(\frac{3}{4} \times \frac{1}{4} \times \frac{1}{4}) \times 3 = 9/64$	33	$(0.7576 \times 0.2424 \times 0.2424) \times 3 = 0.1335$	30.7	20717	30.05
187	$C_6H_3{}^{37}Cl^{37}Cl^{37}Cl$	$(\frac{1}{4} \times \frac{1}{4} \times \frac{1}{4}) = 1/64$	3.7	$(0.2424)^3 = 0.0142$	3.3	2241	3.3

3.4.1.4 Calibration Gas

Figure 3.33 shows the spectrum for the calibration gas, at $E/N = 200$ Td. The integration

time was 60 s. The protonated parent ions decreased at higher E/N, whilst m/z 51, 75, 77,

91, 95, 103, 111 and 129 all appear as predicted by the previous study of fragmentation of

the compounds. (The peak at m/z 169 is 1,3-dinitrobenzene, (m.w. = 168.017 amu,

protonated m.w. = 169.024 amu), still resident in the reaction chamber nine days after

colleagues had been investigating this.)

Figure 3.33: Calibration gas spectrum at $E/N = 200$ Td

3.4.2 Discussion

Table 3.9 shows the percentage of MH$^+$ and product ions assigned to the five chlorobenzene compounds at E/N =140 Td and 245 Td. Trichlorobenzene appears to be the most stable, having 61% of MH$^+$ remaining at E/N = 245 Td. As can be seen from the branching ratios, the percentage of a species at intermediate E/N values can be more, or less, than that found at E/N = 245 Td.

Table 3.9: Percentage product ions of chlorobenzenes at E/N = 140 Td and 245 Td.
Shaded rows are the MH$^+$ m/z values: 113 = chlorobenzene (CB) 147 = dichlorobenzenes (DCB) and 181 = 1,2,4-trichlorobenzene (TCB)

m/z	Proposed Formula	CB C_6H_5Cl Td		o-DCB 1,2-$C_6H_4Cl_2$ Td		m-DCB 1,3-$C_6H_4Cl_2$ Td		p-DCB 1,4-$C_6H_4Cl_2$ Td		1,2,4-TCB 1,2,4-$C_6H_3Cl_3$ Td	
		140	245	140	245	140	245	140	245	140	245
39	$C_3H_3^+$	-	4	-	9	-	9	-	9	-	-
50	$C_4H_2^+$	-	10	-	-	-	-	-	-	-	-
51	$C_4H_3^+$	-	15	-	-	-	-	-	-	-	-
65	$C_5H_5^+$	-	-	-	4	-	4	-	4	-	-
73	$C_6H_3^+$	-	-	-	-	-	-	-	-	-	8
75	$C_6H_3^+$	-	-	-	26	-	27	-	27	-	-
77	$C_6H_5^+$	-	42	-	-	-	-	-	-	-	-
94				-	2	-	2	-	2	-	-
95		1	1	-	-	-	-	-	-	-	-
99				-	-	-	-	-	-	-	7
109	$C_6H_2Cl^+$	-	-	-	-	-	-	-	-	-	5
111	$C_6H_4Cl^+$	-	-	-	17	-	17	-	17	-	-
113	$C_6H_6Cl^+$	100	28	-	4	-	4	-	4	-	-
128				-	-	-	-	-	-	-	5
129				-	2	-	2	-	2	-	-
146	$C_6H_4Cl_2^+$									-	15
147	$C_6H_5Cl_2^+$			100	40	100	40	100	39		
181	$C_6H_4Cl_3^+$									100	61

The spectra of chlorine-containing compounds are generally easy to identify as they always display at least two peaks separated by 2 amu in height ratios that relate to the relative abundance of the isotopes and the number of chlorine atoms in the compound. However,

peaks in these mono- di- and tri-chlorobenzene spectra proved to be much more difficult to assign than those of the alkylbenzenes. The next section analyses the product ions and fragmentation behaviour of these compounds and explains how some unlikely peaks at *m/z* 94/95 and *m/z* 128/129 were identified.

3.4.2.1 Product Ion Analysis

m/z 129 in Dichlorobenzenes

An unexpected peak appeared in the dichlorobenzenes at *m/z* 129 which is 18 amu less than the MH$^+$ peak at *m/z* 147. The isotope peaks of the species at *m/z* 129 have the characteristics of a single chlorinated ion, with two peaks separated by 2 amu in the ratio of 3:1 (Figure 3.34). However, *m/z* 129 cannot be a product ion of MH$^+$ at *m/z* 147, a loss of

Figure 3.34: *p*-Dichlorobenzene spectrum with *m/z*129 peak magnified

18 amu representing a loss of one carbon and six hydrogen atoms. Since the protonated molecule only has four hydrogen atoms, this is clearly an impossible fragmentation pathway.

Figure 3.35: Branching ratios for *p*-dichlorobenzene including *m/z* 129 and *m/z* 94.

The branching ratios for p-dichlorobenzene, including m/z 129, are shown in Figure 3.35.

The peak seen in the PTR-MS was at m/z 129.00: a NIST molecular weight search suggested protonated monochlorophenol, $(C_6H_6ClO^+)$, as the most likely compound, m.w. 129.01 amu (neutral m.w.128.00 amu). Monochlorophenol is a common pollutant in the environment, being widely used in manufacturing processes (El-Sayed *et al.* 2009). The peak at m/z 94 is included in Figure 3.35 as this may have the same origin as m/z 95 in chlorobenzene (see Figure 3.42).

It was not possible to identify this fragment initially. A conclusion was reached but only after extensive work which is described in §3.4.2.1.

m/z 128 and *m/z* 163 in 1,2,4-Trichlorobenzene

This compound displayed a species at m/z 128, with peaks similar to the dichlorobenzenes' m/z 129 peak, and a new compound at m/z 163 (Figure 3.36), possibly a protonated dichlorophenol (DCP), $C_6H_5Cl_2O^+$, m.w. 162.97 amu (neutral $C_6H_4Cl_2O$ m.w. 161.96 amu).

Figure 3.36: 1,2,4-Trichlorobenzene (TCB) at E/N = 210 Td with magnifications of m/z 128 and m/z 163.

TCB Branching Ratios Product Ions

Figure 3.37: Branching ratios for trichlorobenzene (TCB) showing *m/z* 128 and *m/z* 163.

The isotope peaks at *m/z* 163 are characteristic of a compound with two Cl atoms and those at *m/z* 128 show one Cl atom. The behaviour of the *m/z* 128 branching ratio (Figure 3.37) is similar to that of *m/z* 129 in dichlorobenzene (Figure 3.35) and *m/z* 95 in chlorobenzene (Figure 3.42), although it does not show an actual maximum but appears to be levelling out at *E/N* ~245 Td.

Fragments in the Calibration Gas: *m/z* **129 and** *m/z* **94**

The 'unexpected' peak at *m/z* 129 appears in the calibration gas spectrum (Figure 3.38) along with evidence of a contribution to *m/z* 94, the ^{13}C peak for toluene (see §3.4.1).

Figure 3.38: Calibration gas at *E/N* = 200 Td with an enlargement of *m/z* 129

m/z 111 $C_6H_3Cl^+$

This product ion only occurs in the dichlorobenzenes and a spectrum demonstrates that it

has one chlorine atom (Figure 3.39) where the counts for *m/z* 111 and *m/z* 113 are 39807

Figure 3.39: Spectrum of *m/z* 111 showing isotope peaks
of an ion containing Cl

and 13041 respectively, giving a ratio of 3.05:1. This ion is therefore the result of the loss

of HCl from the parent ion at *m/z* 147:

$$C_6H_4Cl_2H^+ \longrightarrow C_6H_4Cl^+ + HCl$$

m/z 147   *m/z* 111

m/z 109 $C_6H_2Cl^+$

This product ion occurs in trichlorobenzene (Figure 3.40). It has only one chlorine atom

although the size of the peak at *m/z* 111 is rather large. This is probably due to the loss of

HCl from the dichlorobenzene impurity at *m/z* 147.

Figure 3.40: Spectrum of *m/z* 109 showing isotope peaks
of an ion containing Cl

The m/z 109 product ion is the result of the loss of H_2Cl from the product ion at m/z 146:

$$C_6H_4Cl_2^+ \longrightarrow C_6H_2Cl^+ + H_2Cl$$

$$m/z\ 146 \qquad\qquad m/z\ 109$$

m/z 95 in Chlorobenzene

The protonated parent ion, MH^+, for chlorobenzene ($C_6H_5ClH^+$) occurs at m/z 113. The peak at m/z 95.05 is 18 amu less than the MH^+ peak (Figure 3.41) representing a loss of one

Figure 3.41: Chlorobenzene spectrum at 180 Td with m/z 95 peak magnified in b)

carbon and six hydrogen atoms. This would leave a product ion of C_5Cl^+. However, it is clear from the peak pattern (Figure 3.41b) that this fragment does not contain any chlorine atoms as there is no peak at m/z 97 representing the ^{37}Cl isotope. It is therefore very unlikely that this product ion originated from the fragmentation of m/z 113.

A NIST molecular weight search suggests that m/z 95.06 is most likely to be protonated phenol, $C_6H_6OH^+$, molecular weight = 95.049 amu (94.042 amu neutral). The ^{13}C isotope

counts at m/z 96 are 6% of the counts at m/z 95 which accords well with six carbon atoms

(expected 6.6%) and the peak amu is at 95.05 amu. The peak at m/z 97 is much more than

would be expected for the ^{18}O isotope, being 5% of the m/z 95 counts, where only 0.4% is

Figure 3.42: Branching ratios for chlorobenzene including m/z 95.

expected so an accurate identification for phenol cannot be made using this isotope. Figure

3.42 shows the branching ratios for chlorobenzene where m/z 95 is included: this is similar

in shape to that found for m/z 129 in the dichlorobenzenes (Figure 3.35).

m/z 75 $C_6H_3^+$

This product ion is found in the dichlorobenzene spectrum and has no chlorine atoms

(Figure 3.43).

Figure 3.43: Spectrum of m/z 75

It appears to be the result of the loss of HCl from the fragment ion at m/z 111:

$$C_6H_4Cl^+ \longrightarrow C_6H_3^+ + HCl$$

$$m/z \; 111 \qquad\qquad m/z \; 75$$

m/z **73**

Figure 3.44 shows spectra of *m/z* 73 in 1,2,4-trichlorobenzene for a) $E/N = 210$ Td, b) $E/N = 230$ Td and c) $E/N = 245$ Td. It is not clear what the composition of this ion is: in Figure

a)

Figure 3.44: Spectra for *m/z* 73 in 1,2,4-trichlorobenzene at a) $E/N = 210$ Td, b) $E/N = 230$ Td and c) $E/N = 245$ Td

3.44a) and b), there appears to be one Cl atom. However, the single Cl isotope pattern has disappeared at $E/N = 245$ Td (Figure 3.44c). This suggests a possible composition of $C_3H_2Cl^+$, molecular weight 72.984 amu produced as a result of *m/z* 146, $C_6H_4Cl_2^+$, splitting into two ions of $C_3H_2Cl^+$:

$$C_6H_4Cl_2^+ \longrightarrow C_3H_2Cl^+ + C_3H_2Cl^+$$

$$m/z \; 146 \qquad\qquad m/z \; 73 \qquad m/z \; 73$$

However, this does not explain the pattern seen at E/N = 245 Td.

m/z 65

This product ion appears in the dichlorobenzenes as shown in Figure 3.45 for *p*-dichlorobenzene. It is most likely to be produced from *m/z* 94. Possible formulae are C_4OH^+

Figure 3.45: Spectrum of *m/z* 65

(m.w. = 65.003 amu) or $C_5H_5^+$ (m.w. = 65.04 amu). The maximum *m/z* values for this peak are shown in Table 3.10 and the ^{13}C isotope peak at *m/z* 66 in Figure 3.53 is 6% of the peak counts at *m/z* 65 (expected ratio of 5.5% for 5 carbon atoms).

Table 3.10: Peak maximum for *m/z* 65 (wet) relates to the humid conditions described in the Clusters with H_2O section

Compound	Peak *m/z*	E/N /Td
p-DBC (wet)	65.01	190
p-DBC (wet)	65.02	220/245
m-DCB	65.04	190/220/245
o-DCB	65.07	190/220/245
p-DBC (dry)	65.03	170/190
p-DBC (dry)	65.04	220/245

From these data, it can be inferred that this peak represents the $C_5H_5^+$ ion, resulting from the following reaction:

m/z 39 C₃H₃⁺

This product ion appears in the spectra of the chloro- and dichlorobenzenes. The peak at

m/z 39 in the PTR spectrum is generally larger than that expected solely as a result of

fragmentation of MH⁺ since it is always present as the isotope of the first water dimer at *m/z*

37, $H_3O^+.(H_2O)$.

Figure 3.46 shows the *m/z* 39 peak to be bigger than that expected for the *m/z* 37 peak: the

Figure 3.46: Spectrum of *m/z* 39 in *p*-dichlorobenzene

presence of *m/z* 37 has been compensated for as explained in §2.4.3. In chlorobenzene, it

seems most likely that *m/z* 39 is produced by the loss of C_3H_2 from *m/z* 77 to form $C_3H_3^+$

(*m/z* 39), the cyclopropenyl ion.

$$C_6H_5^+ \longrightarrow C_3H_3^+ + C_3H_2$$

m/z 77   *m/z* 39

In the dichlorobenzenes it is possible that this is formed by fragmentation of *m/z* 111 which

loses C_3HCl:

$$C_6H_4Cl^+ \longrightarrow C_3H_3^+ + C_3HCl$$

m/z 111   *m/z* 39

3.4.2.1 Identifying Product Ion Fragments *m/z* 95 and 128/9

The procedure adopted to identify the origins and structures of fragments at *m/z* 95, 128 and

129 beyond all reasonable doubt was firstly, to consider if they were impurities: the purity of

all of the chlorobenzene chemicals was specified as > 99% (Table 3.3). However, the PTR-TOF-MS is able to detect impurities in the sample (~ 1%), especially if the vapour pressure of such an impurity is 100 times that of the compound under investigation. In these circumstances, they would have the same concentration in the drift tube, sufficient to present uncertainties when examining the fragmentation patterns of each of these compounds. Then, if found not to be impurities, to investigate if they could result from secondary reactions and finally if they might be clusters of recognised fragments with water. These lines of enquiry are described below.

Impurities

If these peaks actually represent impurities, there should be a signal at lower E/N values which would reduce with increasing E/N instead of increasing, as found here. Normalised counts for m/z 95 in chlorobenzene and m/z 129 in p-dichlorobenzene are shown in Figures 3.47 and 3.48.

Figure 3.47: m/z 95 counts normalized to 10^6 H_3O^+counts

p-Dichlorobenzene *m/z* 129 Normalised to 10^6 (19+37)

Figure 3.48: *m/z* 129 counts normalised to 10^6 ($H_3O^+ + H_3O^+.(H_2O)$)

The shape of the curve warranted further investigation – if this were an impurity, there would have been more of it present at lower *E/N* values and it was necessary to check how phenol itself behaved in a changing *E/N* scenario. The curve in Figure 3.49 was obtained for normalised counts of phenol at *m/z* 95: the MH^+ counts decreased as *E/N* was increased. So it seems unlikely that the species at *m/z* 95 is an impurity in chlorobenzene and the calibration gas.

Figure 3.49: Graph of normalized counts for phenol.

Also, for completeness, the vapour pressures for each of the monochlorophenol isomers are given in Table 3.11. The vapour pressure of *p*-DCB is 234.7 Pa @ 275 K ((ATSDR) 1998) which is of the same order of magnitude as two of the monochlorophenols, indicating that if

Table 3.11: Vapour pressures of the three monochlorophenol isomers

	2-MCP ortho	3-MCP meta	4-MCP para
Vapour pressure	139 Pa at 25 °C	125hPa at 25 °C	51 Pa at 25 °C

these peaks represent the phenols, then it would be possible for them to be detected in the PTR-TOF.

By way of comparison with the behaviour of m/z 95, the peak at m/z 46 was similarly investigated. With only C, H and Cl atoms available, it is difficult to find a composition for this ion, as well as being problematical to see how it could be formed from any of the major species. A branching ratio graph including this ion is shown in Fig 3.50 and displays the behaviour of an impurity, appearing as it does at all E/N values. It is not clear why there is a sudden increase in both this ion and m/z 50 after $E/N = 230$ Td.

Figure 3.50: Branching ratios for chlorobenzene with m/z 46

The main piece of evidence leading to the conclusion that these fragments are not impurities is the appearance of both m/z 94 and m/z 128 in the calibration gas as mentioned above.

Secondary Reactions

Having ascertained that a possible compound for m/z 95 in chlorobenzene could be phenol, and that for m/z 129 in dichlorobenzene could be chlorophenol, the possibility presented itself of a pattern emerging whereby one chlorine atom was being replaced by an OH group. These may be regarded as secondary reactions:

$$C_6H_5Cl\,H^+ \;+\; H_2O \;\longrightarrow\; C_6H_5OHH^+ \;+\; HCl$$

Chlorobenzene   Phenol

$$C_6H_4Cl_2\,H^+ \;+\; H_2O \;\longrightarrow\; C_6H_4ClOHH^+ \;+\; HCl$$

Dichlorobenzene   Chlorophenol

However, calculations of the enthalpy, ΔH, for these reactions show that both have positive ΔHs: for the chlorobenzene reaction, $\Delta H = 62.8$ kJ/mol (0.65 eV) and for the dichlorobenzene reaction $\Delta H = 692.54$ kJ/mol (7.2 eV) (see Appendix 1). These results confirm that neither of these reactions can occur spontaneously.

Clusters with H$_2$O

"When you have eliminated the impossible, whatever remains, *however improbable*, must be the truth."

Sherlock Holmes: The Sign of Four (1890) Arthur Conan Doyle

The branching ratios graph for *p*-dichlorobenzene including *m/z* 129 and *m/z* 94 is shown in Figure 3.35 and is repeated here as Figure 3.51.

Figure 3.51: Branching ratios for *p*-DCB highlighting *m/z* 94 and *m/z* 129

Considering just the *m/z* 129 signal in *p*-dichlorobenzene, a further investigation examined *p*-dichlorobenzene in more humid conditions (see Figure 3.52), passing the buffer gas (laboratory air) through water at room temperature. This revealed a moisture dependence,

with the m/z 129 peak yield value being ~ 20% higher in these more humid conditions.

There was also a shift in the peak towards a higher E/N value from 200 to ~ 210 Td.

Branching ratios of m/z 129 in p-DCB

Figure 3.52: Comparison of m/z 129 branching ratios in wet and dry conditions

Using O_2^+ as reagent gas

By way of further confirmation regarding humidity, an E/N investigation of p-dichlorobenzene was carried out using oxygen as the reagent ion (O_2^+) to reduce humidity effects. The parent ion resulting from non-dissociative electron charge transfer with oxygen (O_2^+) appears at m/z 146 as can be seen in Figure 3.53. Peaks for the other product ions, m/z 111, m/z 75 and m/z 50, all appear at the same values as in the samples using H_3O^+. In these conditions, m/z 111 is the result of the loss of a Cl atom. There is no product ion at m/z 129

Figure 3.53: Spectrum of p-dichlorobenzene in oxygen

but there are peaks at m/z 99 and m/z 85 as can be seen in Figure 3.54.

Figure 3.54: Spectrum of p-dichlorobenzene
product ions m/z 85 and m/z 99

Branching ratios for p-Dichlorobenzene in O_2^+ are shown in Figure 3.55.

Figure 3.55: Branching ratios of p-dichlorobenzene in oxygen (O_2^+)

Conclusion

Having concluded that m/z 129 could neither have come from the dissociation of m/z 147

nor from a secondary reaction and that it has one chlorine atom, as can be seen in Figure

3.56, it would appear that the only explanation remaining is that it is a cluster of m/z 111

($C_6H_3Cl^+$) with an H_2O molecule. This structure ($C_6H_3Cl^+$).H_2O is surprising as such a

construct would seem to be most unlikely to form at such high E/N values. Further

investigation is warranted here.

3.5   Sensitivity Results

The calibration gas was studied using two different procedures as described in §3.2.2: varying

E/N holding the DT pressure constant, and holding E/N constant and varying the DT pressure.

The data from the foregoing work was used to apply fragmentation coefficients where

compounds fragment, producing an ion at an m/z value of another compound's MH^+. This is

described in more detail in the following section.

3.5.1   Fragmentation Correction

Product ions from fragmentation processes contribute signal to other compounds' MH^+ peaks.

For example, styrene, m/z 105, ethylbenzene and the xylenes, m/z 107, and trimethylbenzene,

m/z 121, all yield product ions at m/z 79, the m/z where the protonated benzene parent ion is

found (Table 3.12).

Table 3.12: Compounds that contribute signal to other peaks:

	Contribution from:					
m/z	105	107 Xylenes	107 Ethylb.	121	147	181
79	x	x	x	x		
105		x		x		
107				x		
113					x	
147						x

m/z 105, 107 and 121 contribute to m/z 79;
m/z 107 (xylenes) and m/z 121 contribute to m/z 105;
m/z 147 contributes to m/z 113;
m/z 181 contributes to m/z 147.

In order to account for these contributions the following formula was applied at each E/N:

$$[C^{Corr}] = [C^{MH+}] - \sum_{i=1}^{n} F_i \times C_i$$

Where

C^{Corr} = number of counts for MH^+ corrected for product ion contributions;

C^{MH+} = actual number of counts for MH^+;

C_i = corrected number of counts for the contributing compound;

F_i = fragmentation coefficient of the contributing compound.

A series of such calculations were executed working from the highest to lowest m/z values.

The fragmentation coefficient is the ratio of the percentages of product ion to its remaining

Table 3.13: Branching ratio data extract for ethylbenzene
Showing % ions at m/z 79, 91 and 107 at E/N = 140, 150 and 160 Td

E/NTd	m/z		
	79	91	107
140	37%		63%
150	52%		48%
160	63%	1%	36%

Table 3.14: Non-normalised counts from calibration gas at $E/N = 140$ Td
Isotopes and the M^+ peaks are included.

E/N Td	m/z 79	m/z 93	m/z 105	m/z 107 (Xylenes)	m/z107 (EB)	m/z 113	m/z 121	m/z 147	m/z 181
140	15374	11905	13424	42547	9087	13834	27372	34382	9972

MH^+ at a given E/N. These percentages are taken from the data used to plot the branching ratio curves. An extract of this data is shown in Table 3.13 for ethylbenzene. From this and Table 3.14 it can be seen that the adjusted counts for m/z 79 at $E/N = 140$ Td are:

$$C^{Corr} = 15374 - \frac{37}{63} * 9087 = 10053$$

C_i is described as being 'corrected' as it may itself have received a contribution from another compound's product ion. For example, at $E/N = 200$ Td, styrene (m/z 105) fragments to yield a product ion at m/z 79 but has itself gained contributions from the di- and trimethylbenzenes (m/z 107 and m/z 121). All isotopes were included in these calculations as well as any signal at M^+ appearing as a result of non-dissociative charge transfer from the oxygen present in the system.

Initially, m/z 93 produced an unfeasibly high result at high E/N values. As can be seen in the foregoing, the dichlorobenzenes (m/z 147) fragment to yield a product ion at m/z 94 which had to be excluded from the calculations. This was resolved by calculating the isotope counts at m/z 94 directly from the counts at m/z 93, considered to be purely attributable to protonated toluene:

$$[\text{Counts at } m/z \text{ 94}] \quad = \quad [\text{Counts at } m/z \text{ 93}] \times 0.077$$

Ethylbenzene and the xylenes at m/z 107 are isobaric: the known ppbv ratio for these compounds was used to assign the counts at m/z 107 to each of these compounds.

Having found the counts for each m/z at a specific E/N value, these counts were then normalised to 10^6 H_3O^+ or 10^6 $(H_3O^+ + H_3O^+ \cdot H_2O)$, depending on the compound's proton affinity and previously established information regarding the specific behaviour of, for example, benzene and toluene (Hayward 2002). It was not possible to ascertain the proton affinity for trichlorobenzene, so it was assumed that it would have a PA similar to that of the other chlorobenzenes and so was normalised only to m/z 19.

3.5.1.1 Varying E/N at Constant Pressure

Figure 3.56 shows two spectra for the calibration gas, the red line E/N = 140 Td and the black line is the spectrum for E/N = 240 Td. The integration time was 60 s in both cases. In all cases, the protonated parent ion decreased at higher E/N, whilst m/z 50, 51, 75, 77, 91, 103, and 111 all appear as predicted by the previous study of fragmentation of the compounds, along with a peak at m/z 169, 1,3-dinitrobenzene, (m.w. = 168.017 amu, protonated m.w. = 169.024 amu), still resident in the reaction chamber nine days after colleagues had been investigating this.

Figure 3.56: Calibration gas spectra at *E/N* values 140 Td and 240 Td.

Sensitivities for the calibration gas compounds over a range of *E/N* values are shown in Figure 3.57 and the data are given in Table 3.15. Figure 3.57a shows the sensitivity without accounting for fragmentation, and Figure 3.57b includes the fragmentation. These show that ignoring the fragmentation of compounds and their contribution to other peaks distorts the results by exaggerating sensitivities, primarily in the compounds most susceptible to fragmentation e.g. ethylbenzene/xylenes, and compounds that receive product ions from several other species.

Table 3.15: Data for sensitivity with fragmentation in Figure 3.56b
Values are normalised counts per second

E/N [Td]	*m/z* 79	*m/z* 93	*m/z* 105	*m/z* 107	*m/z* 113	*m/z* 121	*m/z* 147	*m/z* 181	H_3O^+ (counts/s)	$H_2O.H_3O^+$ (counts/s)
100	28	41	7	20	35	8	18	18	1,198,507	3,951,201
120	8	10	6	7	10	6	7	3	8,507,890	4,125,601
140	5	6	5	6	7	6	5	2	20,194,916	3,193,754
160	5	5	5	5	6	5	4	1	29,649,534	2,025,131
180	4	5	4	5	5	4	3	1	36,912,652	1,178,849
200	3	5	2	4	4	4	2	1	42,464,939	697,470
220	3	4	2	4	3	4	2	1	47,707,494	426,523
240	2	3	1	3	3	2	1	1	52,084,163	297,105

a)

b)

Figure 3.57: Sensitivity for calibration gas, E/N =120–240 Td at constant pressure = 0.8 mbar where 'Up' refers to results as E/N was increased.
a) no fragmentation correction coefficients applied; b) fragmentation correction coefficients applied.
(19) = counts normalised to 10^6 H_3O^+
(19+37) = counts normalised to 10^6 (H_3O^+ H_3O^+. (H_2O))

The results for benzene and ethylbenzene/xylenes are shown separately in Figures 3.58a) and b). For benzene, the graph shows the over-estimation in the sensitivity results if fragmentation is not taken into account in this type of complex chemical mixture. This is to be expected for most compounds at high E/N values, but for benzene it can be seen that even at 140 Td there is a 50% over-estimation resulting from the fragmentation of ethylbenzene contributing a product ion at m/z 79.

Figure 3.58: Sensitivity a) with and b) without fragments
for a) benzene and b) ethylbenzene/xylenes

Figure 3.58b shows that there is an under-estimation in sensitivity.

It can be seen that the general trend is for the sensitivity to reduce as E/N increases. This increases the velocity of H_3O^+ ions as they traverse the reaction chamber resulting in a reduction in reaction time: reaction time is inversely proportional to E/N.

3.5.1.2 Varying Pressure with Constant E/N

Figures 3.59a) and b) show the sensitivity behaviour with and without fragment correction as the drift tube pressure is varied from 0.8 mbar to 1.32 mbar, and E/N is held at a constant 140 Td by adjusting the relevant voltages. This value of E/N was chosen as this is the most frequently used value in work undertaken here. The only compound to vary as a result of these changes is benzene (m/z 79). This displays a sensitivity where fragmentation is not accounted for (~7–12 ncps ppbv^{-1}) higher than with fragmentation ($\sim$ 4–7 ncps ppbv^{-1}) both values normalised to 10^6 H_3O^+. This is the result of ethylbenzene fragmenting at $E/N = 140$ Td to yield product ions at m/z 79. The effect on ethylbenzene sensitivity results is masked because it is included with the xylenes at m/z 107.

a)

Sensitivity No Fragment Correction E/N 140 Td

b)

Sensitivity with Fragment Correction E/N 140 Td

Figure 3.59: Sensitivity for calibration gas, pressure 0.8 – 1.32 mbar at constant E/N = 140 Td.
a) has no fragmentation correction; b) applies fragmentation correction. Note that benzene (m/z 79) moves from second lowest position with fragments to almost the highest position without fragments

3.5.2 Toluene:Benzene Sensitivity Ratio – Comparison with Theory

In order to check the 'validity' of the data, the sensitivity ratio for benzene and toluene was calculated. The expected ratio of sensitivity for toluene:benzene = 1.2 ± 0.3 (Warneke *et al.* 2001). This is calculated from the rate coefficients in H_3O^+ for benzene ($1.9 \pm 0.4 \times 10^{-9}$ $cm^3/mol/s$) and toluene ($2.2 \pm 0.4 \times 10^{-9}$ $cm^3/mol/s$)

Figure 3.60 shows the results for this sensitivity ratio over the E/N range 100 Td – 240 Td: it falls within the expected values for E/N = 120 Td to 220 Td. The upper curve is corrected for fragmentation; the lower curve has no fragmentation correction. It is not surprising that these graphs are so different, as benzene is particularly affected by contributions from other compounds.

Figure 3.60: Graph showing the ratio of sensitivities for toluene:benzene

3.6 Further Discussion

3.6.1 Variation in Spectra in p-Dichlorobenzene as E/N Increases

An unexpected pattern of spectra was observed for the protonated parent ion during an E/N

investigation of deuterated p-dichlorobenzene, (m/z 151) (Figure 3.61). At E/N = 90 Td, the

Figure 3.61: Deuterated p-dichlorobenzene spectra with changing E/N

Figure 3.62: p-Dichlorobenzene spectra with changing E/N

mass spectrum looks very similar to non-deuterated p-dichlorobenzene (Figure 3.62a). As E/N increases, however, the deuterated species becomes much more complex with MH^+ and isotope peaks appearing at varying m/z values.

The series of spectra for non-deuterated p-dichlorobenzene as E/N varies shows the normal behaviour for isotope ratios (Figure 3.62). However, inspection of the ^{13}C isotope peak at m/z 148 shows a much higher signal than expected. This is related to the peak at m/z 146 produced by non-dissociative charge transfer with oxygen in the system. Not all peaks display this non-dissociative charge transfer peak as can be seen in Figure 3.63 where m/z 94 displays

Figure 3.63: Peaks with and without a non-dissociative charge transfer peak.

a peak at m/z 93, but m/z 99 has no peak at m/z 98. Where such peaks appear, the signal has been included in the counts for the MH^+ peak.

The m/z 146 M^+ peak has a ^{37}Cl isotope peak at m/z 148. Consequently, the peak at m/z 148 consists of the sum of the ^{13}C isotope for MH^+ plus the ^{37}Cl isotope peak for M^+. It should be noted that M^+ has a ^{13}C isotope at m/z 147 which also must be removed from the MH^+ signal (Table 3.16). This shows that the ratio of the actual counts for the peaks at m/z 147 and m/z

Table 3.16: Actual and adjusted counts in p-dichlorobenzene at 230 Td for peaks at m/z 146 to m/z 148

	m/z 146	m/z 147	m/z 148	148:147
Actual counts	20112	105983	20482	19.32%
^{13}C isotope from m/z 146		1327		
Adjusted counts		104656		
^{37}Cl isotope from m/z 146			13408	
Adjusted counts			7074	
Adjusted ratio				6.8%

148 before any adjustments are made is 19.32%. After removing the ^{13}C isotope counts for the peak at M^+ from the counts at m/z 147, and also removing the ^{37}Cl isotope counts at m/z 148 for M^+, the ratio of the adjusted peaks m/z 147 and m/z 148 becomes 6.8%, very close to the expected 6.6% for the six carbon atoms in $C_6H_5Cl_2^+$.

3.6.2 Anomalies for m/z 85 and m/z 87

These product ions appear in the dichlorobenzenes and their spectra change as E/N changes (see Figure 3.64). If the spectrum is examined at $E/N = 240$ Td there appears to be an ion at

Figure 3.64: Spectra of m/z 85 and m/z 87 at $E/N =$ a) 190 Td, b) 210 Td and c) 240 Td

m/z 85 with two chlorine atoms; if inspected at $E/N = 190$ Td, there seems to be an ion at m/z 87 with one chlorine atom. These product ions make only a very small contribution to the whole branching ratio picture and so have been excluded from the BR graph.

3.6.3 PTR-MS vs. Electron Impact Mass Spectra

Results for the highest E/N values become similar to those found in electron impact (EI) spectra: a comparison of both mass spectra shows that many product ions occur at the same m/z, apart from M^+ which appears, as expected, at $(m+1)/z$ in the PTR spectrum (Figure 3.65). This result is surprising considering the very different energy conditions in the two processes:

a)

Benzene, chloro-
MASS SPECTRUM

NIST Chemistry WebBook (http://webbook.nist.gov/chemistry)

b)

Chlorobenzene 245 Td

Figure 3.65: Spectra for chlorobenzene
for a) electron impact and b) PTR showing relative intensities

EI takes place at ~70 eV and proton transfer at energies of ~ 2eV.

The two different types of reactions can be described in the following way.

For EI ionisation the following reaction takes place:

$$e^- + M \longrightarrow (M^+)^* + 2e^-$$

where M = analyte, e^- = electron and * represents an excited species.

$(M^+)^*$ may then fragment, either sequentially or in parallel, into $(A+)^*$, B^+, C^+, etc.:

$$(M^+)^* \quad \begin{cases} (A^+)^* \\ | \\ B^+ \\ | \\ C^+ \end{cases}$$

The parent peak and fragments appear at m/z, where m = molecular weight and z = charge.

For proton transfer reactions, the following reaction occurs:

$$H_3O^+ + M \longrightarrow (MH^+)^* + H_2O$$

In this case, the parent peak appears at $(m+1)/z$. If sufficient energy is available after protonation, $(MH^+)^*$ can fragment further:

$$(MH^+)^* \longrightarrow A^+ + B \text{ (e.g. } H_2),$$
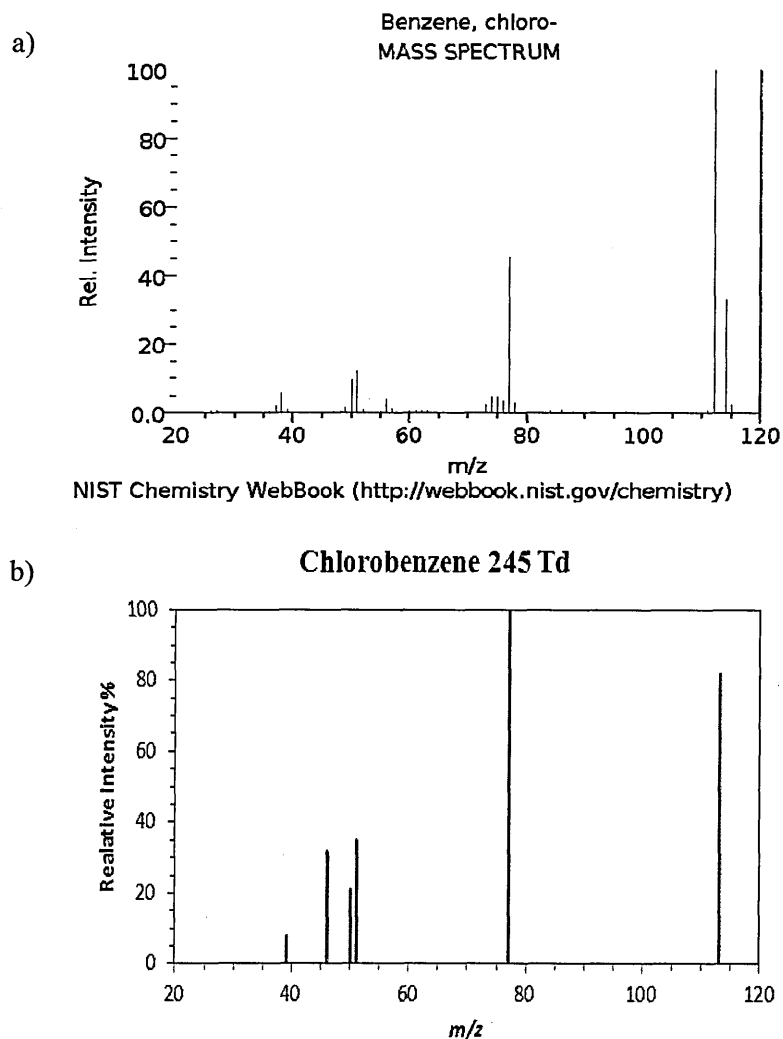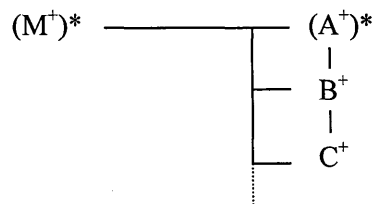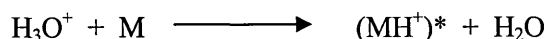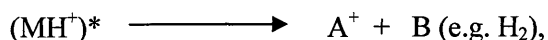
The surplus collisional energy can then result in A^+ fragmenting in the same way as that observed in EI, resulting in fragments appearing at m/z, rather than the protonated $(m+1)/z$ normally seen in PTR-MS.

3.7 Conclusion

Sensitivity measurements for E/N = 90 Td to 245 Td and m/z = 79 to 181 found a value of 4-6 ncps ppbv^{-1} normalised to 10^6 H_3O^+. Each of the 14 compounds in the calibration gas used here was separately investigated over the same E/N range to establish fragmentation behaviour and possible interfering contributions. Several were found to have product ions occurring at m/z 79, mostly occurring at higher energy levels (E/N > 160 to 170 Td). Ethylbenzene was a notable exception: it is reduced by ~ 40% at E/N = 140 Td producing m/z 79. Other effects became apparent on closer inspection of these data: an unlikely cluster formed in the di-chlorobenzenes at m/z 129 appears to be formed by a product ion at m/z 111 ($C_6H_4Cl^+$) associating with a molecule of water, H_2O. This is especially puzzling as it only appears at higher E/N values, reaching a peak at ~ 200 Td. The isomeric compounds ethyl benzene and xylenes produce very different fragmentation patterns in a wide energy range, so enabling

their possible differentiation, although the individual xylene isomers cannot be distinguished

using this method

Page 112

Chapter 4 – Hexenols

"[The] structural theory is of extreme simplicity.... this theory has always proved capable of providing a different structure for every different compound ... there are never more isomeric forms than the theory permits."

Nevil Vincent Sidgwick

Presidential Address to the Chemical Society (16 Apr 1936),

Journal of the Chemical Society (1936),

4.1 Introduction

The C_6 unsaturated alcohols (hexenols) form part of the hexenal family, a series of volatile compounds whose characteristic odour is that of cut grass. This work examines the effect of energy changes in the PTR-TOF-MS on all four of the hexen-1-ol isomers, *cis*-2-hexen-1-ol, *trans*-2-hexen-1-ol, *cis*-3-hexen-1-ol ('leaf alcohol') and *trans*-3-hexen-1-ol (hereafter referred to as *cis*-2, *trans*-2, *cis*-3 and *trans*-3).

These species are found in the atmosphere, being produced by the leaves of many plants during the course of wounding, drying and pathogen attack. In this latter case, *cis*-3 is found as a signalling chemical to trigger defence responses (Heiden 2003, Hatanaka 1993, Farag 2005 and Laothawornkitkul 2009). Investigations in the 1950s and '60s showed that the presence in the atmosphere of small amounts of these and other biogenic VOCs contribute to ozone formation (Fall 1999a). These examples illustrate the interdisciplinary nature of investigations involving these VOCs and are of interest to atmospheric chemists with respect to modelling regional and global VOC emisions (e.g. Guenther 1999), botanists regarding VOC roles in plant biology and ecology, and entomologists are concerned with VOCs as signalling agents (reviewed by Laothawornkitkul 2009).

Studies of hexenols also appear in other application areas involving complex chemical environments, such as flavour analysis (Aharoni 2000, Buhr 2002) and fragrance synthesis (Froissard 2011 and Ibdah 2011). It is particularly important to be able to identify the full range of active components in flavour analysis where efforts have been made to relate molecular structure to aroma since at least 1971 (Bedoukian 1971, Blake 2009).

Various techniques have been used to examine these compounds, *viz.* GC-MS for *cis*-3 (Heiden *et al.* 2003), selected ion flow tube-MS (SIFT-MS) studies of *cis*-2 and the 3-hexen-1-ols (Schoon *et al.* 2007), FA-SIFT-MS experiments with *cis*-3 and *trans*-2 (Dhooghe *et al.* 2009) and all four isomers (Dhooghe *et al.* 2012), and, most pertinently for this study, proton transfer reaction mass spectrometry: Demarcke 2010 (*cis*-2 and *trans*-3), Buhr 2002 (*cis*-3) and Fall *et al.* 1999b (*trans*-2 and 3-hexen-1-ols).

There has been much interest of late in studying how changing the collisional energy conditions within the reaction chamber of a PTR-MS influences the product ion branching ratios (Brown *et al.* 2010, Demarcke 2010, Ennis *et al.* 2005). This work advances that of previous researchers (Fall *et al.* 1999b, Demarcke *et al.* 2010) by studying all four of the hexenol isomers over a wider E/N range on a PTR time of flight instrument. Fall *et al.* examined the fragmentation patterns of the *cis*-3, *trans*-3 and *trans*-2 isomers in a quadrupole PTR-MS instrument. The E/N at which this was carried out was not specified but is considered most likely to be 120 Td. These results are summarised in Table 4.1. Demarcke *et al.*'s work also used a quad PTR-MS and covers the E/N range of 80 Td to 140 Td for *cis*-3 and *trans*-2. Details of this work are also given in § 4.4.

Table 4.1: Research to date for hexen-1-ols
Analysed by author, instrument and buffer gas for SIFTs, the product ions detected (m/z) and which isomers were inspected. Not all of the product ions were found for all of the isomers listed for an author.

Work Done By	Instrument (Buffer gas)	*m/z*	Hexenol(s)
Fall *et al.*(1999b)	PTR-MS quad	55 ($C_4H_7^+$), 69 ($C_5H_9^+$)* 83 ($C_6H_{11}^+$) 101 ($C_6H_{12}OH^+$)	*Cis*-2, *trans*-3 and *trans*-2
Buhr *et al.* (2002)	PTR-MS quad	55, 83 84 ($C_5H_9^+$)[a]	*Cis*-3
Demarcke *et al.* (2010)	PTR-MS quad	39 ($C_3H_3^+$) 41 ($C_3H_5^+$) 55, 83, 101, 119	*Cis*-3 and *trans*-2
Custer *et al.* (2003)	FA-SIFT (He)	67 ($C_6H_{11}^+$)* 69 ($C_5H_9^+$)* 81 ($C_6H_9^+$)* 83 99 ($C_6H_9OH^+$ or $C_7H_{15}^+$) 101	*Cis*-2, *trans*-3 and *trans*-2
Schoon *et al.* (2007) Noted that no MH+ for 2-hexen-1-ols	SIFT (He)	83, 99, 101	*Cis*-2, *cis*-3, *trans*-2 and *trans*-3
Dhooghe *et al.* (2009)	FA-SIFT (Ar)	83, 101, 119 ($C_6H_{12}OH^+(H_2O)$) 137 ($C_6H_{12}OH^+(H_2O)_2$) 155 ($C_6H_{12}OH^+(H_2O)_3$)*	*Cis*-3 and *trans*-2
Dhooghe *et al.* (2012)	FA-TMS (Ar)	29 (C3H5+)†* 31 (C3H7+)†*, 41† 43 ($C_3H_7^+$)† 53 ($C_4H_5^+$), 55, 83	*Cis*-2, *cis*-3, *trans*-2 and *trans*-3. (Data from CID of *m/z* 83)

* = Product ions not seen in this work
† = Product ions only seen at energies > 2eV
[a] = Could be the isotope for *m/z* 83

4.2 Experimental

4.2.1 The Hexenol Isomers $C_6H_{11}OH$

Hexenol has the molecular formula $C_6H_{11}OH$. The structures of the four isomers investigated in this PTR-MS study are shown in Figures 4.1a) to d).
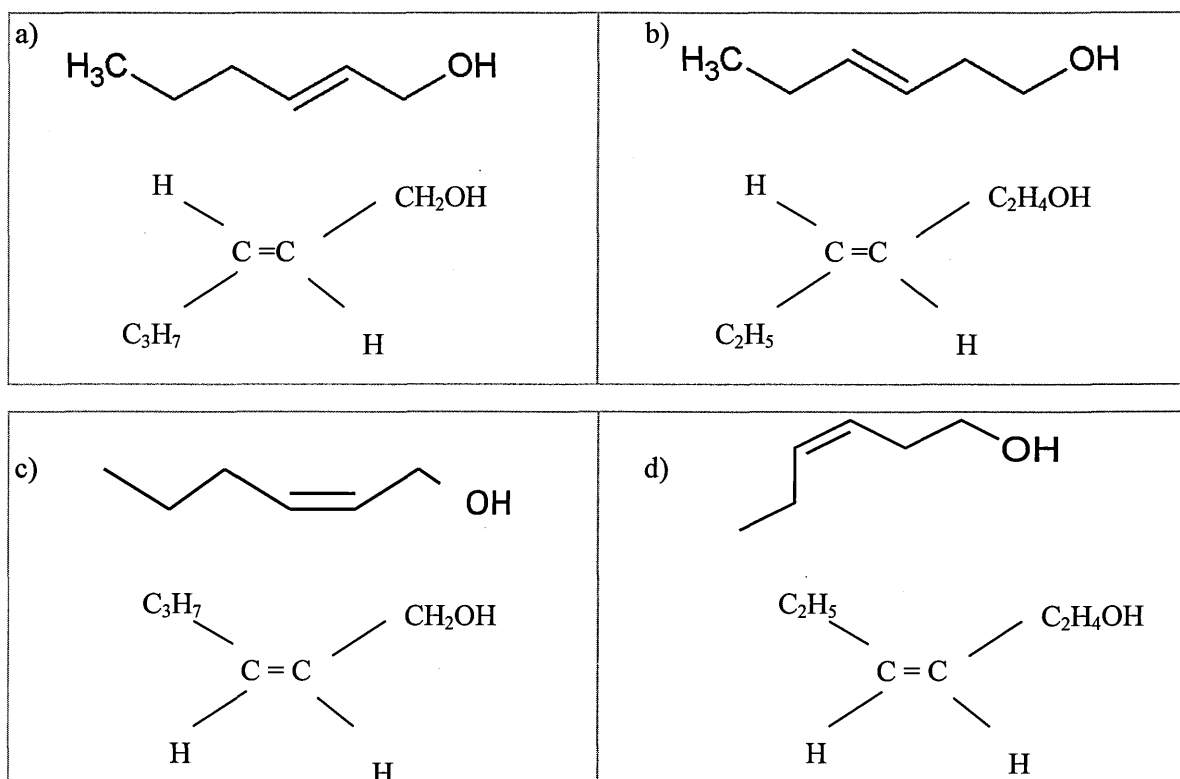
Figure 4.1: Schematic structures of the four hexen-1-ol isomers:
a) *Trans*-2-hexen-1-ol (*E*-2-hexen-1-ol); b) *Trans*-3-hexen-1-ol (*E*-3-hexen-1-ol); c) *Cis*-2-hexen-1-ol (*Z*-2-hexen-1-ol); d) *Cis*-3-hexen-1-ol (*Z*-3-hexen-1-ol)

The *trans*-hexenols have the substituent groups on differing sides of the carbon chain, whereas in the *cis*-hexenols, these groups are on the same side of the C chain.

Chemicals were obtained from Sigma-Aldrich (purities ≥ 99%) and used with no further purification.

4.2.2 Set-up

A syringe and syringe drive were used to introduce each sample into the reaction chamber of the PTR-TOF-MS which was held at a temperature of 303 ± 1 K and a pressure of 1.0 mbar. 1 mL of sample was deposited onto cotton wool inside the syringe (Figure 4.2). This was then
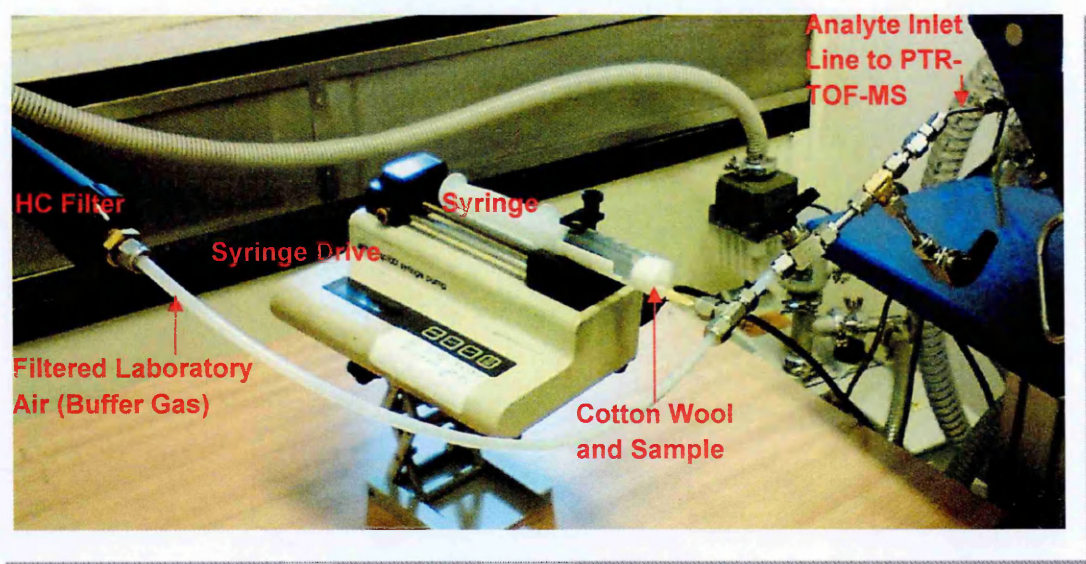
Figure 4.2: Experimental set-up for hexenols

filled with filtered lab air (Agilent HC trap HT200-4) and the syringe needle was inserted into a septum connected to a ¼ in Teflon tube through which filtered laboratory air was flowing. The Teflon tube was connected to the PTR-TOF-MS inlet needle valve using Swagelok connectors. No further changes were made, for example to reduce humidity, in an attempt to replicate normal operational conditions when field analysis for such chemicals is performed. Fifteen *E/N* settings were used, from 100 Td to 170 Td in steps of 5 Td. Three spectra were taken at each *E/N* value both without (background) and with the analyte. A separate set of identical equipment was used for each chemical.

4.2.3 Data Analysis

4.2.3.1 Background Measurement Correction

Measurements with filtered laboratory air were taken over the same *E/N* range before each isomer was studied. The data for each background *m/z* were subtracted from the analyte *m/z* values.

4.2.3.2 Product Ions Investigated

The product ions investigated here are primarily taken from the work of various authors on the hexenols (Table 4.1). This work sees m/z 117 which is not mentioned in any of the foregoing research. As it is always seen in conjunction with m/z 99 it is presumed to be its hydrate, $C_6H_9OH^+(H_2O)$.

4.2.3.3 Product Ions at m/z 39 and m/z 55

Issues arise when determining product ions at m/z 39 ($C_3H_3^+$ mass 39.0229 amu) and m/z 55 ($C_4H_7^+$ mass 55.0542 amu): with pure water vapour alone in the drift tube, the protonated water dimer's ^{18}O isotope is always present at m/z 39 (39.0327 amu) and the protonated water trimer itself is found at m/z 55 (55.039 amu) (see §2.2.2.1). The resolution of the instrument is insufficient to distinguish such small differences in mass (0.0107 amu for the m/z 37 product ions and 0.0152 amu for those at m/z 55). Methods for dealing with these difficulties are explained below.

- m/z 39 Product ion $C_3H_3^+$

  The method used to estimate the product ion counts at m/z 39 is the same as that used in Chapter 3 for the alkyl benzenes: the ^{18}O isotope counts expected from the water dimer, $H_3O^+.(H_2O)$ at m/z 37 are calculated and subtracted from the actual counts at m/z 39. This is satisfactory for E/N values > 140 Td and accounts for the m/z 39 branching ratios starting at $E/N \geq 140$ Td.

- *m/z* 55 Product ion C$_4$H$_7^+$

This *m/z* is slightly easier to deal with than counts at *m/z* 39, since the water trimer signal at *m/z* 55 completely disappears as *E/N* becomes greater than ~ 120 Td, based on investigations using only purified air in the drift tube (see §2.2.2.1).

The signal at *m/z* 56, the ^{13}C isotope of C$_4$H$_7^+$ was used to determine the signal at *m/z* 55 for this product ion, representing 4.4% of the product ion's signal at *m/z* 55. With no analyte (i.e. background counts for just air), the protonated water trimer produces a signal at *m/z* 56 of 0.2% of the signal at *m/z* 55, representing the ^{2}H isotope. These counts were subtracted from the analyte counts at *m/z* 56 and the result was divided by 0.044 to calculate the total expected counts resulting from the fragment C$_4$H$_7^+$.

4.3   Results

4.3.1   2-Hexen-1-ols

4.3.1.1   *Trans*-2-hexen-1-ol

Figure 4.3 shows spectra for *trans*-2 at (a) *E/N* = 115 Td and (b) 170 Td. The (M-H$_2$)H$^+$ product ion at *m/z* 99 and its hydrate at *m/z* 117 can be seen in Figure 4.3a). There is a very small signal at *m/z* 101, at 115 Td which may be the protonated parent. The peak at *m/z* 55 for *E/N* = 115 Td contains a significant amount of the protonated water trimer, H$_3$O$^+$.(H$_2$O)$_2$. However, at 170 Td, the contribution from this has almost completely disappeared, based on investigations using only purified air in the drift tube, leaving only the signal from the product ion C$_4$H$_7^+$. This applies to all of the isomers.

a)

Trans-2-hexen-1-ol 115 Td

Counts /30s

8000
7000
6000
5000
4000
3000
2000
1000
0

55
$C_4H_7^+$

83
$(M-H_2O)H^+$

$(M-H_2)H^+$
99

$(M-H_2).(H_2O)H^+$
117

$C_3H_3^+$
39

30   40   50   60   70   80   90   100   110   120
m/z

b)

Trans-2-hexen-1-ol 170 Td

Counts /30s

3000
2500
2000
1500
1000
500
0

55

83

39
$C_3H_5^+$
41
43

99

30   40   50   60   70   80   90   100   110   120
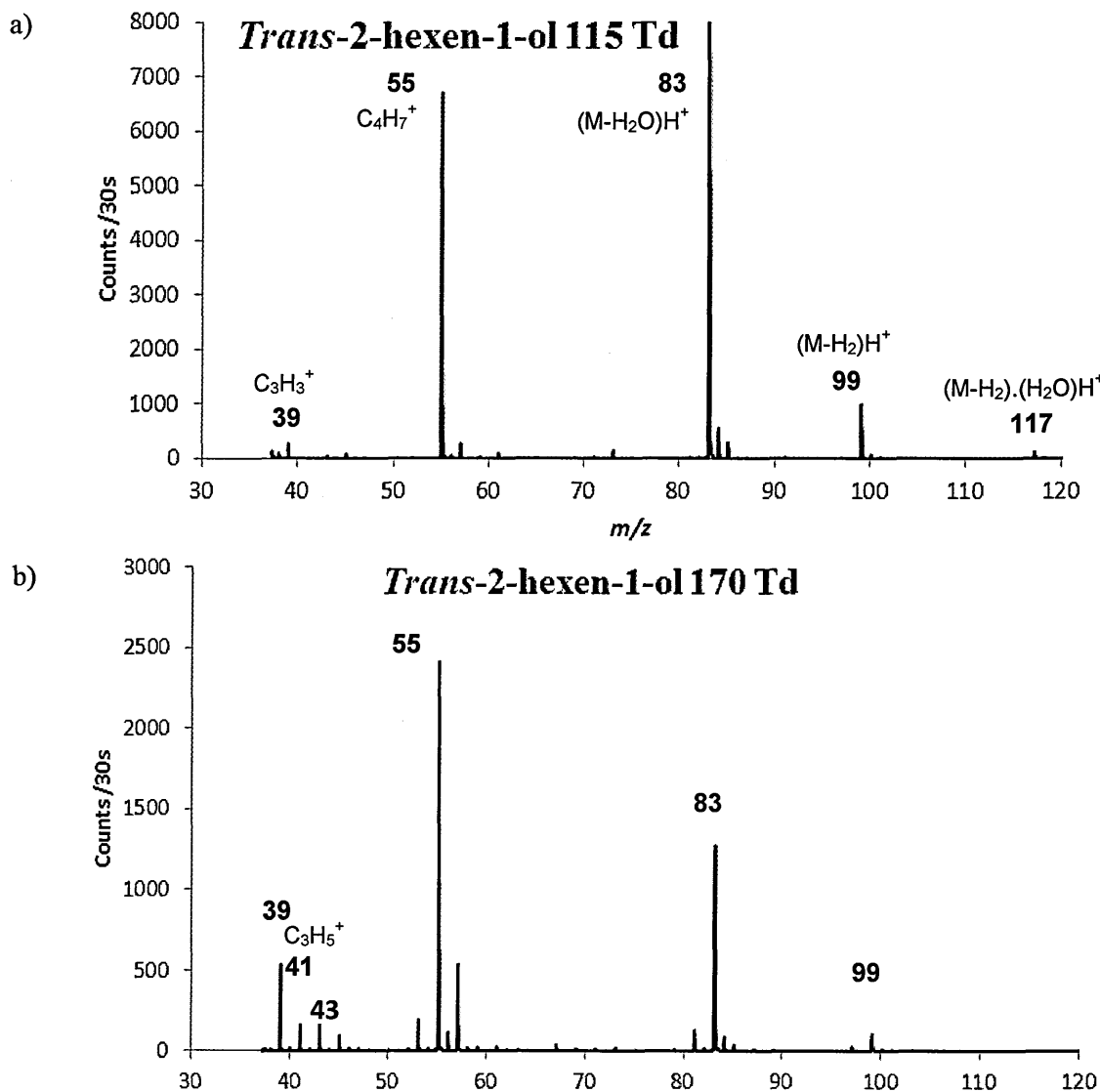
Figure 4.3: Spectra for *trans-2* at a) 115 Td and b) 170 Td
The product ion at *m/z* 99 is seen in a) with its hydrate at *m/z* 117 and
is much reduced at *E/N* 170 Td in b). The product ion at *m/z* 117 has
completely disappeared. Product ion at *m/z* 41 is absent at lower *E/N*
values. There is a very small peak for MH⁺ at 115 Td. (Note the
different counts scales for the two graphs.)

Figures 4.4a) and b) illustrate the product ion ratio percentages (branching ratios) for *trans-2* over the full range of *E/N* values from 100 Td to 170 Td. Figure 4.4a) shows the major product ions; Figure 4.4b) displays minor product ions at the lower branching ratio percentages of < 12%.

a)

Trans-2-hexen-1-ol Major Product Ions

b)

Trans-2-hexen-1-ol Minor Product Ions < 12%
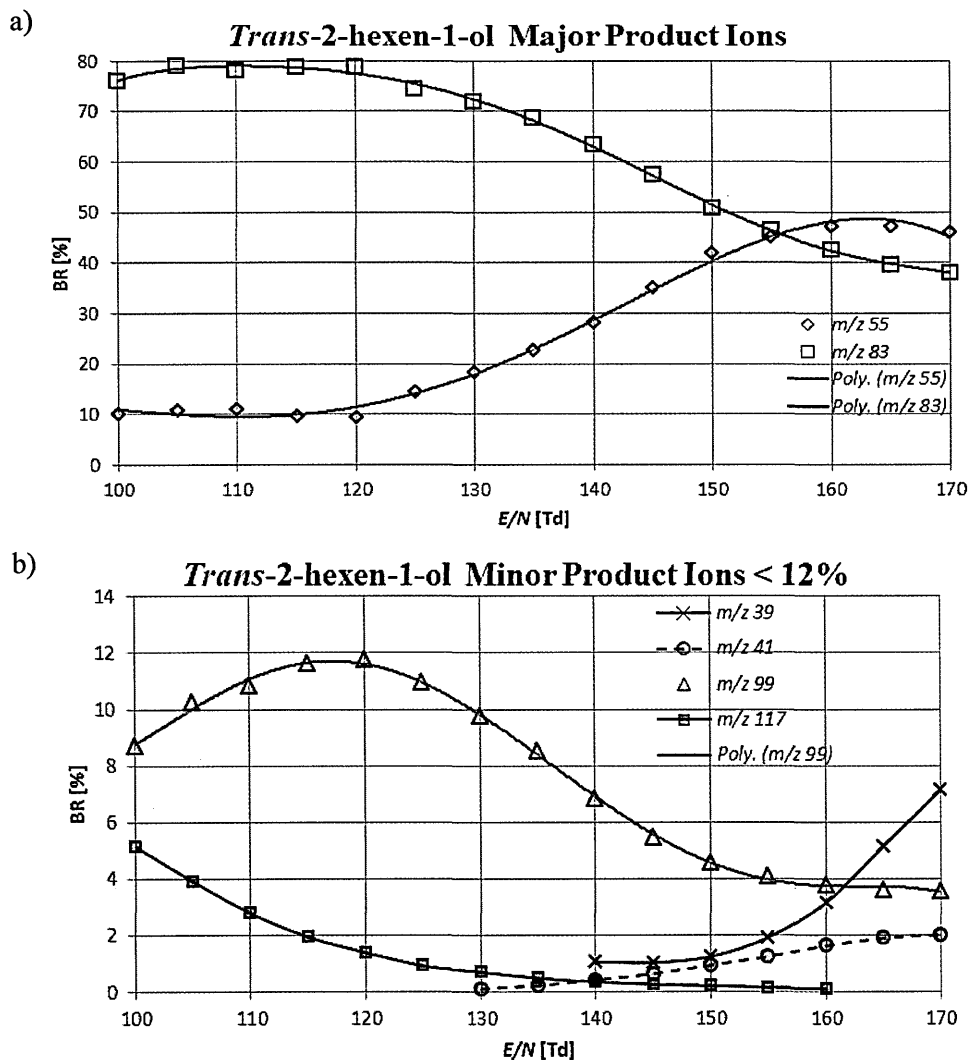
Figure 4.4: Branching ratios for *trans*-2.
b) has an expanded BR % scale.

Demarcke *et al.* 2010 and Fall *et al.* 1999b) investigated *trans*-2 on a PTR-MS (quad), with Demarcke varying E/N from 80 Td to 140 Td. Percentage fragmentations for Fall and Demarcke's results for *trans*-2 at E/N 120 Td are given in Table 4.2 along with those from this work. The Demarcke values are estimated from the product ion distribution graphs in their paper.

In order to enable a comparison of results from this work with those of the above two authors, values are given for E/N = 140 Td, the setting regularly used on this PTR-TOF-MS instrument as the standard where the ratio of m/z 19:m/z 37 < 10%. (For further information, see Chapter 2.)

These results are largely in agreement with those found by Demarcke *et al.* 2010. The main

Table 4.2: Comparison of branching ratios (BR%) for *trans*-2 by Fall *et al.* (1999b), Demarcke *et al.* (2010) and this work. Demarcke's data estimated from their product ion distributions.

	Trans-2							
m/z	39	41	55	69	83	99	101	117
Demarcke *et al.*[*]	-	< 1%	18%	-	79%	-	-	-
Fall *et al.*[†]	-	-	23%	0.8%	76%	-	0.2%	-
This work[+]	1%	< 1%	28%	-	63%	7%	-	<1%

[*] E/N = 120 Td has been used to enable comparison with Fall 1999b.
[†] No E/N value reported
[+] E/N = 140 Td for comparative moisture levels

difference is the product ion at *m/z* 99 which is found in this work but is not mentioned at all by Demarcke.

Trans-2 has also been investigated in FA-SIFT instruments by Dhooghe *et al.* 2009 and Custer *et al.* 2003. The latter study finds major product ions at *m/z* 83 and 55, and minor ions at *m/z* 101, 99 and 95. No further details are given, except that the minor product ions are present at less than half the intensity of the major product ions. Dhooghe *et al.* 2009 react *trans*-2 with $H_3O^+.(H_2O)_n$ for n = 0 to 3. Their results are given in Table 4.3. Of the

Table 4.3: Summary of FA-SIFT results for *trans*-2 from Dhooghe *et al.* (2009) Reactions with *trans*-2 showing % yield of product ions and the mechanisms by which they form.

Reaction	Product ion *m/z*	%	Mechanism	
H_3O^+	83	99	Proton transfer with loss of H_2O:	$M + H_3O^+ \rightarrow C_6H_{11}^+ + 2H_2O$
$H_3O^+.(H_2O)$	83	~100	Dissociative proton transfer:	$M + H_3O^+.(H_2O) \rightarrow C_6H_{11}^+ + 3H_2O$
$H_3O^+.(H_2O)_2$	101	4	Non-dissociative proton transfer:	$M + H_3O^+.(H_2O)_2 \rightarrow MH^+ + 3H_2O$
	119	N	Ligand switching with loss of H_2O:	$M + H_3O^+.(H_2O)_2 \rightarrow MH^+.(H_2O) + 2H_2O$
	137	N	Ligand switching:	$M + H_3O^+.(H_2O)_2 \rightarrow MH^+.(H_2O)_2 + H_2O$

M = Parent molecule $C_6H_{11}OH$
N = No data given

ions described by Dhooghe, this work only finds *m/z* 83 and Dhooghe does not find *m/z* 99.

4.3.1.2 *Cis*-2-hexen-1-ol

Figure 4.5 shows spectra for *cis*-2 at a) $E/N = 115$ Td and b) 170 Td. As found for the *trans*-

a)

b)
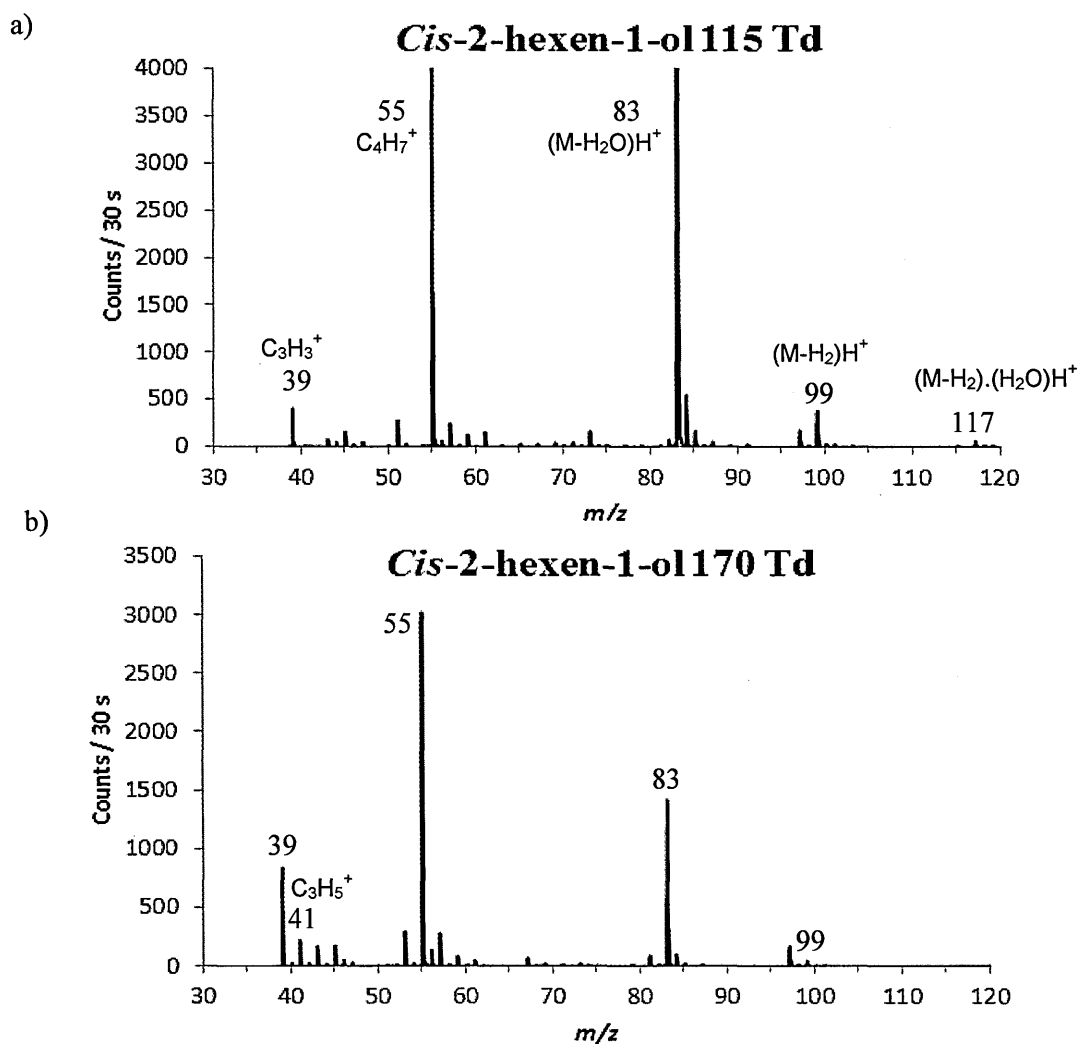
Figure 4.5: Spectra for *cis*-2 at a) 115 Td and b) 170 Td. The product ion at *m/z* 99 is seen in a) with its hydrate at *m/z* 117 but these have mostly disappeared at E/N 170 Td in b); *m/z* 41 is absent at lower *E/N* values.

2 fragmentation, there is a very small protonated parent signal, *m/z* 101 at 115 Td. The (M-H)H$^+$ product ion at *m/z* 99 can be seen in Figure 4.5a) and the hydrate signal at *m/z* 117 is also discernible but has disappeared completely at $E/N = 170$ Td.

The product ions found over the full energy range for cis-2 are m/z 99, 83, 55, 41 and 39 and the branching ratios for the major product ions are shown in Figure 4.6a). Figure 4.6b) shows the minor product ions with branching ratios < 10%.

a)

Cis-2-hexen-1-ol Major Product Ions

b)

Cis-2-hexen-1-ol Minor Product Ions < 10%
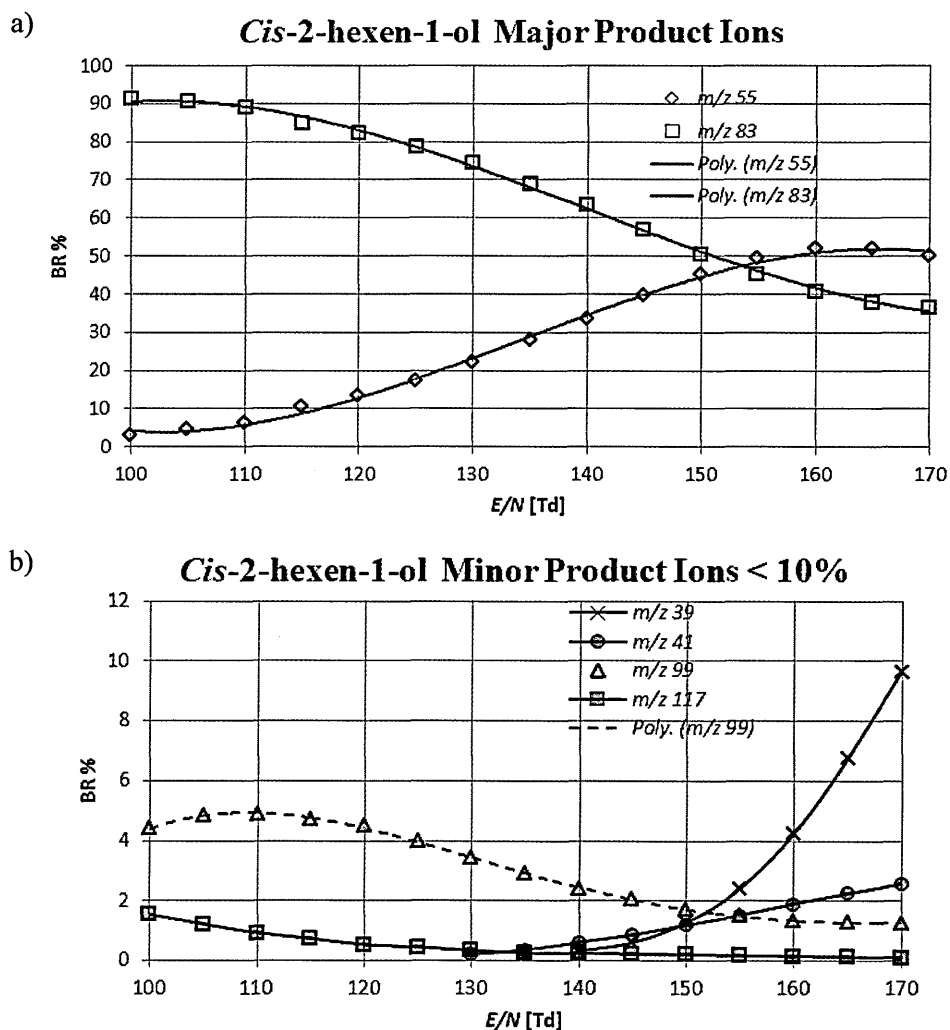
Figure 4.6: Branching ratios for cis-2.
Product ions in a) and b) are shown at different scales of BR percentages. No protonated parent ion (m/z 101) appears.

There is very little work reported in the literature concerning cis-2. Two groups report on all four isomers: a FA-TMS study (Dhooghe et al. 2012) which looks only at the CID of the m/z 83 product ion and the SIFT work of Schoon et al. 2007. This is the only group to report m/z 99 as a product ion for either of the 2-hexen-1-ols and consider it to be $(M-H)^+$ being a product of the reaction with H_3O^+ with a 3% reaction channel. The current work finds ≈ 5% branching ratio at the lowest energy, 100 Td, which compares favourably with

that result, bearing in mind that the SIFT work is at thermal energies (~ 300 K) and so ions

are less likely to fragment in that system. (Table 2.3, Chapter 2 shows that 100 Td in this

PTR-TOF-MS is equivalent to 1054 K, approximately three times greater than in the SIFT.)

4.3.2 3-Hexen-1-ols

4.3.2.1 *Trans*-3-hexen-1-ol

Figure 4.7a) and b) show spectra for *trans*-3 at E/N = 115 Td and 170 Td. Peaks at m/z 83
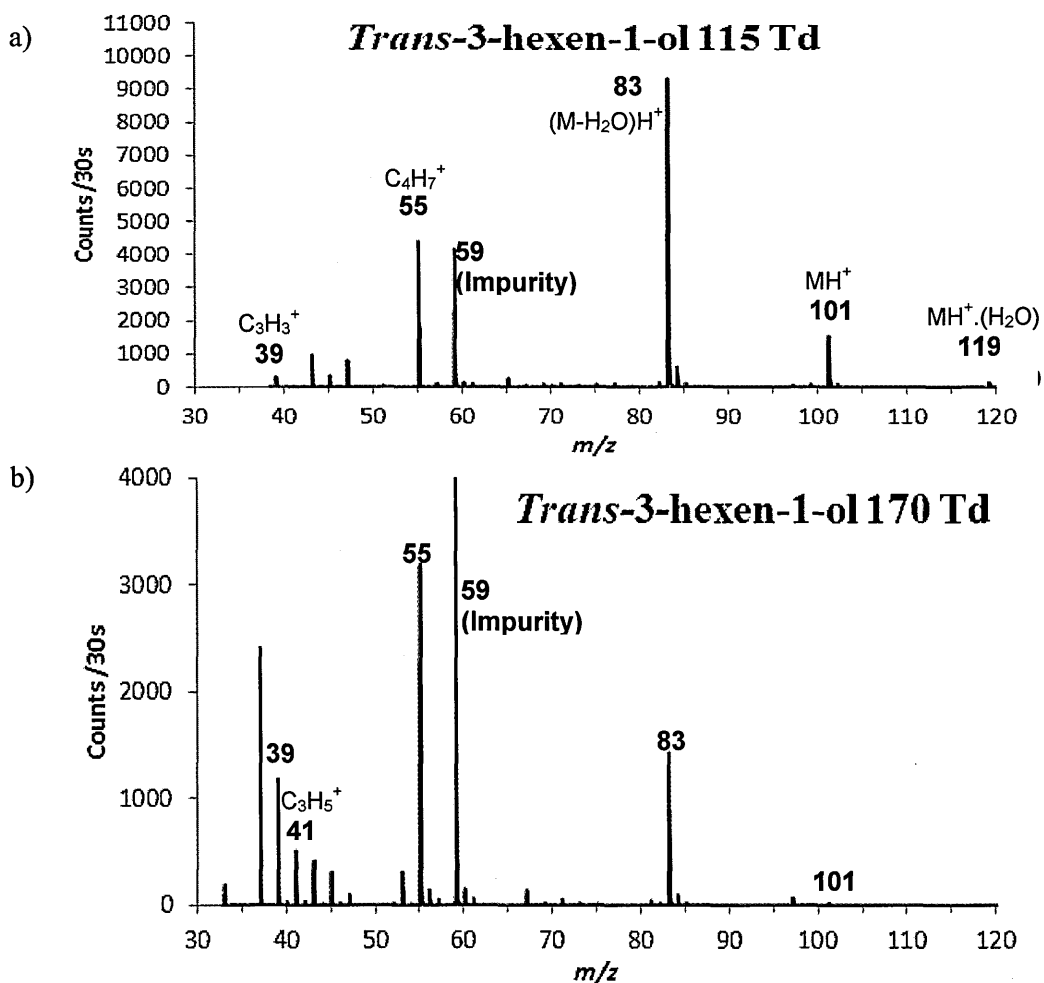
Figure 4.7: Spectra for *trans*-3 at a) 115 Td and b) 170 Td
MH^+ at m/z 101 is clearly seen in a) with its hydrate at m/z 119. The large peak at
m/z 59 in both a) and b) can be seen to be of a similar magnitude, ~ 4000 counts,
and is therefore considered to be an impurity.

and m/z 55 occur in differing ratios at the two E/N values. The protonated parent signal at

m/z 101 is easily visible at E/N = 115 Td but has almost disappeared at E/N = 170 Td. The

large peaks at m/z 59 are most likely to be protonated acetone ($CH_3COCH_3H^+$), an impurity,

---

Page 124

as the signal at this peak value remains fairly constant throughout the collisional energy range. Fall *et al.* 1999b report a large percentage of *m/z* 59 (20%) for this compound, (Table 4.3), commented on by Dhooghe *et al.* 2012 who also consider this to be an acetone impurity.

The branching ratios for *trans*-3 over the full range of *E/N* values are shown for the major product ions in Figure 4.8a) and enhanced for the minor product ions at branching ratios < 12% in Figure 4.8b).

a)

Trans-3-hexen-1-ol Major Product Ions

b)

Trans-3-hexen-1-ol Minor Product Ions < 16%
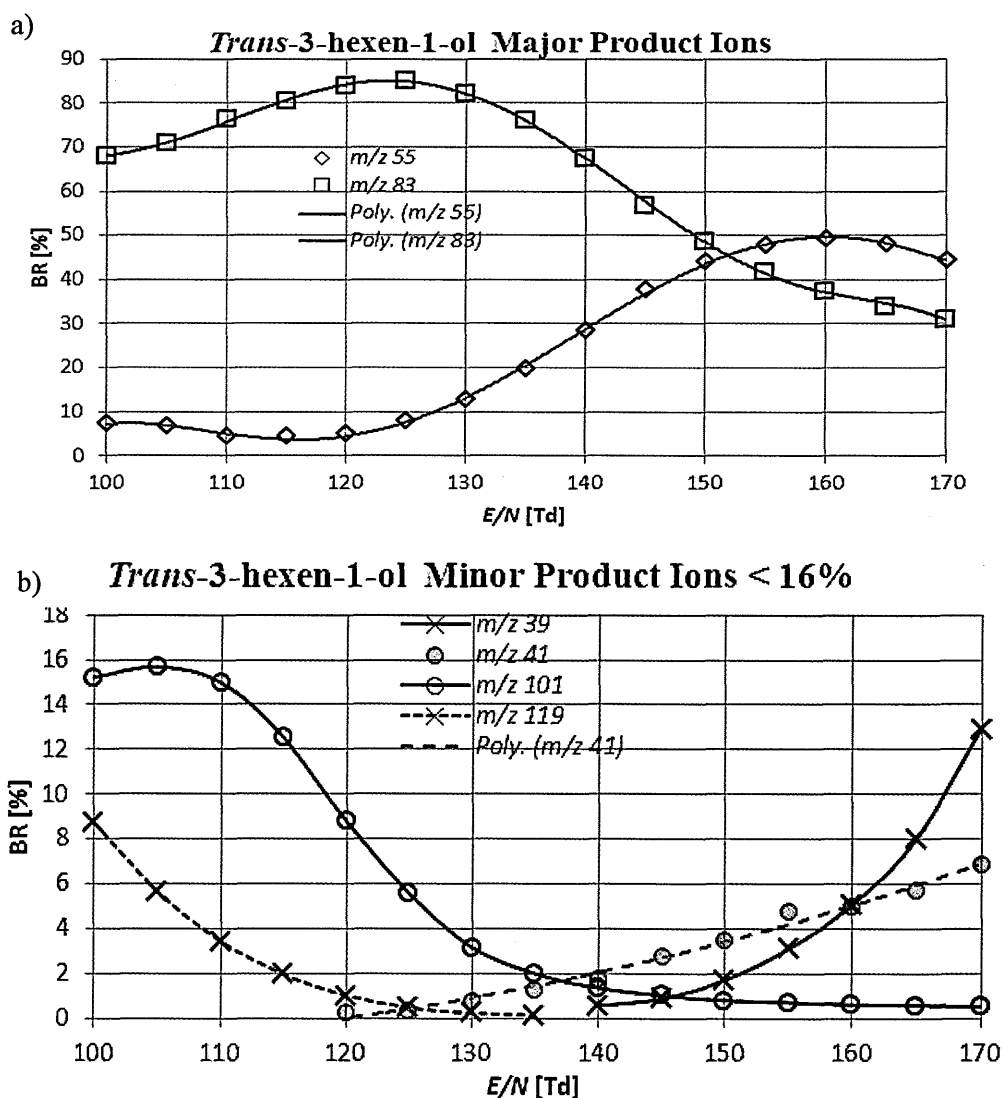
Figure 4.8: Branching ratios for *trans*-3.
Product ions in a) and b) are shown at different scales of BR percentages. The protonated parent is seen at *m/z* 101 and the first water monomer at *m/z* 119.

The protonated parent ion, *m/z* 101, is clearly visible (~18% at *E/N* = 100 Td) along with its associated water monomer, $C_6H_{12}OH^+.(H_2O)$ at *m/z* 119. In their SIFT work on *trans*-3

reactions with H_3O^+, Schoon *et al.* 2007 find a reaction channel of < 6% for *m/z* 101 and 93% for *m/z* 83. We find ~ 60% at the lowest energy for *m/z* 83.

4.3.2.2 *Cis*-3-hexen-1-ol

Figure 4.9 shows spectra for *cis*-3 at E/N = 115 Td (a) and E/N = 170 Td (b). The protonated parent ion at *m/z* 101 and its hydrate at *m/z* 119 can be seen for E/N = 115 Td but it has virtually disappeared at E/N = 170 Td and, as expected, no *m/z* 119 is observed. A small but significant peak for *m/z* 41 can be seen in Figure 4.9b) and Figure 4.9b) confirms this.
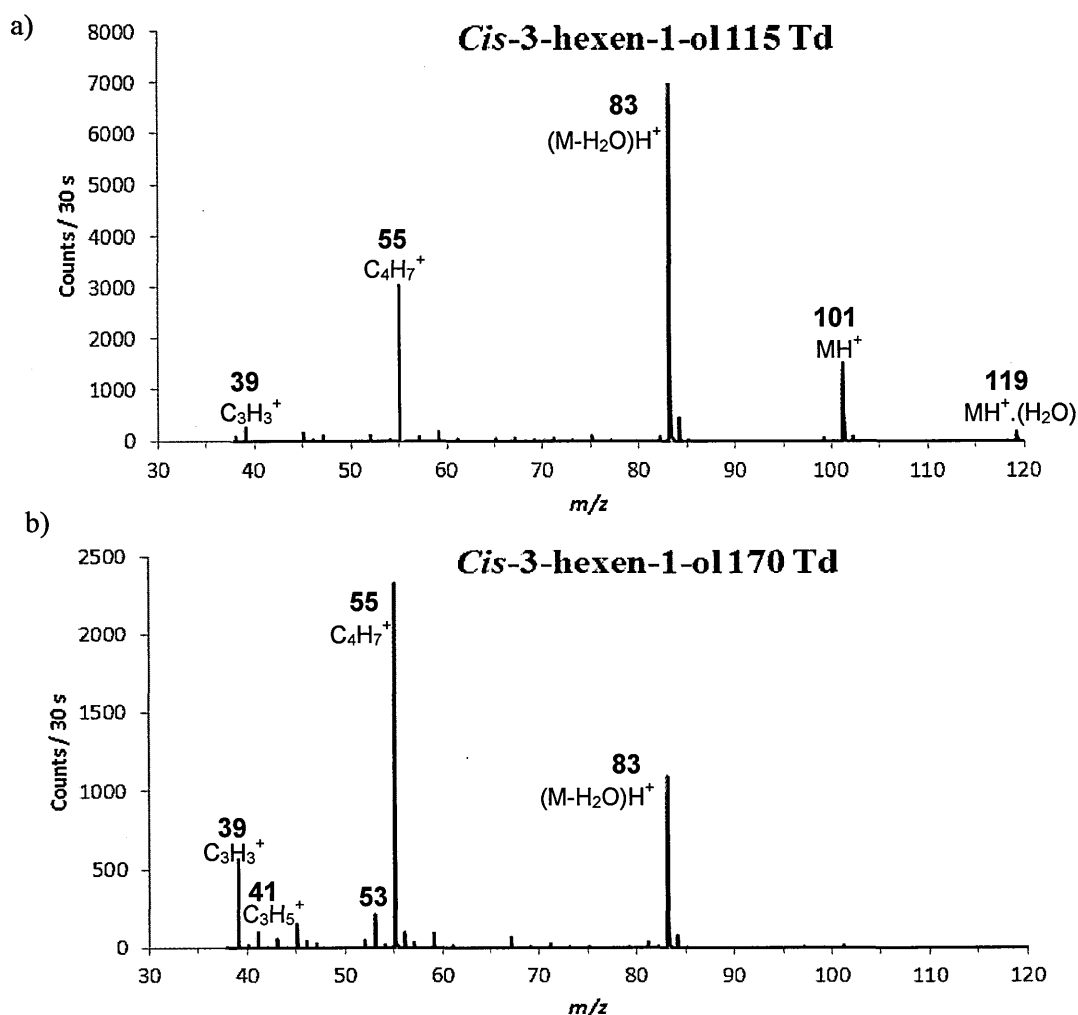
Figure 4.9: Spectra for *cis*-3 at a) 115 Td and b) 170 Td.

The product ion distribution for the whole E/N range is shown in Figures 4.10a) and b): Figure 4.10a) shows the major product ions and Figure 4.10b) amplifies the scale for the product ions with BRs < 14% where the protonated parent's hydrates can be seen.

a)

Cis-3-hexen-1-ol Major Product Ions

b)

Cis-3-hexen-1-ol Minor Product Ions < 14 %
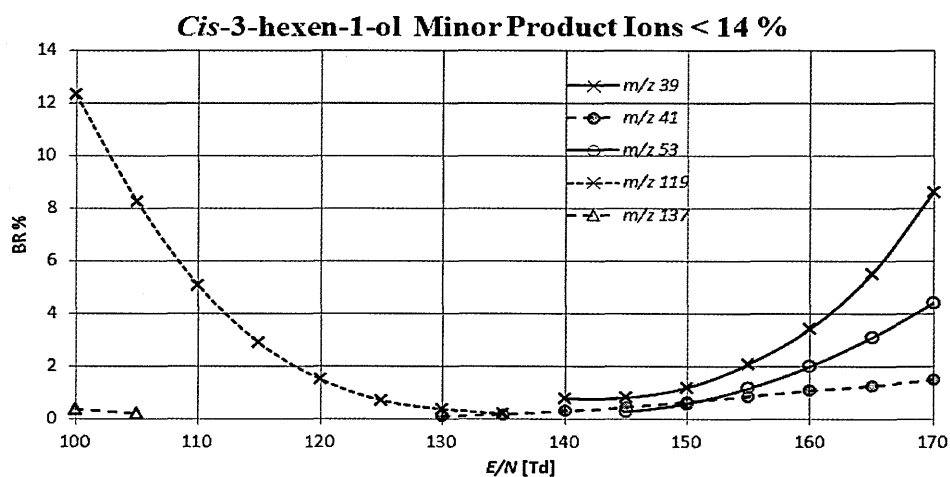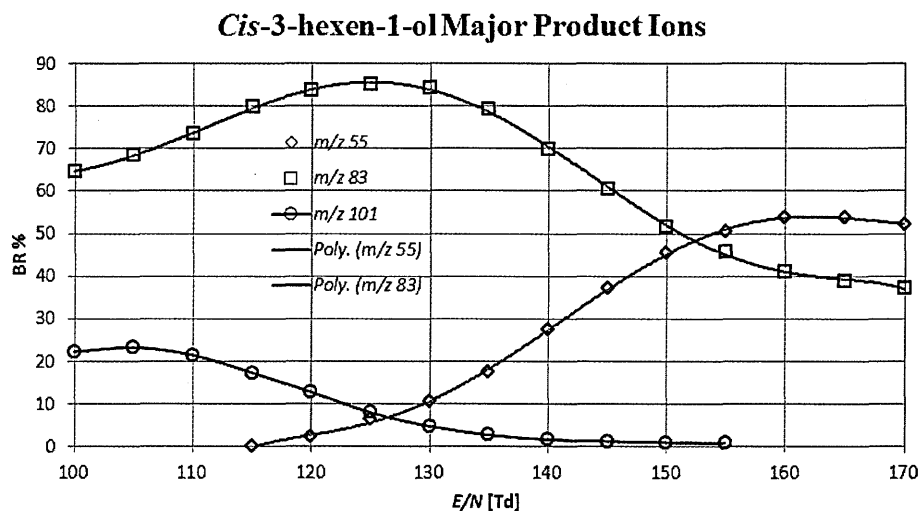
Figure 4.10: Branching ratios for a) cis-3 major and b) minor (<14%) product ions.
The protonated parent is seen at m/z 101, the water monomer at m/z 119 and dimer at m/z 137.

Demarcke et al. 2010 and Fall et al. 1999b investigated cis-3 on a PTR-QUAD-MS, with Demarcke varying E/N from 80 Td to 140 Td. Their results for cis-3 percentage fragmentations at E/N 120 Td are shown in Table 4.4 along with those from this work at E/N = 140 Td for the same reasons as stated for trans-2 in §4.3.2.1.. The Demarcke values are estimated from product ion distributions in their paper (2010).

Table 4.4: Comparison of branching ratios (BR%) for *cis*-3
by Fall *et al.* (1999b) and Demarcke *et al.* (2010) and this work.
Demarcke's data estimated from their product ion distributions.

	Cis-3					
m/z	**39**	**41**	**55**	**59**	**83**	**101**
Demarcke *et al.**	< 1%	-	18%	-	75%	2%
Fall *et al.*[†]	-	-	22%	5%	74%	1%
This work[+]	< 1%	< 1%	28%	-	70%	2%

*E/N = 120 Td data to enable comparison with Fall 1999b.
[†] No E/N value reported
[+] E/N = 140 Td for comparative moisture levels

These results are largely in agreement with those found by Demarcke *et al.* 2010. The main

difference is the product ion at *m/z* 59 in Fall's work which is not found in this work and is

again, as mentioned in §4.3.2.3 *Trans*-3, an acetone impurity.

Cis-3 has also been investigated in a SIFT instrument by Dhooghe *et al.* 2009 and in a FA-

SIFT by Custer *et al.* 2003. The latter study was primarily interested in negative ion (OH⁻)

reactions, but presents data from reactions with H_3O^+ for comparison. For *cis*-3 they find

only one major product ion at *m/z* 83 and the three minor ions *m/z* 101, 99 and 67. No

further details are given, except that the minor product ions are present at less than half the

intensity of the major product ions.

Reactions in the SIFT with *cis*-3 and $H_3O^+.(H_2O)_n$ for n = 0 to 3 carried out by Dhooghe *et*

Table 4.5: *Cis*-3 reactions with protonated water clusters (SIFT)
producing ions at *m/z* 83, 101, 119, 137 and 155. % channel where available
(Dhooghe *et al.* 2009)

m/z	**83**	**101**	**119**	**137**	**155**
H_3O^+ (*m/z* 19)	95%	4%	-	-	-
$H_3O^+.(H_2O)$ (*m/z* 37)	12%	33%	55%	-	-
$H_3O^+.(H_2O)_2$ (*m/z* 55)	-	-	Y*	Y*	-
$H_3O^+.(H_2O)_3$ (*m/z* 73)	-	-	-	Y*	Y*

Y* = presence of ion, no % given

al. 2009 are presented in Table 4.5. This shows how *cis*-3 fragments when reacted with

each reagent ion, H_3O^+, $H_3O^+.(H_2O)$, $H_3O^+.(H_2O)_2$ and $H_3O^+.(H_2O)_3$. Taking *m/z* 83 as an

example, the table shows that 95% of the parent molecule reacts with H_3O^+ (*m/z* 19) in a

non-dissociative proton transfer and the loss of H_2O to form m/z 83. The parent ion also

reacts with $H_3O^+.(H_2O)$ (m/z 37) but with only a 12% yield of m/z 83.

The inference from this is that, in the PTR-TOF-MS at low E/N, where there is more

$H_3O^+.(H_2O)$ than H_3O^+, less m/z 83 will be seen than at higher energy values. Figure 4.11

shows the branching ratios for water dimers in the cis-3 data as E/N is increased and is

introduced to demonstrate how the water dimer ratios have affected the product ion

percentages and behaviour vis $à$ vis the values in Table 4.5. In Figure 4.11 it can be seen

that the proportion of H_3O^+ increases from a very low level ($\sim$ 8%) at low E/N to become

the dominant species at $E/N \geq$ 120 Td. It also shows that the water trimer, $H_3O^+.(H_2O)_2$, m/z

55, is present for E/N = 100 Td to 130 Td and that $H_3O^+.(H_2O)_3$, m/z 73, is only just
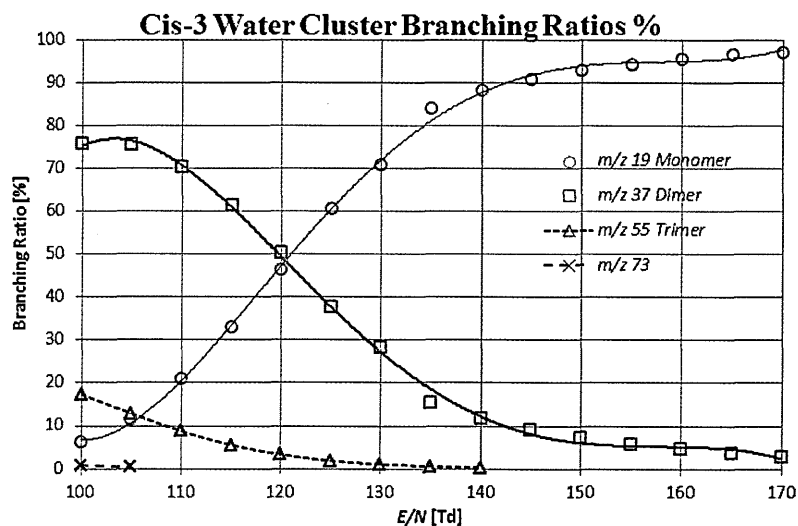
Figure 4.11: Water clusters from cis-3 data.
At low E/N there is very little m/z 19 (H_3O^+), the dominant
species being m/z 37 ($H_3O^+. H_2O$) with a small but significant
amount of m/z 55 and a very small amount of m/z 73

discernible for the two lowest E/N values. Note that the contribution from the cis-3 product

ion at m/z 55 has been deducted to give the values shown here.

To demonstrate how product ions m/z 83, 101, 119 and 137 are affected by these levels of

water cluster ions, their branching ratios are superimposed on the water clusters graph in

Figure 4.12. Equations for the reactions described below can be found in Table 4.3.

Looking at each product ion in turn and starting with m/z 83, it can be seen from Table 4.5 that this is mostly produced by a reaction of m/z 101 with H_3O^+ (95%) by dissociative
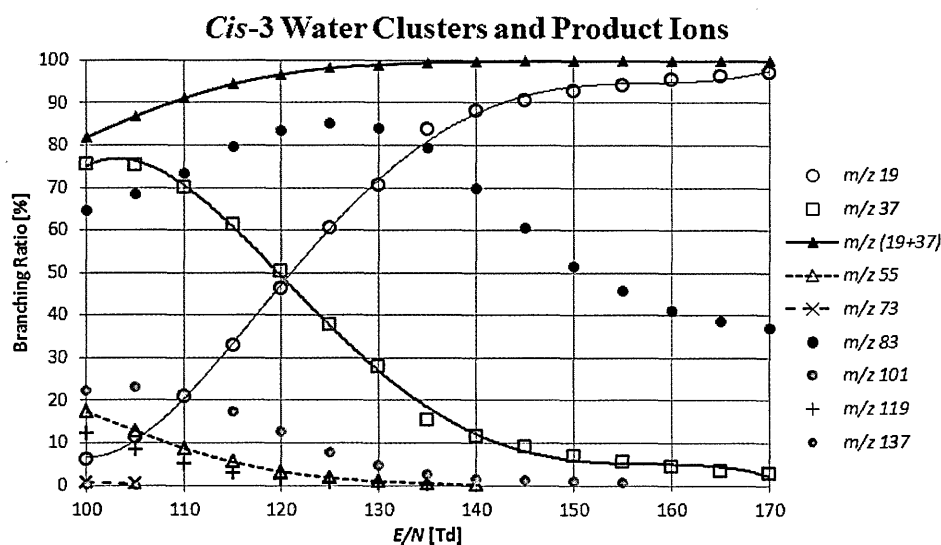
Figure 4.12: Branching ratios for *Cis*-3 product ions m/z 83, 101, 119 and 137 and water cluster ions H_3O^+ (m/z 19), H_3O^+.(H_2O) (m/z 37), H_3O^+.(H_2O)$_2$ (m/z 55), and H_3O^+.(H_2O)$_3$ (m/z 73). The contribution from the *cis*-3 product ion to m/z 55 has been subtracted. Markers for product ions are not connected by lines. m/z (19+37) = Total BR% for water dimers at m/z 19 and 37.

proton transfer. However, at E/N < 115 Td there is very little H_3O^+ but the significant amount of H_3O^+.(H_2O) gives rise to most of the m/z 83 and this latter continues to rise as E/N is increased and the proportions of H_3O^+ and H_3O^+.(H_2O) change with an overall increase in their sum total. This increase in m/z 83 appears to follow (H_3O^+ + H_3O^+.(H_2O)) until E/N = 125 Td when the collisional energy is sufficient to fragment m/z 83 quite significantly to produce m/z 55 as can be seen in Figure 4.10a.

The signal at m/z 101 is a result of non-dissociative protonation of the parent molecule with H_3O^+ (4%) and H_3O^+.(H_2O) (33%) (Table 4.5). As so much more of the protonated parent molecule is produced by reacting with H_3O^+.(H_2O), it is not surprising to see the branching ratio for m/z 101 follow this as it reduces.

The product ion at m/z *119* results from ligand switching of M with H_3O^+.(H_2O) and H_3O^+.(H_2O)$_2$. In the SIFT the percentages of m/z 83, 101 and 119 are 12%, 33%, 55%. In the PTR-MS instrument used here, there is much less m/z 119 than either of the other two product ions for all E/N values. This is most likely because the higher collision energies in

the PTR cause fragmentation of this hydrated protonated parent ion. It can also be seen that the ratio of m/z 119 follows the line of the water trimer: Dhooghe et $al.$ indicate that m/z 119 is seen as a result of a ligand switching reaction with $H_3O^+.(H_2O)_2$ and the subsequent elimination of H_2O but no data are available for their percentage yield.

Finally, m/z 137, the protonated parent water dimer, is the product of reactions with both $H_3O^+.(H_2O)_2$ and $H_3O^+.(H_2O)_3$. However the contributions from each reagent ion are not provided (Table 4.5). It would appear from Figure 4.12 that all of the signal for m/z 137 is a result of a ligand switching reaction and a loss of H_2O with $H_3O^+.(H_2O)_3$.

No signal was observed at m/z 155 in this work.

4.4 Summary and Discussion

The graphs in Figure 4.13 and 4.14 summarise the fragmentation behaviour described above by showing the branching ratios for the isomers analysed by product ion. Figures 4.13a) to d) show graphs for m/z 39, 41, 55 and 83. All isomers produce these ions over the E/N range used here
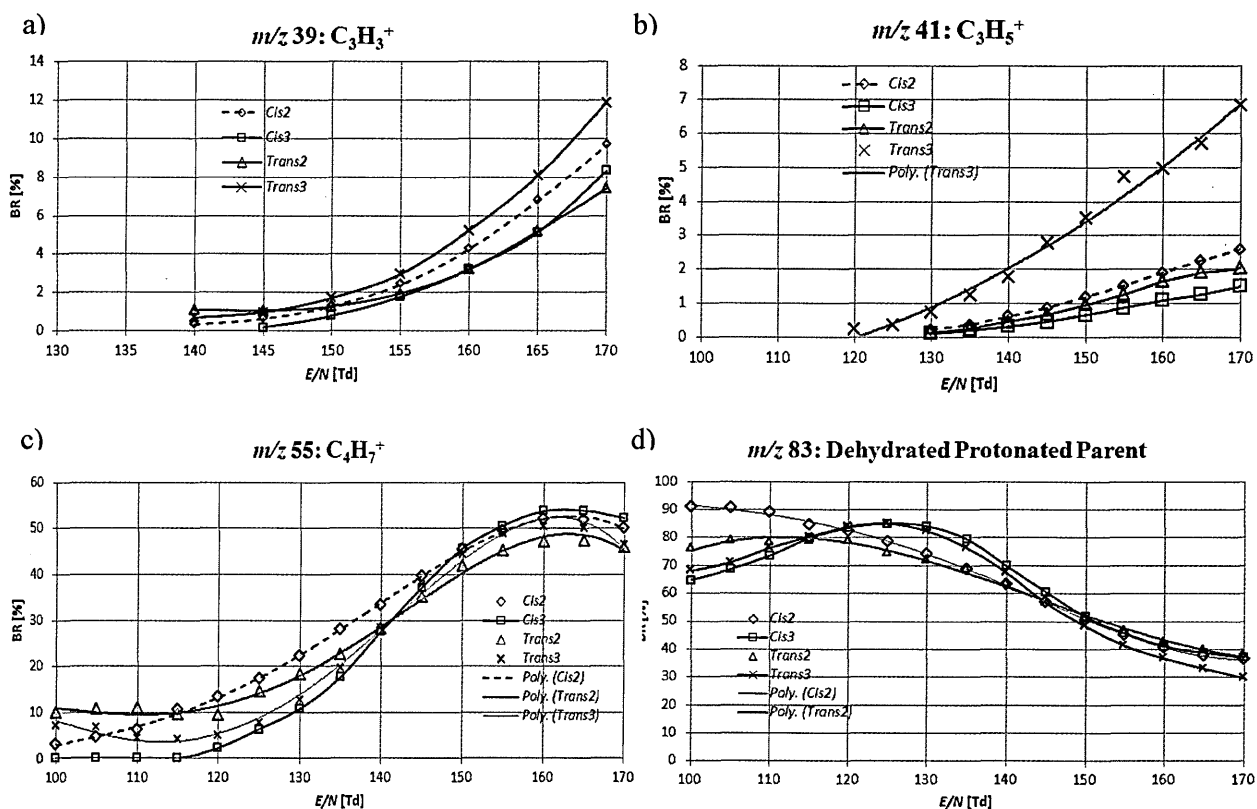
Figure 4.13: Branching ratios for isomers grouped by product ions
a) m/z 39, b) m/z 41, c) m/z 55 and d) m/z 83. Fragmentation behaviour appears to be related to the position of the C=C bond for all product ions except for m/z 41.

and there is some evidence that the branching ratios depend on the position of the C=C bond (also see Schoon *et al.* 2007). For example, in Figures 4.14a) to d), m/z 99 and 117 are only seen for the 2-hexen-1-ols, and m/z 101 and 119 for the 3-hexen-1-ols. Several hydrated ions are observed, m/z 117, m/z 119, and m/z 137 which can be seen in the low percentage branching ratio graph for *cis*-3 (Figure 4.10b).
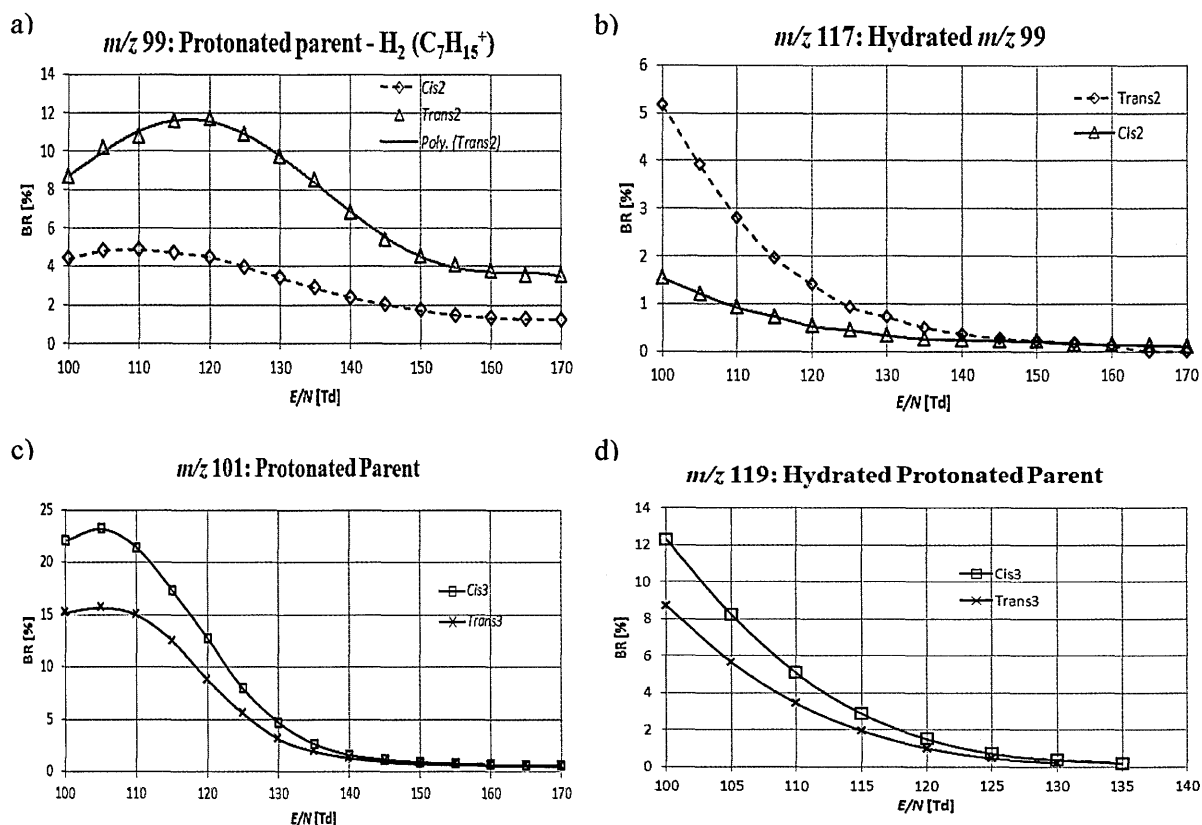
Figure 4.14: Branching ratios for a) m/z 99, b) m/z 117, c) m/z 101 and d) m/z 119
These graphs further demonstrate the effect of the C=C position in the molecule.

Dhooghe *et al.* 2012 have further investigated all four isomers in a flowing afterglow tandem MS (FA-TMS) using argon as the carrier gas, examining the m/z 83 product ion resulting from their reaction with H_3O^+. As that instrument operates at higher energies than the PTR-MS, only the results for the lowest energy, below 1.8 eV, are quoted in this work. At these energies, identical fragmentation patterns were found for all four isomers, producing ions at m/z 55 ($C_4H_7^+$, $\approx$ 90%) and m/z 41 ($C_3H_5^+$, $\approx$ 10%) (Figure 4.15):

$$C_6H_{11}^+ \quad + \quad Ar \quad \longrightarrow \quad (C_6H_{11}^+)^* \quad + \quad Ar$$

90% — $C_4H_7^+$ + neutrals

$C_3H_5^+$ + neutrals

10%

Figure 4.15: Reactions for *m/z* 83 with H_3O^+ in a FA-TMS to form ions at *m/z* 55 ($C_4H_7^+$), 90%, and *m/z* 83 ($C_3H_5^+$), 10%. (Dhooghe *et al.* (2101))

The FA-TMS study found other product ions at higher collision energies, *viz. m/z* 29 ($C_2H_5^+$), 31 ($C_3H_7^+$), 41 ($C_3H_7^+$) and 43 ($C_3H_9^+$). Only *m/z* 41 is seen in this work.

A table of energies in eV and corresponding *E/N* values used on the PTR-TOF-MS can be found in Table 2.3, §2.2.2.2. The maximum energy used in this work is 0.394 eV.

Table 4.6 illustrates how all four isomers fragment in the PTR-TOF-MS. A pattern is immediately apparent here: all four isomers produce ions at *m/z* 39, 41, 55 and 83 but

Table 4.6: Product ions > 1% by isomer seen at any *E/N*

	39	41	55	83	99	101	117	119
Trans-3	Y	Y	Y	Y	-	Y	-	Y
Trans -2	Y	Y	Y	Y	Y	-	Y	-
Cis-3	Y	Y	Y	Y	-	Y	-	Y
Cis -2	Y	Y	Y	Y	Y	-	Y	-

differences become apparent at *m/z* values > 83. As noted earlier, the protonated parent ion at *m/z* 101 is absent for the 2-hexenols but present for both of the 3-hexenols. The 2-hexenols produce *m/z* 99; this is also found by Schoon 2007 where it is described as a result of a minor 3% reaction channel when *cis*-2 reacts with H_3O^+ in their SIFT instrument, having the structure $(M-H)^+$.

The difference regarding the absence of the protonated parent in the 2-hexenols is in agreement with the work by Demarcke 2010 and Schoon 2007. Because Demarcke only examined one each of the (2) and (3) isomers, there is no reference with which to compare the relative BRs within each of the *m/z* 99 and 101 product ions. A summary of this work is given in Table 4.7.

Table 4.7: Summary of branching ratios (BR%) for E/N = 80-140 Td.
(Demarcke *et al.* 2010)

m/z	39	41	55	83	101	119	137
Trans-2	Y	Y	Y	Y	-	Y$^+$	Y$^+$
Cis-3	Y	-	Y	Y	Y	Y$^+$	Y$^+$

$^+$ =SIFT experiments (Schoon *et al.* 2007)

Figure 4.16a, (repeat of Figure 4.14c), and Table 4.8 show that there is more *cis*-3 MH$^+$ (*m/z* 101) at a specific E/N value than appears in the *trans*-3 species for E/N < 140 Td, e.g. Table 4.8

a)
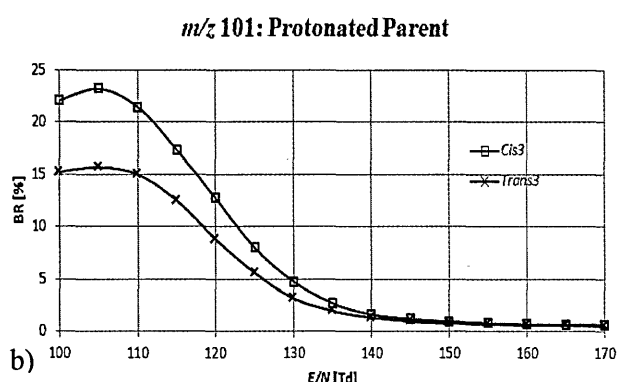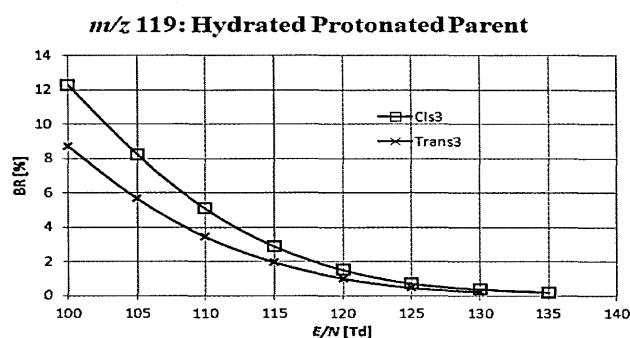
Table 4.8: Comparison of BR %s for *m/z* 101 for *cis*-3 and *trans*-3, E/N = 100 Td – 140 Td

m/z 101: Protonated Parent

b)

m/z 119: Hydrated Protonated Parent

E/N	Cis-3 %	Trans-3 %
100	22	15
105	23	16
110	21	15
115	17	13
120	13	9
125	8	6
130	5	3
135	3	2
140	2	1

Figure 4.16: Branching ratios for a) *m/z* 101 and b) *m/z* 119 for *cis*-3 and *trans*-3.

demonstrates that at E/N = 110 Td there is a 21% yield for *cis*-3 and a 15% yield for *trans*-3.

Figure 4.14a) shows that there is more *m/z* 99 from the *trans*-2 isomer at all E/N values than for *cis*-2. This leads to the conclusion that whichever product ions are present at *m/z* > 83 depends on the position of the C=C bond: the 2-hexen-1-ols fragment to *m/z* 99 but no MH$^+$ is seen. The 3-hexen-1-ols produce the protonated parent at *m/z* 101 but no *m/z* 99. This would then seem to be related to the positioning of the proton within the molecule and the subsequent fragmentation of the excited protonated molecule. It would be helpful to have the proton affinities for these individual configurations but, at present, they are not available.

The existence of fragmentation differences may help to identify these isomers in a mixture where other interfering compounds are absent. Examples of such compounds are given in Table 4.9 with a breakdown of their reported product ions and % values on reaction with H_3O^+ in both the SIFT and PTR-MS (extracted from Dhooghe 2012).

Table 4.9: Interfering compounds for detection of hexenols at m/z values where $\geq$ 5% is likely to be seen (Dhooghe *et al.* 2012)

Mass	Compound	H_3O^+ Product Ion	SIFT[1] %	PTR-MS[2] %
100	Hexanal	101	50	5
		83	50	73
		55	-	73
142	*Cis*-3-hexenyl acetate	83	85	61
142	*Trans*-2-hexenyl acetate		-	66

[1] = Španel *et al.* 1997, [2] = Fall *et al.* 1999b

A possible method is presented as a flow chart in Figure 4.17 where the identification of a C_6 alcohol is determined initially by detecting peaks at m/z 39, 41, 55 and 83 at $E/N \geq$ 160 Td. It would then be necessary to reduce E/N to less than 115 Td to detect either m/z 101 or m/z 99. If m/z 101 is detected at this E/N value then either the *cis*-3 or *trans*-3 isomers are present with the percentage yield giving an indication of which configuration it is. Similarly, if m/z 99 is detected this would indicate the presence of the 2-hexen-1-ol configurations, the percentage yield again enabling identification.

```
                        ┌──────────────┐
                        │    Start     │
                        └──────────────┘
                               │
                               ▼
                        ╱────────────╲
                       ╱  m/z 39, 41   ╲
                      ╱   and 55         ╲        No      ┌──────────────┐
                     ╱    and 83          ╲──────────────▶│  Not a C₆    │
                      ╲   over a wide     ╱               │  unsaturated │
                       ╲  range of E/N   ╱                │   alcohol    │
                        ╲──────────────╱                  └──────────────┘
                               │
                             Yes
                               │
                               ▼
┌───────────┐              ╱──────╲                  ┌───────────┐
│  Trans 2  │    Yes      ╱        ╲      No          │   Cis 3   │
│    Or     │◀───────────╱   m/z    ╲────────────────▶│    Or     │
│   Cis 2   │            ╲    99    ╱                  │  Trans 3  │
└───────────┘             ╲        ╱                   └───────────┘
      │                    ╲──────╱                          │
      │                                                 E/N ≤ 110
      │                                                      │
      ▼                                                      ▼
   ╱──────╲                                              ╱──────╲
  ╱ 110 Td ╲    < 10%    ┌─────────┐                    ╱         ╲   < 20%   ┌───────────┐
 ╱    ≥     ╲───────────▶│  Cis 2  │                   ╱   m/z     ╲──────────▶│  Trans 3  │
 ╲  E/N     ╱            └─────────┘                   ╲   101     ╱           └───────────┘
  ╲ ≤ 125 Td╱                                           ╲         ╱
   ╲──────╱                                              ╲──────╱
      │                                                      │
    ≥ 10%                                                  ≥ 20%
      │                                                      │
      ▼                                                      ▼
┌───────────┐                                          ┌─────────┐
│  Trans 2  │                                          │  Cis 3  │
└───────────┘                                          └─────────┘
```
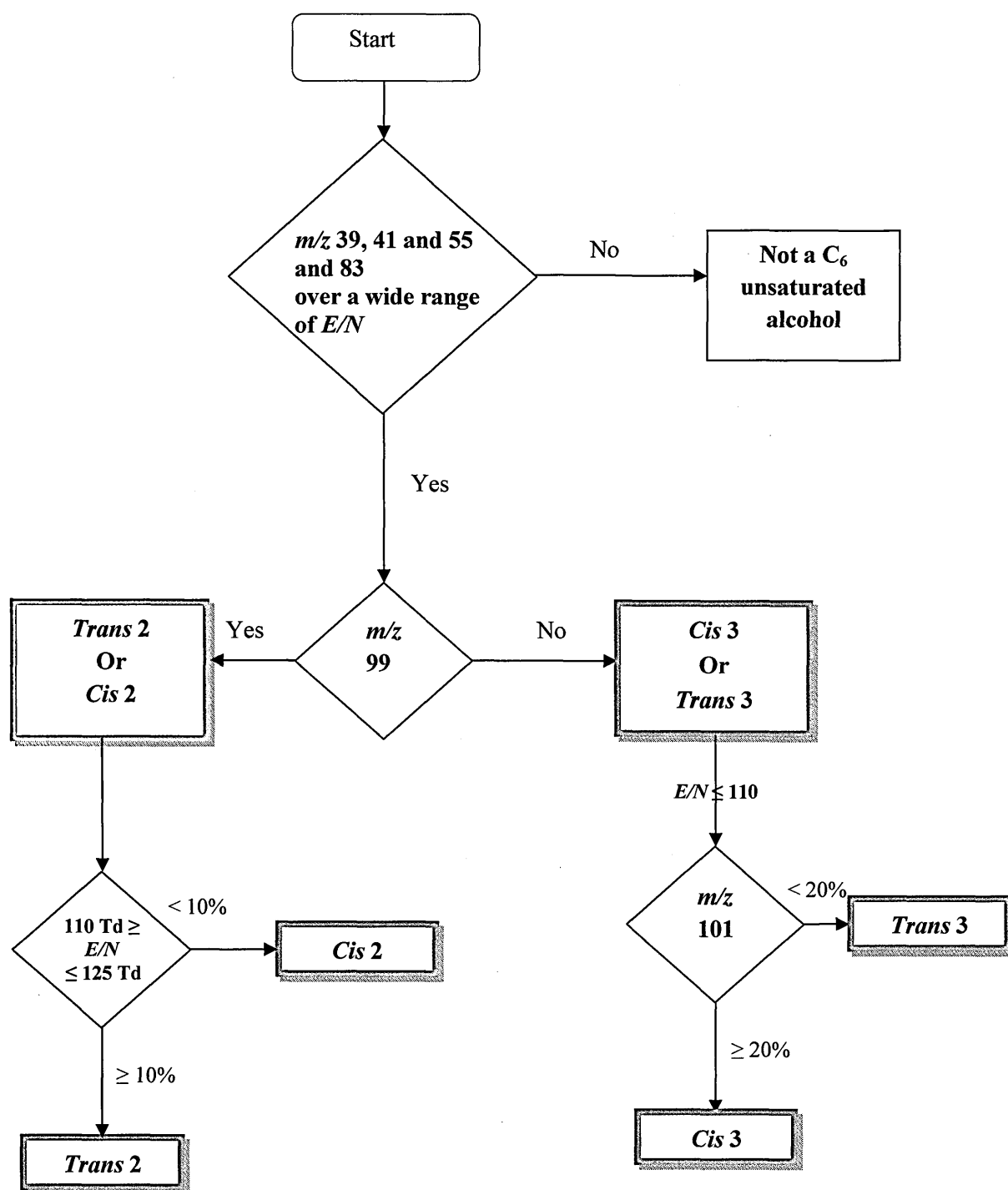
Figure 4.17: Flow chart for hexenol isomer identification.

Following an *E/N* study and calculation of BRs, it may be possible to identify a hexenol isomer from a mixture, depending on the absence of other species which could contribute to the peaks found here.

4.5   Conclusion

This work has shown that the same four product ions are seen for all of the hexenol isomers, m/z 83, 55, 41 and 39 when reacted with H_3O^+ in a PTR-TOF-MS. These results compare favourably with those of other groups working on both SIFT-MS and PTR-MS. However, this work finds that where the protonated parent ion, m/z 101 is absent, m/z 99 becomes apparent but this is not mentioned in any other study. It is this aspect of the hexenols' behaviour that has led to the possibility of discriminating between the 2-hexenols and the 3-hexenols. It may also be possible to identify the *cis-* and *trans-* isomers. However, both product ions involved in this procedure are minor contributors to the branching ratios, and so the instrument's sensitivity will limit the success of this method.

Chapter 5 – Discussion

5.1 Introduction

This chapter discusses the major findings and practical developments described in the foregoing chapters. Practical innovations, both hardware and methodology, are discussed in the light of their necessity for improving measurements and how they have led to permanent instrument development.

The results of experimentation are discussed with regard to their importance in the light of their contribution to advances in the field of Proton Transfer Reaction Mass Spectrometry and possible further applications in specific areas.

5.2 Instrument Development

A primary requirement for analytical use of the PTR-TOF-MS instrument is knowledge and control of the reduced electric field, which is the ratio of the electric field strength (E) to the buffer gas number density (N), E/N, that characterises the collisional energy of reagent ions with neutrals and the product ions with the buffer gas, and hence the degree of fragmentation. This ratio can be determined from the temperature and pressure of the drift tube and the voltage drop across the drift tube. The only accurately measureable parameter on the original 'as received' instrument was the temperature (§2.3 *Optimisation of the Instrument*): there was no readily available method for measuring the voltage drop and the pressure gauge was not sufficiently sensitive. Thus it was necessary to install real-time accurate monitoring of the voltage applied across the reaction chamber and the absolute pressure of the reactant gas inside it.

The manufacturers (Kore) had suggested a method for measuring these voltages without actually attaching a permanent voltmeter. This involved measuring the voltages and calibrating the relevant potentiometers accordingly. This assumes a linear relationship between the potentiometer scale and the change in voltage – an assumption found to be invalid. Instead a digital voltmeter was added for the measurement of the voltages at the relevant electrodes: at the entrance and exit of the chamber and on a plate, 9 cm from the entrance of the chamber. The original reason for this inner electrode (plate 26) was to create a

short region of much higher energy, (E/N), referred to as a collision-induced dissociation (CID) region (Blake *et al.* 2009) as the ions left the reaction chamber in order to break up any water clusters and so simplify the mass spectrum. The main disadvantage of using this method is that the VOC concentrations were underestimated as humidity increased: it was found that an elevated E/N in the CID region relative to the rest of the drift tube led to an overestimate of the amount of H_3O^+, which included contributions from fragmented $H_3O^+(H_2O)_n$ ions (Warneke *et al.* 2005). It is also not clear if and how an E/N measurement could have been established, so making any results difficult to compare with those of other groups. It was for these reasons that, having the capability to set voltages on all three electrodes, they were deployed such that the inner electrode was invisible to the ions in the reaction chamber.

A Pirani pressure gauge was originally used to measure the pressure in the reaction chamber using the principle that the heat conduction of a gas depends on its pressure. The sensitivity of this type of gauge is dependent on the surface condition of the filament and inaccurate readings can be caused by the presence of organic vapours. (Harris 1997). A Pirani gauge is not absolute and in operation it was insufficiently sensitive. It was therefore replaced by a capacitance gauge which measures absolute pressure by sensing the deflection of a diaphragm between the sample volume and a sealed reference volume. The deflection is caused by forces due to a pressure differential which changes the capacitance between an electrode on the diaphragm and a rigid reference (Harris 1997). This gauge performed much better, both in response time, sensitivity and level of accuracy.

Both of these innovative, yet simple enhancements have had a direct benefit for other users in the field by improving the operational control of PTR-TOF-MS instruments now being offered by the manufacturer (Kore).

5.3 Calibration and Benchmarking

Characterising the instrument was essential for future studies relating to sensitivity and mass transmission dependencies, both of which are important for concentration determinations and

comparison of results with those of other instruments. In this study, a calibration gas comprising of 14 aromatic compounds was used to obtain the sensitivity measurements for a wide range of m/z values (79 to 181) and produced a value of 4-6 ncps ppbv^{-1} normalised to 10^6 H_3O^+ (Chapter 3). Each of the constituents of the calibration gas (§3.2.2 *Calibration Gas*) was separately investigated over a wide E/N range in order to determine the behaviour of the reactions with H_3O^+. Significantly, results showed that product ions other than the protonated parent must be accounted for when a complex chemical mixture is subjected to analysis, otherwise the concentrations will be incorrectly determined. For example, if a fragment ion contributes to an m/z corresponding to a protonated parent of interest, then the concentration for the corresponding neutral will be overestimated if that contribution is not taken into account. Conversely, suppose the reaction of H_3O^+ with a molecule, M, were to lead to the protonated parent and a fragment channel, with no contribution from other ions at the corresponding m/z. Then, if the product ion corresponding to that channel is not taken into account, [M] will be underestimated. Thus the calculation of concentrations using PTR-MS is not as easy as proposed in some review articles e.g. Blake *et al.* 2009. This problem has been highlighted in the book by Ellis and Mayhew (Ellis 2014), but as yet few studies have been undertaken. The investigations in this thesis have illustrated how this issue can be addressed. Hence, the aromatic VOCs study has enhanced our knowledge of not only how E/N can be used to change fragmentation patterns in order to improve selectivity but also how these patterns can be used to aid in the determination of neutral concentrations. The determination of absolute concentrations is crucial for many environments including in particular the environmental and food sciences (Ellis 2014).

5.4   Techniques and Methodologies

During the course of pilot studies for pears and bacterial samples not reported in this thesis, it was recognised that it would be advantageous if the headspace for these types of samples could remain undiluted, not only whilst the VOCs were being introduced into the PTR-TOF-MS but also for the duration of the whole investigation, in one case being over 27 days. A

simple technique was devised whereby a small Nalophan® expansion bag was included inside

the sample container (§2.4.1 *Preventing Dilution of VOCs from Biological Sources*). This was

arranged such that the bag could expand and replace the extracted headspace VOCs without

diluting the volatiles. It should be noted that Nalophan® produces its own background VOCs:

isopropanol (protonated at *m/z* 61), ethyl acetate (protonated at *m/z* 89) and toluene

(protonated at *m/z* 93) (Fortune 2012). These VOCs can be mostly removed by placing the

bags in an odour free environment for a period of time (Miller 2008). However, the

Nalophan® used for the indole trials retained indole for some considerable time, long after the

investigations ended. This suggests that new bags should be used for each separate trial.

Another issue to consider is the permeability of the material of the expansion chamber and its

connections in order to limit the leakage of VOCs and air. The concept is viable as the

technique can be used for any system to maintain constant sample concentrations. Further

work is required to establish a reliable container of this type, investigating the use of different

materials and types of closures.

5.5 Application to Non-aromatic Organic Compounds

Results of the study of the four hexen-1-ol isomers, *cis*-2-hexen-1-ol, *cis*-3-hexen-1-ol, *trans*-
2-hexen-1-ol and *trans*-2-hexen-1-ol, compared favourably with the findings of other groups

working on both SIFT-MS and PTR-MS: the same four product ions were found for all of the

isomers, *viz.* those at *m/z* 83, 55, 41 and 39 when reacted with H_3O^+ in a PTR-TOF-MS. None

of these represent the protonated parent ion, *m/z* 101, which is only detected in the *cis*-3- and

trans-3-hexen-1-ols. This work finds that either the protonated parent ion, *m/z* 101, (from the

3-hexen-1-ols) or the fragment at *m/z* 99 (from the 2-hexen-1-ols) is present in the spectrum.

It should be noted that *m/z* 99 is a product ion which is not mentioned in any other study. The

conclusion drawn from this is that the fragmentation of the excited, protonated molecule

depends on the position of the C=C bond and is related to the positioning of the proton. These

observations lead to a possible method for discriminating between the 2- and 3-hexenols with

a smaller likelihood of differentiating between the *cis-* and *trans-* isomers themselves. Both of these are dependent on the instrument's sensitivity as the ions at m/z 99 and 101 form minor contributions to the fragmentation patterns observed (m/z 99 occurs at 7 % ± 3 % at $E/N <$ 140 Td and m/z 101 occurs at 15 % ± 5 % at $E/N <$ 130 Td). The approach of varying E/N adds to work already done in this field and provides a possible way forward for further work as mentioned above.

5.6 Application to Aromatic Compounds

Trichlorobenzene (Chapter 3) and pilot studies with indole revealed issues with certain molecules which took tens of minutes to reach a constant concentration in the reaction chamber of the instrument. Such compounds are often referred to as 'sticky' and, if not corrected for, this will lead to lowered sensitivities, increase reaction times and result in traces of the compounds remaining in the instrument for extended periods of time. The traditional method for dealing with this was used, *viz.* to heat the inlet lines and reaction chamber to avoid condensation (Mikoviny 2010).

The E/N investigations of individual alkylbenzenes and chlorobenzenes (Chapter 3) and hexen-1-ols, (Chapter 4), provided a possible method of discriminating between isobaric compounds, i.e. those with the same molecular mass, by examining fragmentation patterns of VOCs to determine if they vary in a systematic manner within the operating parameters of the PTR-MS system. The fragmentation patterns are represented on branching ratio diagrams which show the relative percentages of product ion channels *vs* E/N values. In particular, branching ratios for ethylbenzene and the xylenes show very different fragmentation patterns when examined by changing the energy conditions in the reaction chamber: ethylbenzene starts to fragment at significantly lower E/N values than the xylenes (§3.3.2.1 *Comparison of the Isomeric Compounds Ethylbenzene and Xylenes*). This illustrates how the selectivity of PTR-MS can be significantly enhanced, changing what is essentially a one-dimensional instrument into a multidimensional one.

The application of this method to a real, complex sample was explored by examining results for ethylbenzene and xylene using the calibration gas as if nothing were known about its contents (§3.2.2 *Calibration Gas*). Some progress was made to this end by looking at the difference in counts as *E/N* was varied and this difference used to estimate the amount of xylene present (§3.3.2.1 *Comparison of the Isomeric Compounds Ethylbenzene and Xylenes*). The counts resulting from this method were found to be a factor of 2 too high when compared with the known counts of xylene in the calibration gas. Further work in this area is desirable as these VOCs are important environmental compounds and it is important to be able to distinguish them in real situations (Karl *et al.* 2001).

The study of chlorobenzenes (Chapter 3) revealed some unanticipated effects: an unlikely cluster in the dichlorobenzenes at *m/z* 129 formed as *E/N* was varied. Extensive investigation of the *m/z* 129 peak revealed that its sole provenance could only have been as a result of an association of the product ion at *m/z* 111 ($C_6H_3Cl^+$) with an H_2O molecule (§3.4.2.1 *Product Ion Analysis*)

Unexpected patterns were observed in spectra for several of the chlorobenzene compounds as *E/N* was increased: specifically for *p*-dichlorobenzene (*m/z* 147), all spectra displayed a much higher signal than expected at *m/z* 148, the ^{13}C isotope peak. It is considered that this is related to the peak at *m/z* 146 produced by non-dissociative charge transfer with the O_2^+ impurity in the system (§3.6.1 *Variation in Spectra in p-Dichlorobenzene as E/N Increases*). Not all peaks display this non-dissociative charge transfer peak: *m/z* 94 displays a peak at *m/z* 93, but *m/z* 99 has no peak at *m/z* 98. These non-dissociative peaks are not mentioned elsewhere in the literature but should be taken into acount when quantitive measurements are required.

Product ions at *m/z* 85 and *m/z* 87 appear in the dichlorobenzenes and their relative intensities change as *E/N* changes (§3.6.2 *Anomalies for m/z 85 and m/z 87*): at *E/N* = 240 Td there is an ion at *m/z* 85 which appears to have two chlorine atoms; at *E/N* = 190 Td, the ion at *m/z* 87 appears to have one chlorine atom based on the intensities of *m/z* 87 and 89,. It is not clear

why these apparent anomalies occurred and they warrant further investigation, perhaps being examined with O_2^+ as the analyte gas.

5.7   Summary

The investigations here examined known VOCs and their behaviours under differing energy conditions. This was found to be helpful when discriminating between isobaric and isomeric compounds. It has presented a new, cogent exposition of the problems to avoid when investigating a complex environment a) for calibrating the instrument and b) in a real world situation such as is found in the environmental sciences.

Chapter 6 - Conclusion and Further Work

6.1   Conclusion

After making the necessary modifications to the PTR-TOF MS (Kore Technologies Ltd. Ely) it proved to be a sensitive and reliable instrument. Sensitivity measurements produced a value of 4-6 ncps ppbv^{-1} normalised to 10^6 H_3O^+ with results showing that it was essential to account for fragmentation in a complex chemical mixture. It has been shown here that failure to take this into account leads to an erroneous sensitivity, the true value being less.

Varying E/N was used as a technique to examine the fragmentation behaviours of VOCs and, in so doing, revealed a method for discriminating isobaric (ethylbenzene and xylenes) and isomeric (hexen-1-ols) compounds, all important constituents in the environmental sciences. This work gives further weight to those few studies already performed and requires further investigation to refine the experimental and analytical processes. A peak at m/z 99, a product ion which is not mentioned in any other study, was seen only in the absence of the protonated parent ion, m/z 101. This suggests that the presence of one or other peaks (m/z 99 or 101) depends on the position of the C=C bond and may be related to the positioning of the proton within the molecule and its subsequent fragmentation. This suggests a likely avenue for identification of the individual isomers within the hexen-1-ols. Results for fragmentation channels with m/z values < 99 compared favourably with those of other groups that had used both SIFT-MS and PTR-MS to study these VOCs.

6.2   Further Work

Likely areas for future work are in the analysis of food stuffs (e.g. fruit ripening) and other bio-matter (e.g. bacteria, especially in the pressing and topical arena of antibiotic resistance and plasmids).

References

(ATSDR) Agency for Toxic Substances and Disease Registry *Toxicological Profile for 1,4-Dichlorobenzene (Update)* Public Health Service, U.S. Department of Health and Human Services, Atlanta, GA. (1998) http://www.atsdr.cdc.gov/toxguides/toxguide-53.pdf (Accessed 11/05/2012)

(http://plantphys.info/plants_human/fruitgrowripe.shtml (Accessed 5-5-2010))

"ToxGuide for Styrene" US Dept of Health and Human Services

Abanda-Nkpwatt, Muesch, Tschiersch, *et al.*, "Molecular interaction between *Methylobacterium extorquens* and seedlings: growth promotion, methanol consumption, and localization of the methanol emission site", *J. Exp. Bot.* (2006) 57 4025

Agarwal, Petersson, Juerschik, *et al.*," Use of proton transfer reaction time-of-flight mass spectrometry for the analytical detection of illicit and controlled prescription drugs at room temperature via direct headspace sampling" *Anal and Bioanal Chem* (2011) 400 8 2631–2639

Aharoni, Keizer, Bouwmeester *et al.* "Identification of the *SAAT* gene involved in strawberry flavor biogenesis by use of DNA microarrays", *The Plant Cell*, 2000) 12 647–661

Amiot, Tacchini, Aubert, *et al.*, "Influence of cultivar, maturity stage, and storage conditions on phenolic composition and enzymatic browning of pear fruits", J. *Agric. Food Chem.* (1995) 43 1132–1137

Balding, Blaby and Summers, "A mutational analysis of the ColE1-encoded cell cycle regulator Rcd confirms its role in plasmid stability", *Plasmid* (2006) 56 68–73

Bedoukian, "The seven primary hexenols and their olfactory characteristics", *Jnl. Agricultural and Food Chem.* (1971) 19 6 1111–1114

Beghi and Guillot, "Use of poly(ethylene terephthalate) film bag to sample and remove humidity from atmosphere containing volatile organic compounds", *J. Chromatography A* (2008) 1183 1–5

Biasioli, Gasperi, Aprea, *et al.*, "Fingerprinting mass spectrometry by PTR-MS: heat treatment vs. pressure treatment of red orange juice-a case study", *Int. J. Mass Spectrom.* (2003) 343 223–224

Biasioli, Yeretzian, Gasperi, *et al.*, "PTR-MS monitoring of VOCs and BVOCs in food science and technology", *Trends in Analytical Chemistry* (2011) 30 7 968–977

Blake, Monks and Ellis, "Proton-Transfer Reaction Mass Spectrometry", *Chem. Rev.*, (2009), 109: 3 861–896

Blake, Whyte, Hughes, *et al.*, "Demonstration of proton-transfer-reaction time-of-flight mass spectrometry for real-time analysis of trace volatile organic compounds", *Anal. Chem.* (2004) 76 3841–3845

Bohme, Mackay and Schiff, "Determination of proton affinities from the kinetics of proton transfer reactions. VII. The proton affinities of O_2, H_2, Kr, O, N_2, Xe, CO_2, CH_4, N_2O, and CO", *Journal of Chemical Physics*, (1980) 73 10) 4976–4986

Borisov and Garrett, "Structure and Isomerization of Arenonium Ions of Dichlorobenzenes in the Gas Phase: A Theoretical Study", *Russ. Chem. Bull.* (1998) 47 9 1677–1682

Boschetti, Holzinger, Prazeller, *et al.*, "PTR-MS real time monitoring of the emission of volatile organic compounds during postharvest aging of berry fruit", *Postharvest Biol. Technol.* (1999) 17 143

Bouchoux, Salpin and Leblane, "A relationship between the kinetics and thermochemistry of proton transfer reactions in the gas phase, *Int. J. Mass Spec. and Ion Procs.* (1996) 153: 37–48

Breslow and Groves, "Cyclopropenyl cation. Synthesis and Characterization", J. Am. Chem. Soc. (1970) 92 4 984–987

Brown, Watts, Märk, *et al.* "Proton transfer reaction mass spectrometry investigations on the effects of reduced electric field and reagent ion internal energy on product ion branching ratios for a series of saturated alcohols", *Int. J. Mass Spec.* (2010) 294 103–111

Buczynska, Krata, Stranger, *et al.*, "Atmospheric BTEX-concentrations in an area with intensive street traffic", *Atmospheric Environment* (2009) 43 311–318

Budzikiewicz, Djerassi and Williams, *Mass Spec. of Org. Compounds*, (1967) Publ. Holden-Day, Inc.

Buhr, van Ruth and Delahunty, "Analysis of volatile flavour compounds by Proton Transfer Reaction-Mass Spectrometry: fragmentation patterns and discrimination between isobaric and isomeric compounds", *Int. J. Mass Spec.* (2002) 221 1–7

REFERENCES

Bunge, Araghipour, Mikoviny, Dunkl, *et al*. On-line monitoring of microbial volatile metabolites by proton transfer reaction-mass spectrometry", *Applied and Environmental Microbiology*, (2008) 74 7 2179–2186

Burg, "The physiology of ethylene", *Ann. Rev. Plant Physiol.* (1962) 13 265–302

Cappellin, Probst, Limtrakul, *et al*., "Proton transfer reaction rate coefficients between H_3O^+ and some sulphur compounds", *Int. J. Mass Spec.*, (2010) 295 1–2 43-48

Chervin, Truett, and Speirs, "Alcohol dehydrogenase expression and alcohol production during pear ripening", *J. Amer. Soc. Hort. Sci.* (1999) 124 1 71–75

Chiavarino, Crestoni, Dopfer, *et al*., "Benzylium versus Tropylium Ion Dichotomy: Vibrational Spectroscopy of Gaseous $C_8H_9^+$ Ions", *Angewandte Chemie-International Edition* (2012) 51 20 4947–4949

Cooper, Gerratt and Raimondi, "The electronic structure of the benzene molecule", *Nature* (1986) 323, 699–701 (A possibly controversial paper: "The view that delocalized electrons provide essentially the correct description for this type of system ...... We show that the π-electrons in benzene are almost certainly localized and that the characteristic properties of such a system arise from the mode of spin coupling.")

Cresp, Cristeau, de Ronde, *et al*., "PTR-MS detects rapid changes in volatile metabolite emission by *Mycobacterium smegmatis* after the addition of specific microbial agents", *J. Microbiological Methods* (2011) 86 8–15

Custer, Kato, Fall, *et al*., "Negative-ion CIMS: analysis of volatile leaf wound compounds including HCN", *Int. J. Mass Spec.* (2003) 223–224 427–446

de Gouw and Warneke, "Measurements of volatile organic compounds in the earth's atmosphere using proton-transfer-reaction mass spectrometry", *Mass Spectrometry Reviews*, (2007) 26 223–257

de Gouw, Warneke, Holzinger, *et al*., "Inter-comparison between airborne measurements of methanol, acetonitrile and acetone using two differently configured PTR-MS instruments", *Int. J. Mass Spec.* (2004) 239 129–137

Demarcke, Amelynck, Schoon, *et al.*, "Laboratory studies in support of the detection of biogenic unsaturated alcohols by proton transfer reaction-mass spectrometry", *Int. J. Mass Spec.* (2010) 290 14–21

Demarcke, Amelynck., Schoon, *et al.*, "Laboratory studies in support of the detection of sesquiterpenes by proton-transfer-reaction-mass-spectrometry", *Int. J. of Mass Spec.* (2009) 279 156–162

Derwent, "Ozone formation downwind of an industrial source of hydrocarbons under European conditions" *Atmospheric Environment* (2000) 34 3 689–3700

Dhooghe, Amelynck, Rimetz-Planchon, *et al.*, "Flowing afterglow selected ion flow tube (FA-SIFT) study of ion/molecule reactions in support of the detection of biogenic alcohols by medium-pressure chemical ionization mass spectrometry techniques", *Int. J. Mass Spec.* (2009) 285 1–2 31–41

Dhooghe, Vansintjan, Schoon, *et al.*, "Studies in search of selective detection of isomeric biogenic hexen-1-ols and hexanal by flowing afterglow tandem mass spectrometry using $[H_3O]^+$ and $[NO]^+$ reagent ions", *Rapid Commun. Mass Spectrom.* (2012) 26 1868–1874

Ellis and Mayhew, "Proton Transfer Reaction Mass Spectrometry: Fundamentals and Applications", John Wiley & Sons Ltd (In preparation)

El-Sayed, Ismaeil and El-Beih, "Isolation of 4-chlorophenol-degrading bacteria, *Bacillus subtilis* OS1 and *Alcaligenes sp.* OS2 from petroleum oil-contaminated soil and characterization of its catabolic pathway", *Austral. J. of Basic and Appl. Sciences* (2009) 3(2) 776–783

Ennis, Reynolds, Keely, *et al.* "A hollow cathode proton transfer reaction time of flight mass spectrometer" *Int. J. Mass Spec.* (2005) 247 72

EUGRIS Portal for Soil and Water Management in Europe:

http://www.eugris.info/FurtherDescription.asp?e=6&Ca=2&Cy=0&T=Benzene,%20 Toluene,%20ethylbenzene,%20and%20xylene (Accessed 31/05/2012)

EuroChlor Risk Assessment for the Marine Environment "monochlorophenols" Feb 2002: http://www.eurochlor.org/media/49352/8-11-4-14_marine_ra_monochlorophenols.pdf   (Accessed 10/07/2012)

Fall, "Biogenic emissions of volatile organic compounds from higher plants", *Reactive Hydrocarbons in the Atmosphere*, Chapter 2 Ed. Hewitt (1999a) Academic Press, Harcourt Brace & Co.

Fall, Karl, Hansel, *et al.*, "Volatile organic compounds emitted after leaf wounding: On-line analysis by proton-transfer-reaction mass spectrometry", *J. Geophys. Res.* (1999b) 104 D13

FAO: The Food and Agriculture Organisation of the United Nations Statistics Database website. Production data archive. http://faostat.fao.org/site/567/default.aspx#ancor (Accessed 04/02/2013)

Farag, Fokar, Zhang, *et al.* "(Z)-3-Hexenol induces defense genes and downstream metabolites in maize", *Planta* (2005) 220 6 900–909

Fateley and Lippincott, "The vibrational spectrum and structure of the tropylium ion", *J. Am. Chem. Soc.*, (1955) 77 (1) 249–250

Fortune, Henningsen, Tuday, *et al.* "Chemical and odor evaluation of various potential replacement films for sampling bags", (2012) *Env. Fed. / Air & Waste Managmnt. Assn.*: Odors and Air Pollutants, Louisville, KY:

> http://www.fivesenses.com/Documents/Library/52%20Sample%20Bag%20Material%20Perf ormance%20Paper%20-%20WEFOdor2012.pdf (Accessed May 2014))

Froissard, Fons, Bessiere, *et al.*, "Volatiles of French ferns and "fougere" scent in perfumery", *Natural Product Communications* (2011) 6 11 1723–1726

Gombosi, T.E *Gaskinetic Theory*, (1994) Cambridge Atmospheric and Space Series, Cambridge University Press

Guenther, "Modeling biogenic volatile organic compound emissions to the atmosphere", *Reactive Hydrocarbons in the Atmosphere*, Chapter 3 Ed. Hewitt (1999) Academic Press, Harcourt Brace & Co.

Hansel, Jordan, Holzinger, *et al.*, "Proton-Transfer Reaction Mass-Spectrometry - Online Trace Gas - Analysis at the ppb Level.", *Int. J. Mass Spec.and Ion Processes.* (1995) 15 150 609–19

Hanson, Greenberg, Henry, *et al.*, "Proton transfer reaction mass spectrometry at high drift tube pressure", *Int. J. Mass Spec.* (2003) 223–224 507–518

Harris, "Modern Vacuum Practice" (1997) McGraw Hill ISBN 0-070707099-2

Hatanaka, "The biogeneration of green odour by green leaves", *Phytochemistry* (1993) 34 1201–1218

Hayes, Leek, Curran, *et al.*, "The influence of diet crude protein level on odour and ammonia emissions from finishing pig houses", *Bioresource Technology*, (2004) 91 3 309–315

Hayward, Hewitt, Sartin, *et al.*, "Performance characteristics and applications of a PTR-MS for measuring VOCs in ambient air", *Environ. Sci. Technol.* (2002) 36 1554–60

Heenan, Soukolis, Silcock, *et al.*, "PTR-TOF-MS monitoring of *in vitro* and *in vivo* flavour release in cereal bars with varying sugar composition", *Food Chemistry* (2012) 131 2 477–84

Heiden, Kobel, Langebartels, *et al.* "Emissions of oxygenated volatile organic compounds from plants Part I: emissions from lipoxygenase activity", *J. Atmos. Chemistry* (2003) 45 143–172

Hitzfield, Gehre and Richnow, "A novel online approach to the determination of isotopic ratios for organically bound chlorine, bromine and sulphur", *Rapid Commun. Mass Spec.* (2011) 25 3114–3122

House, "Refinement of PTR-MS methodology and application to the measurement of (O)VOCS from cattle slurry" PhD thesis (2008) **http://nora.nerc.ac.uk/9370/** (Accessed 27/06/2013)

http://www.nrcresearchpress.com/doi/pdf/10.1139/v86-334 Accessed 03/05/2012

Hunter and Lias, "Evaluated gas basicities and proton affinities of molecules: an update", *J. Phys Chem. Ref. Data* (1998) 27 3

Ibdah, Lavid, Lewinson, *et al.*, "Green routes to green notes", *Chem. Eng. Trans.* (2010) 20

Inomata, Tanimoto, Aoki, *et al.*, "A novel discharge source of hydronium ions for proton transfer reaction ionization: design, characterization, and performance", *Rapid Communications in Mass Spec.* (2006) 20 6 1025–1029

Inomata, Tanimoto, Kameyana, *et al.*, "Technical Note: Determination of formaldehyde mixing ratios in air with PTR-MS: Laboratory experiments and field measurements", *Atmos Chem and Phys*, (2008) 8 273–284

Ionicon Analytik Gesellschaft m.b.H http://www.ionicon.com/products/ptr-ms/ptrtofms/ Accessed 16/05/2013

Jaksch, Margesin, Mikoviny, *et al.* "The effect of ozone treatment on the microbial contamination of pork meat measured by detecting the emissions using PTR-MS and by enumeration of micro-organisms", *Int. J. Mass Spec.* (2004) 239 209–214

Jobson, Volkamer, Velasco, *et al.*, "Comparison of aromatic hydrocarbon measurements made by PTR-MS, DOAS and GC-FID", *Atmos. Chem. Phys.*, (2010) 10

Jordan, Haidacher, Hanel, *et al.* "An online ultra-high sensitivity proton-transfer-reaction mass-spectrometer combined with switchable reagent ion capability (PTR+SRI-MS)", *Int. J. Mass Spec.* (2009) 286 32–38

Jordan, Hansel, Holzinger, Lindinger, "Acetonitrile and benzene in the breath of smokers and non-smokers investigated by proton transfer reaction mass spectrometry (PTR-MS)", *Int J. Mass Spec. and Ion Processes*, (1995) 148 1–2 L1–L3

Karl, Crutzen, Mandl, *et al.*, "Variability-lifetime relationship of VOCs observed at the Sonnblick Observatory 1999 - estimation of HO-densities", *Atmos. Environ.* (2001) 35 31 5287–5300

Koning, "Fruit Ripening", *Plant Physiology Information Website* (1994):

Kore Technology (2013) Private correspondence

Laothawornkitkul, Taylor, Paul, *et al.*, "Biogenic volatile organic compounds in the Earth system", *New Phytologist* (2009) 183: 27–51

Lasekan and Otto, "In vivo analysis of palm wine (Elaeis guineensis) volatile organic compounds (VOCs) by proton transfer reaction-mass spectrometry", *Int. J. Mass Spectrom.* (2009) 45 282

Lee and Sato, "Toluene, benzene, xylene and styrene", chapter in *Drugs and Poisonings in Humans* Pub. Springer, Berlin Heidelberg (2005) II 149–152

Lifshitz, "Tropylium ion formation from toluene: solution of an old problem in organic mass spectrometry", *Acc. Chem. Res.* (1994) 27 138–144

Lin, Lin, Hsieh, *et al.*, "Vertical and diurnal characterization of volatile organic compounds in ambient air in urban areas", *Journal of the Air & Waste Management Association* (2011) 61

Lindinger, Hansel and Jordan, "On-line monitoring of volatile organic compounds at pptv levels by means of proton-transfer-reaction mass spectrometry (PTR-MS) medical applications, food control and environmental research", *Int. J. Mass Spectrom. Ion Process.* (1998) 173 191

Lindinger, Hirber, Paretzke, "An ion/molecule-reaction mass-spectrometer used for online trace gas-analysis", *Int. J. Mass Spec.and Ion Processes* (1993) 79–88

Lindinger, Yeretzian and Blank, "When machine tastes coffee: successful prediction of coffee sensory profiles by instrumental methods based on on-line PTR-MS", *Chimia* (2009) 63 5 292

Lirk, Bodrogi, Raifer, *et al.*, "Elective haemodialysis increases exhaled isoprene", *Nephrology Dialysis Transplantation* (2003) 18 5 937–41

Little and von Engel, "The hollow-cathode effect and the theory of glow discharges", *Proceedings of the Royal Society of London. Series A, Mathematical and Physical Sciences* (1954) 224 1157 209–227

Loudon, *Organic Chemistry* (2002) Oxford University Press

Malcolm, Howe and Dobson, "Chlorobenzenes other than hexachlorobenzene: Environmental aspects", *Concise international chemical assessment document 60,* World Health Organization (2004) ISBN 92 4 153060 X

Mamyrin, Pokhunkov, Dubenskii, *et al.*, "Mass-reflectron research of gas-composition in upper layers of atmosphere using satellites", *Zhurnal Tekhnicheskoi Fiziki* (1993) 63 11 200–205

Mathew and Parpia, "Food browning as a polyphenol reaction", *Adv. Food Res.* (1971) 19 75–145.

Mayer "Polyphenoloxidase in plants-recent progress", *Phytochemistry* (1987) 26 11–20

Mayhew, Sulzer, Petersson, *et al.*, "Applications of proton transfer reaction time-of-flight mass spectrometry for the sensitive and rapid real-time detection of solid high explosives", *Int. J. Mass Spec.* (2010) 289 58–63

Mayr, Margesin, Klingsbichel, *et al.*, "Rapid detection of meat spoilage by measuring volatile organic compounds by using proton transfer reaction mass spectrometry", *Appl. and Environ. Microbiology,* (2003) 69 8 4697–4705

Mayr, Margesin, Schinner, *et al.*, "Detection of the spoiling of meat using PTR–MS", *Int. J. Mass Spectrom.* (2003a) 223–224 229–235

McFarland, "Flow-drift technique for ion mobility and ion-molecule reaction rate constant measurements. II. Positive ion reactions of N^+, O^+, and H_2^+ with O_2 and O^+ with N_2 from thermal to ~2 eV", *J. Chem. Phys.*, (1973) 59 6620

Merlo, Jankevics, Takano and Breitling, "Exploring the metabolic state of microorganisms using metabolomics", *Bioanalysis*, (2011) 3 21 2443–2458

Mikoviny, Kaser and Wisthaler, "Development and characterization of a High-Temperature Proton-Transfer-Reaction Mass Spectrometer (HT-PTR-MS)", (2010) *Atmos. Meas. Tech.*, 3, 537–544

> http://www.atmos-meas-tech.net/3/537/2010/amt-3-537-2010.pdf (Accessed May 2014)

Miller and McGinley, "Background odour in Tedlar and Nalophan sample bags", (2008) *WEF/A&WMA*: Odors and Air Emissions, Phoenix, Arizona pp 590-604

Moser, Bodrogi, Eibl, Lechner, *et al.*, "Mass spectrometric profile of exhaled breath - field study by PTR-MS", *Respiratory Physiology & Neurobiology* (2005) 145 295–300.

Munson and Field, "Chemical ionisation mass spectrometry", *J. of Am. Chem. Soc.* (1966) 88 2621

Nhu-Thuc Phan, Ki-Hyun Kim, Eui-Chan Jeon, *et al.*, "Analysis of volatile organic compounds released during food decaying processes", *Environ. Monit. Assess.* (2012) 184 1683–1692

NIST molecular weight search:

> http://webbook.nist.gov/chemistry/mw-ser.html (Accessed 02/02/2012)

NIST:

http://physics.nist.gov/cgi-bin/Compositions/stand_alone.pl?ele=O&ascii=html&isotype=some (Accessed 14/05/2013)

O'Hara and Mayhew, "A preliminary comparison of VOC in the headspace of cultures of *Staph. Aur.* Grown in nutrient, dextrose and brain heart bovine broths measured using a PTR-MS", *J Breath Res.* (2009) 3

O'Hara, O'Hehir, Green, and Mayhew, "Development of a protocol to measure volatile organic compounds in human breath: a comparison of rebreathing and on-line single exhalations using proton transfer reaction mass spectrometry", *Physiological Measurement* (2008) 29 309–330.

Revercomb and Mason, "Theory of plasma chromatography/gaseous electrophoresis – A review", *Analytical Chemistry* (1975) 47 7 970–983

Schoon, Amelynck, Debie, *et al.*, "A selected ion flow tube study of the reactions of H_3O^+, NO^+ and $O_2^{\bullet+}$ with a series of C_5, C_6 and C_8 unsaturated biogenic alcohols", *Int. J. Mass Spec.* (2007) 263 127–136

Shen, Li, Wang, Wang, *et al.*, "Discrimination of isomers and isobars by varying the reduced-field across drift tube in proton-transfer-reaction mass spectrometry (PTR-MS)", *Int. J. Env. Anal. Chem.*, (2012) 92 3 289–301

Smiths Detection www.smithsdetection.com

Španěl and Smith, "Reactions of hydrated hydronium ions and hydrated hydroxide ions with some hydrocarbons and oxygen-bearing organic molecules" *J. Phys. Chem.* (1995) 99 15551–15556

Španěl and Smith, "Selected ion flow tube studies of the reactions of H_3O^+, NO^+ and O_2^+ with several aromatic and aliphatic hydrocarbons", *Int. J. Mass Spec.* (1998) 181 1–10

Španěl, Ji and Smith, "SIFT studies of the reactions of H_3O^+, NO^+ and O_2^+ with a series of aldehydes and ketones", *Int. J. Mass Spec.* Ion Processes (1997) 165/166 25

Stone, Li and Turner, "A high pressure mass spectrometer study of proton transfer between tri-, tetra-, penta-, and hexamethylbenzene", *Can. J. Chem* (1986) 64 2021

Sulzer, Petersson, Agarwal, *et al.* "Proton transfer reaction mass spectrometry and the unambiguous real-time detection of 2,4,6-trinitrotoluene", *Anal. Chem.* (2012) 84 416–4166

Turner, "VOC Analysis by SIFT-MS, GC-MS and electronic nose for diagnosing and monitoring disease", *Volatile Biomarkers* (2013) Publ. Elsevier P.B.

Turner, Private communication (2011)

Verevkin and Emel'yanenko, "Thermochemistry of chlorobenzenes and chlorophenols: ambient temperature vapor pressures and enthalpies of phase transitions", *J. Chem. Eng. Data* (2007) 52 499–510

Wang, Španel and Smith, "A selected ion flow tube study of the reactions of H_3O^+, NO^+ and O_2^+ with some phenols, phenyl alcohols and cyclic carbonyl compounds in support of SIFT-MS and PTR-MS", *Int. J. of Mass Spec.* (2004) 239 139–146

Wannier "On the motion of gaseous ions in a strong electric field" *Phys. Rev.*, (1951) 83 28

Warneke, van der Veen, Luxembourg, *et al.* "Measurements of benzene and toluene in ambient air using proton-transfer-reaction mass spectrometry: calibration, humidity dependence, and field inter-comparison", *Int. J. Mass Spec.* (2001) 207 167

Warneke, de Gouw, Lovejoy, *et al.* "Development of proton-transfer ion trap-mass spectrometry: On-line detection and identification of volatile organic compounds in air", *Am. Soc. Mass Spec.* (2005) *16*, 1316

Wiki Chlorophenol: http://www.chemistry.ccsu.edu/glagovich/teaching/316/ms/aromatic.html (Accessed 13/05/2012)

Yeretzian, Jordan and Lindinger, "Analysing the headspace of coffee by proton-transfer-reaction mass-spectrometry", *Int. J. Mass Spect.* (2003) 115 223–224

Appendix 1 - Thermodynamics for Reactions in Chapter 3

A1 I   Thermodynamic Considerations for Reactions

Formation of *m/z* 95, protonated phenol

Table A1.1: Gas phase thermochemistry constants:
^{a} = NIST;

Compound/species	Proton Affinity kJ/mol	Heat of formation $\Delta_f H^0_{gas}$ kJ/mol
Chlorobenzene (CB) C_6H_5Cl	753.1^a	54.42^a
Chlorobenzene prot (CBH^+) $C_6H_6Cl^+$	-	1258.95 (calc)
Water H_2O	691^a	-241.83^a
Phenol C_6H_5OH	817.3^a	-96.44^a
Phenol prot ($PhenolH^+$) C_6H_6OH+	-	1172.33 (calc)
HCl	-	-92.31^a

To calculate the enthalpy, ΔH, for the reaction:

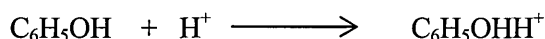$$C_6H_5ClH^+ \ + \ H_2O \longrightarrow C_6H_5OHH^+ \ + \ HCl$$
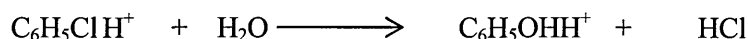
$\Delta H \ = \ \Sigma(\text{Heat of formation products}) - \Sigma(\text{Heat of formation reactants})$

$$\Delta H \ = \ \Delta H_f(PhenolH+) \ + \ \Delta H_f(HCl) \ - \ \Delta H_f(CBH+) \ - \ \Delta H_f(H_2O) \qquad (1)$$

Unknowns are $\Delta H_f(PhenolH+)$ and $\Delta H_f(CBH+)$:

$\Delta H_f(PhenolH^+)$ is formed in the protonation reaction:

$$C_6H_5OH \ + \ H^+ \longrightarrow C_6H_5OHH^+$$

where the proton affinity of phenol, PA(Phenol):

$$PA(Phenol) = \Delta H_f(PhenolH^+) \ - \ \Delta H_f(Phenol) \ - \ \Delta H_f(H^+)$$

$$\Delta H_f(PhenolH^+) = \ PA(Phenol) + \ \Delta H_f(Phenol) \ + \ \Delta H_f(H^+)$$

Similarly, for $\Delta H_f(CBH^+)$:

$$\Delta H_f(CBH^+) = \ PA(CB) + \ \Delta H_f(CB) \ + \ \Delta H_f(H^+)$$

Substituting for both of these unknowns into (1):

$$\Delta H \ = PA(Phenol) + \ \Delta H_f(Phenol) \ + \ \Delta H_f(H+) \ + \Delta H_f(HCl) - (PA(CB) + \ \Delta H_f(CB)$$
$$+ \ \Delta H_f(H+)) \ - \ \Delta H_f(H_2O)$$

➔ $\Delta H \ = (PA(Phenol) - PA(CB)) + (\Delta H_f(Phenol) - \Delta H_f(CB)) + \Delta H_f(HCl) - \ \Delta H_f(H_2O)$

Substituting values from the above table:

$$\rightarrow \quad \Delta H = 62.8 \text{ kJ/mol}$$

Formation of *m/z* 129, protonated dichlorophenol

Table A1.2: Gas phase thermochemistry constants:
[a] = NIST; [b] = Basheer (2006); [c] = Zhu (2003)

Compound/species	Proton Affinity kJ/mol	Heat of formation $\Delta_f H^0_{gas}$ kJ/mol
1,4-Dichlorobenzene (DCB) $C_6H_4Cl_2$	701.67[a]	24.6[a]
Water H_2O	691[a]	-241.83[a] (-469)[b]
Chlorophenol C_6H_5ClOH	1422.59[b]	-131.9 (2-chlorophen)[c] -153.3 (3-chlorophen)[c] -145.8 (4-chlorophen)[c]
HCl	-	-92.31[a]

$$C_6H_4Cl_2H^+ + H_2O \longrightarrow C_6H_4ClOHH^+ + HCl$$
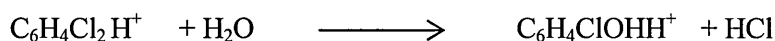
To calculate the enthalpy, ΔH, for the above reaction:

$$\Delta H = \Sigma(\text{Heat of formation products}) - \Sigma(\text{Heat of formation reactants})$$

$$\Delta H = \Delta H_f(\text{ChlPhenH}^+) + \Delta H_f(\text{HCl}) - \Delta H_f(\text{DCBH}^+) - \Delta H_f(H_2O) \quad (2)$$

By comparison with the phenol calculation, this can be seen to be equivalent to:

$$\Delta H = (\text{PA(ChlPhenol)} - \text{PA(DCB)}) + (\Delta H_f(\text{ChlPhenol}) - \Delta H_f(\text{DCB})) + \Delta H_f(\text{HCl})$$
$$- \Delta H_f(H_2O)$$

Substituting values from the above table, using $\Delta_f H^0$ for 2-chlorophenol:

$$\rightarrow \quad \Delta H = 713.94 \text{ kJ/mol}$$

Substituting values from the above table, using $\Delta_f H^0$ for 4-chlorophenol:

$$\rightarrow \quad \Delta H = 700.04 \text{ kJ/mol}$$

Substituting values from the above table, using $\Delta_f H^0$ for 3-chlorophenol:

$$\rightarrow \quad \Delta H = 692.54 \text{ kJ/mol}$$